FZD-473

BI-ANNUAL REPORT 2005/06

RADIATION SOURCE ELBE

Forschungszentrum Dresden Rossendorf

Annual Report 2005/06

Radiation Source ELBE

Editor: U. Lehnert

Forschungszentrum
Dresden Rossendorf

Forschungszentrum Dresden - Rossendorf e.V.
Strahlungsquelle ELBE

Postfach 51 01 19
D-01314 Dresden
Bundesrepublik Deutschland

Leiter   Dr. rer. nat. Peter Michel
Telefon   +49 (351) 260 2101
Fax   +49 (351) 260 3690
e-mail   p.michel@fzd.de

homepage   http://www.fzd.de/FWL

Cover Picture :

3D-Model of the U100 FIR free-electron laser. Central device is the hybrid undulator with 100 mm magnetic period length. Then main technological challenge is the waveguide which transports the optical beam through the undulator up to the first mirror chamber (on the left side). The upstream mirror chamber on the right side containes 3 interchangeable mirrors. The magnetic focussing with an electromagnetic quadrupole triplet and the deflection magnets for the electron beam are also drawn.

Contents

Development of a Superconducting RF photo Gun   79

Preface

In the years 2005 and 2006 the radiation source ELBE has made a very successful transition to a large scale user facility at the research centre Dresden. The original concept for ELBE was to provide a common research facility for the scientific institutes of the FZD and to generate synergy effects. This aim has been achieved. Now ELBE is a broad experimental basic facility for many users inside and outside of the FZD.It became an indispensable tool for the implementation of the main scientific topics of the FZD which are structure of matter, life sciences and environment and security. Both the concept of ELBE as a multiple beam facility and the technical execution have proved as outstanding successful.

In the reporting period, approximately 6000 hours of ELBE secondary beams were delivered for experiments. The users from the FZD came from four institutes.In particular many external users were interested in the ELBE Free Electron Laser beams. Starting in 2005, the ELBE FEL has been operated as a user facility being open to users worldwide. Users from European and associated countries within the EC founded research program "Integrating Activity on Synchrotron and Free Electron Laser Science". First scientific results were gained and published.
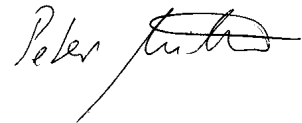
In January 2005 the installation of the second linac module enabled the energy to be increased to 36 MeV. Thus, the data collection was drastically improved for the Channeling radiation experiments and the short-wave IR range in the U27 FEL could be extended down to 3 μm. In August 2006 the installation was completed on the long-wavelength FEL, U100. On August 23rd 2006, first lasing was achieved only a few hours after first injection of the electron beam into the FEL. Thus, the available wave length spectra of the ELBE IR FEL's extends now from 3 to 150 μm.

In the near future it will be possible to use the Elbe IR radiation for experiments in high magnetic fields. The technical installations required for these experiments have been established in the past months. This world-wide collaboration was established for the first time and it should open further synergy effects between groups working in the FZD and outside.

For the commissioning of the ELBE positrons and neutron sources the crucial technical facilities were set up in the past two years. First positron and neutron beams are expected in 2007.

The ELBE accelerator and its secondary radiation facilities have proven to be extraordinarily successful because of its excellent beam parameters and its high availability. This is confirmed

also by the fact that the Elbe technology was adopted by the company ACCEL and will be marketed world-wide for example for the 4GLS project at CCLRC in Daresbury (UK). In addition there are many institutions in the world which show high interest to implement the ELBE technology or parts of it in the frame of future accelerator projects. Thus the FZD with ELBE shifts increasingly into the focus of international institutions, especially those who plan to construct radiation sources of similar kind in the near future.

The ELBE Accelerator Facility - Operation and Machine Development

Besides the user operation and the according maintenance and repair the ELBE staff is continuously working to improve and extend the capabilities of the accelerator. The main extension has been the second accelerator cryomodule installed in January, 2005, thus, makeing available beam energies up to 36 MeV in CW operation. The high-voltage system of the thermionic gun and the RF-system have undergone major revisions. The new pulsed-mode operation of the RF system allows to decrease the heat load to the liquid helium cooling system, thus, enabling us to exceed the design limit of the beam energy. Up to 48 MeV accelerated beam have been demonstrated. Many other systems have seen upgrades with the goal to simplify machine operation and to increase the stability and to reduce failure and down-times.

Experiences on ELBE Operation

P. Michel

Beam time statistics

During this reporting period, significant progress has been made in delivering stable and efficient user beam time at ELBE. The total available beam time in 2005 and 2006 was distributed to 29% bremsstrahlung, 10% channelling radiation and 36% FEL operation. It was common each week to have all three of the secondary radiation beams operational. In addition to the routine beam operation for scientific experiments, there was approximately 25% of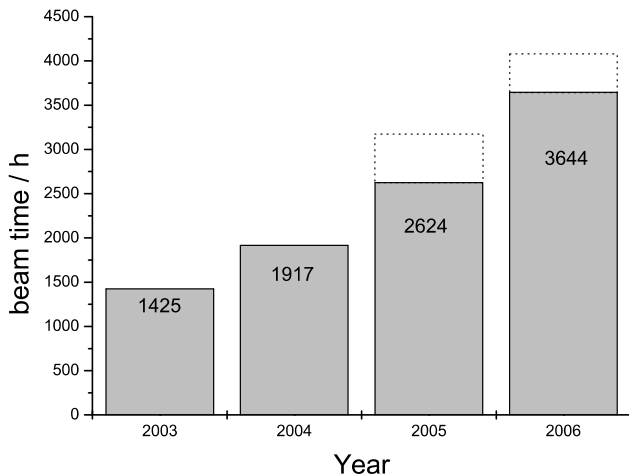 beam time used for machine studies on the accelerator and the secondary radiation targets. Altogether about 6300 hours of beam time were utilized in 2005 and 2006 at ELBE. The statistics in Fig. 1 illustrates the increase of the beam time provided at the ELBE facility since the beginning of the user operation in 2003.

Fig. 1: *Total delivered beam time at ELBE. The scheduled beam time for 2005 and 2006 is shown by the dashed bars. The reliability in the years 2005 and 2006 was 82% and 89%, respectively.*

The theoretical limit for the present ELBE operating regime amounts to 5144 hours (3 shifts daily; five days per week, two week maintenance periods; 4 times per year, one Monday morning maintenance shift each 3 weeks). The difference between the supplied and scheduled time was caused by work on the ELBE infrastructure. The installation work in 2005 was for two accelerator modules and work on the FEL U27, in 2006 it was for the structure of the long-wave FEL U100 [1]. In both years there was unscheduled down time for the helium refrigerator. The problem with the plant was water or nitrogen contamination. The causes for this contamination are not completely understood. The refrigerator is still the most sensitive component of the ELBE plant and will continue to require additional technical and personnel resources for maintenance and repair [2].

Operational Staff

With the reduction of infrastructure work at the ELBE facility, the emphasis shifted to the user program. In November 2004 the ELBE staff transitioned to three-shift operation (5 days per week). In order to accomplish this with the existing personnel, the decision was made that ELBE was to be controlled by a single operator during the night shifts. Three-shift operation and one-man control was a considerable challenge to the ELBE operating crew. All operators were to be cross-trained accordingly. In addition to the mentioned facility infrastructure work another priority was the research project for the development of a super-conducting RF photo gun [3]. The demands on the qualified ELBE operating staff were particularly high for this period of the operation of the FEL. For the FEL, no other aspect of the electron beam parameters was so crucial for the production of secondary radiation like the electron bunch length and energy spread. The first operational experiences in the user program began with the U27 FEL. This experience illustrated the demands on the machine for flexibility and stability when the user required a change in wave length. Work continues to reduce the time after a change in wavelength before the FEL delivers an optimized and stable IR beam. Fig. 2 shows the average time which was needed from switching on ELBE machine to reaching stable lasing for different laser wave lengths.
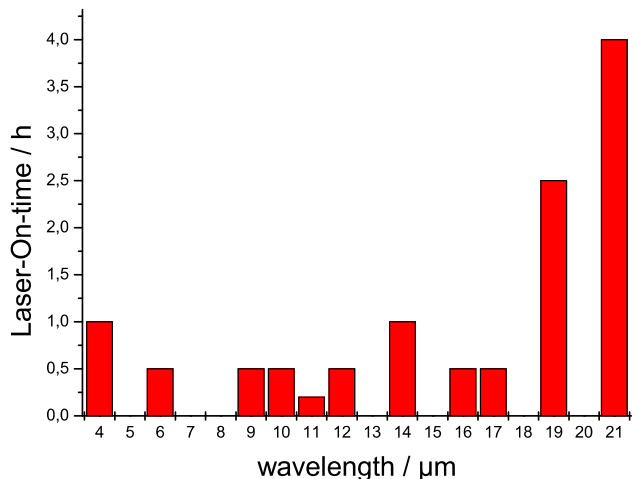
Fig. 2: *Average time needed by the ELBE crew to achieve lasing.*

The operations staff were both educated theoretically in seminars and trained in the practical aspects of operations of the driver accelerator and the FEL by the ELBE scientific staff. An important and successful step was the introduction of the two operation engineers in 2005. Their mission is to be in charge of the coordination for both maintenance and beam operations.

Technical advances

In the passed two years there were many accomplishments and technical improvements on ELBE. Foremost among these achievements is the realization of storing and recalling of all the machine parameters. Thereby it is possible to recover from the changes of the beam paths and energy in a few minutes. Further improvements were attained by the use of magnet cycling (hysteresis) procedures [4]. All dipole and quadrupole magnets (iron core) are automatically switched from zero to maximum values several times and back. The resulting magnetic field gradients are much better defined and the electron beam deviation is significantly less from the ideal beam axis after reloading settings.

Another clear improvement of beam stability was reached by the stabilization of the beam energy [5]. In a dispersive beam line section the energy is measured by means of beam position monitors and fed back over a control loop to the accelerator. This method is in particular useful for long-term experiments in nuclear spectroscopy using the ELBE bremsstrahlung.

Progress was also made with the determination of the absolute electron beam energy. By means of an NMR the magnetic field can be measured with very high accuracy on several ELBE dipoles [6]. A calibration of these field gradients to the beam energy is planned for the near future.

Necessary improvements

Nevertheless there is still another set of possible technical and organizational improvements on ELBE. These are for example:

- further decrease of the tuning times by better qualification of the operating personnel

- development of computer aided procedures for beam tuning and troubleshooting

- development of diagnosis tools for the measurement of system RF phases

- measurement of the absolute beam energy in different places of the beam line

- commissioning of a position-sensitive beam loss detector

- improvement of the position- and energy stability of the electron beam

- improvement of the high voltage characteristics of the thermionic electron gun

[1] FEL U100 commissioning, this report
[2] Cryogenic system, this report
[3] SRF gun , this report
[4] Magnet cycling, this report
[5] Energy stabilisation, this report
[6] NMR based energy measurement, this report

NMR Magnetic Field Measurements and Beam Energy Calibration

U. LEHNERT

The very first parameter which is asked of any accelerator is the beam energy. Unfortunately, accurate measurement of the beam energy is not as easy as it seems. Usually the deflection of the beam in a magnetic field ist used. However, this requires knowledge of the magnetic field strength. In principle this value is related to the drive current of the magnet, but due to hysteresis effects and remanent magnetic fields it depends on the whole history of driving the magnet. Relying on the current alone, therefore, yields a very limited accuracy of beam energy determination.

To overcome all these difficulties an on-line magnetic field measurement was sought. The radiation environment of the magnets, however, precludes any measurement techniques (such as hall probes) which require the use of semiconductor electronics at the place of the measurement. We have choosen an NMR (nuclear magnetic resonance) field measurement technique. A probe containing a sample material which has a nuclear angular momentum (spin) is placed inside the magetic field. The field makes the direction of the momentum rotate about the axis of the field. The frequency of this precession depends on the value of the angular momentum (which is a natural constant characterized by the gyromagnetic factor γ=42.57608MHz/T for protons) and the magnitude of the field. In thermodynamic equilibrium the phases of the precession of all atoms in the sample differ. Around the sample a modulation coil is wound which is driven with an RF signal. If the sample atoms are influenced by an RF field of a frequency close to the precession frequency, the phases will be synchronized. Then a signal can be measured in a second pickup coil wound perpendicular to the modulation coil. An accurate determination of the resonance frequency yields a magnetic field measurement which accuracy is only limited by the homogeneity of the field and the knowledge of the natural constants.
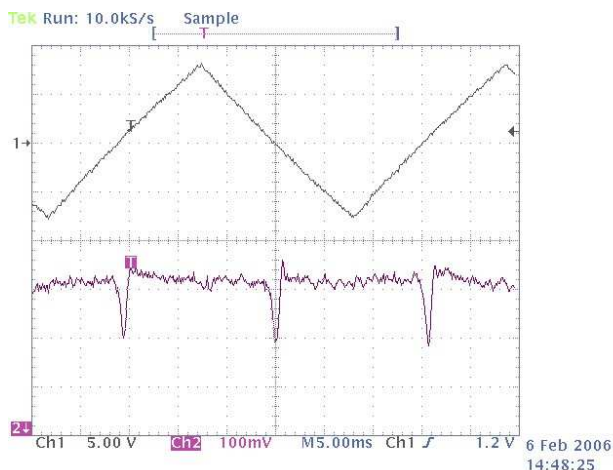
A comercial (METROLAB PT2025) teslameter is used which containes all the electronics to generate and measure the required RF frequencies with an absolute accuracy better that $\pm$5ppm. Fig. 1 shows the signal as the RF frequency is swept through the resonance. Once the PT 2025 has locked on to a signal the internal search algorithm then follows the field by adjusting the center frequency of the sweep to match the resonance.

As the PT2025 can be remote controlled a user interface (see Fig.2) can be run on the diagnostic station in the ELBE control room. This software was written in JAVA and communicates with the PT2025 via RS232 and an RS232-TCP/IP bridge. It allows to comfortably select between the connected magnets and keeps track of the different polarities and calibration factors. The instrument status indicates the presence of and the correct lock on to a NMR resonance. When a valid magnetic field value is received this value is displayed with the computed beam energy in parallel. In addition, an estimation of the magnet current is displayed which is a convenient guide when searching for the resonance. Also implemented was a mode to completely manualy control the PT2025 by switching off the SCAN mode. In this case the center frequency is directly preset by the numerical value of the DAC that controles the oscillator. Valid field measurements, however, can only be obtained in the SCAN-mode, when the center frequency of the sweep automatically follows the resonance. Necessary manual corrections to the (coarse) preset of the DAC are indicated before the tracking algorithm looses the lock.

The described field measurement has been in use for one year now at all beamtimes operating the nuclear physics facility. It has ensured a perfect reproducibility of the beam energy even though, the absolute value of the beam energy is still in dispute due to insufficient knowledge of the alignment and the fringe fields of the used magnets.
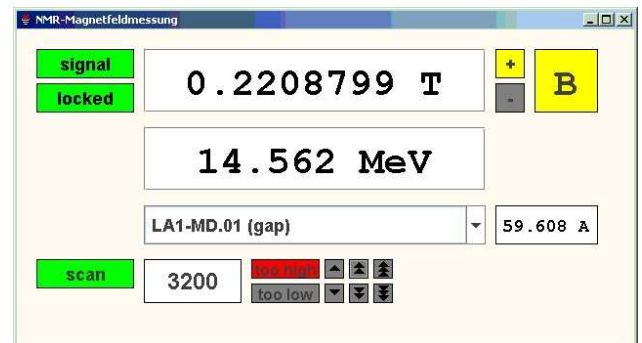

Fig. 1: *The scope signals of the NMR field measurement at resonance. Channel 1 shows the sweep of the RF frequency, channel 2 the pickup RF amplitude.*

Fig. 2: *User interface to the PT2025 NMR teslameter.*

Beam Energy Stabilisation using Transverse Dispersion

M. Justus, P. Evtushenko, U. Lehnert, P. Michel

Stability in mean electron beam energy is of highest interest for a number of experiments performed at the ELBE accelerator. Energy drifts affect parameters of the generated Bremsstrahlung spectra, X-rays or infrared light, as well as the beam trajectory at the production targets or through the FEL waveguide, respectively.

In practise, we observe a slow drifting of the effective accelerating field during the first hours after a machine power-up or after switching to different nominal beam energies. Initially, this effect was compensated manually. A first order automation solution has been developed that corrects the resulting energy drift continuously, using a non-intrusive beam position monitor placed in a transversely dispersive part of the beam guide.

Energy drift of the ELBE accelerator

In Fig. 1 the observable drift in forward and reflected RF power and thus in beam energy is shown exemplarily. A second order delay element was found to represent this behaviour well, for which the step response is

$$x_a(t) = x_a^0 + \Delta x_a^\infty \left(1 - \frac{T_1}{T_1 - T_2} e^{\frac{-t}{T_1}} + \frac{T_2}{T_1 - T_2} e^{\frac{-t}{T_2}}\right) \quad (1)$$

x_a^0 being an output offset, $x_a^0 + \Delta x_a^\infty$ the value the output will settle to and T_1, T_2 the time constants of the system. Good agreement of measured and calculated curve is obtained for $T_1 = 30$ min and $T_2 = 25$ min.

The usual method to compensate for this was to adjust the RF gradient value of the last accelerating module ten-minute-wise, as long as the thermal drift behaviour does not settle. To indicate a change in energy, a $\lambda/4$ strip line beam position monitor (BPM, [1]) placed in a dispersive part of the beam guide, was observed. Intuitively, the first order solution is to perform this correction automatically by a continuous control loop, integrated in the beam control system of ELBE [2].

The control loop

In Fig. 2 the elements building the control loop are displayed exemplarily for the Bremsstrahlung beam line of ELBE, where photo activation experiments are most sensitive to the beam energy. The transfer function FS of the controlled system is the product of:

- the TESLA cavity with al length of 1000 mm

$$F_C = \frac{\partial E_{El}/\mathrm{MeV}}{\partial G_C/(\mathrm{MV/m})} = \cos \varphi \quad (2)$$

- the bending magnet

$$F_D = \frac{\partial x_1}{\partial E_{El}} = \frac{D_D}{E_{nom}} \quad (3)$$

- the drift space

$$F_{Dr} = \frac{\partial x_2}{\partial x_1} = 1 + \frac{D_D'}{D_D} L_{Dr} \quad (4)$$

- the BPM

$$F_{BPM} = \frac{\partial x_2^*}{\partial x_2} = \frac{1}{1 + pT_\Sigma} \quad (5)$$

- a low pass filter in the PLC algorithm

$$F_F = \frac{1}{1 + pT_F} \quad \text{with} \quad T_F = 30\,\mathrm{s}. \quad (6)$$
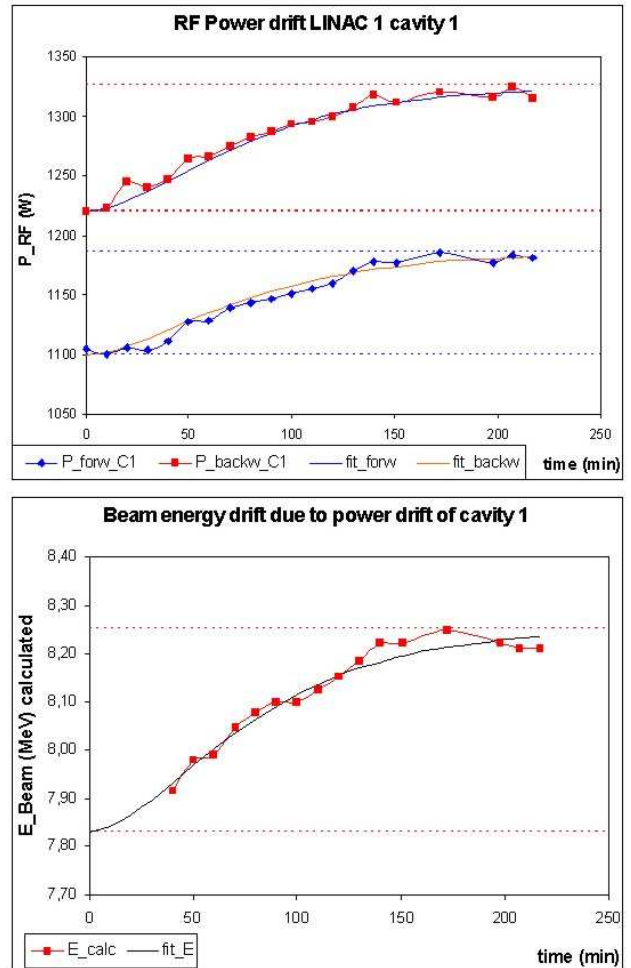
Fig. 1: *RF power and beam energy drift after startup of the accelerator (cavity 1 gradient: 10 MV/m, cavity 2 gradient ≈0, E_{nom}=8 MeV)*

Have a look at Fig. 3 for the corresponding control loop model. The notations used above are :

φ RF phase
G_C RF gradient
x_1, x_2 transverse displacement (horizontal)
D_D dispersion
E_{nom} nominal beam energy
D'_D/D_D horizontal (angular) momentum
L_{Dr} length of drift space
T_F filter time constant

Eq. 2 implies the transit time factor of cavity 2 to be unity. The dispersion is a geometric attribute of the dipole and is not derived here in detail. This may be studied with appropriate literature on particle beam optics [3, 4]. The delay time T_Σ in Eq. 5 is the so called "accumulated delay time" [5], representing all response times of the BPM RF signal transmission, data acquisition and OPC transfer of the BPM results to the PLC. It was found experimentally to be $\approx 0.3\,\text{s}$. The filter is designed as to eliminate higher frequency parts of the BPM signal, which are small but fast deviations of beam deflection and energy, as well as measurement noise. They may result from local charging up effects in the injector section or higher frequent RF modulations and are not to be handled by this control mechanism.
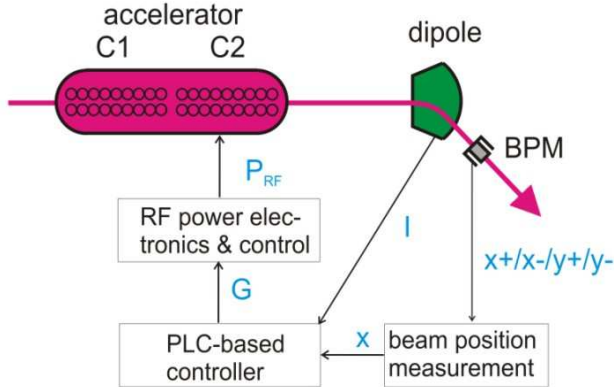

Fig. 2: *Schematic view of the energy stabilization system.*
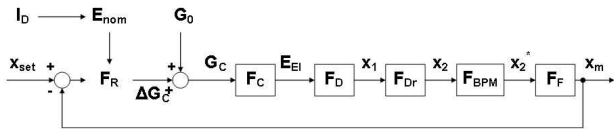

Fig. 3: *Control loop scheme.*

Controller design

Applying general rules of structural design for linear control loops [5], a PI controller is used that compensates for the large delay time TF of the system.

$$F_R = \frac{1 + pT_F}{pT_I} = P + \frac{1}{pT_I} \qquad (7)$$

For the resulting second order control loop, the necessary damping D can be calculated by selecting a certain overshoot h_+ that has to be inserted as a percentage:

$$D = \frac{1}{\sqrt{1 + (\pi/(\ln h_+))^2}} \qquad (8)$$

The open loop transfer function $F_0(j\omega)$ in frequency domain is calculated by developing $F_0 = F_R \cdot F_S$ towards

$$F_0(j\omega) = \frac{V_S}{j\omega_0 T_I(1 + j\omega T_\Sigma)}. \qquad (9)$$

Equating with

$$F_0(j\omega) = \frac{\omega_0^2}{(j\omega)^2 + 2D\omega_0 \cdot j\omega} \qquad (10)$$

and using

$$\omega_0 = \frac{1}{2DT_\Sigma} \quad \text{and} \quad T_I = \frac{V_S}{\omega_0^2 T_\Sigma}, \qquad (11)$$

one can calculate the integration time and the gain of the controller. Here, ω_0 is the eigen frequency of the open loop. This generalized derivation for the controller parameters has been used to meet any ratio of T_F and T_Σ, i.e. if the filter time is modified or one faces data transmission delays other than expected. It is suitable for fully being implemented in the controller software algorithm.

PLC and WinCC implementation

For implementation into the Simatik PLC environment, the Step7 standard function block CNT_CTRL for de facto continuous control is used. In every iteration step (period of 500 ms), the required controller parameters are calculated according to the above standing rules from machine parameters. The filter is a simple discrete delay element using the backwards differentiation method with a period of 50 ms. The controller is adaptive in terms of the dependence of the system gain from the nominal energy, which is calculated from the current set value I_D and the design value $(\Delta I/\Delta E)_D$ of the dipole for nominal deflection angle and radius:

$$E_{nom} = \frac{I_D + I_0}{(\Delta I/\Delta E)_D} \qquad (12)$$

Further, a user interface was created for the visualization environment of ELBE, allowing full control of all loop parameters. It provides the possibility of adding additional steps to the position set point, as well as the RF gradient of the first cavity set value for investigation of the loop performance. The operator can check whether the running conditions (beam is on, the appropriate beam line is selected, a minimum macro bunch length and current are given and pre-alignment has been done) are fulfilled. They are switch-off conditions as well, triggering appropriate error messages. When the controller is activated, the actual gradient

set value is stored as controller output offset, controller parameters are initialized, and the due value at the input is set to zero or to the actual BPM reading, respectively. The direct input options for all beam line elements determining beam current, energy or trajectory are restricted.

Verification

Fig. 4 shows the operation of the control loop over a timescale of 90 minutes in the nuclear physics beam line. One can see that from the moment of switching on, the BPM measurement stays constant (curve `F_in`). The remaining high frequency part of the signal is in the order of $200\,\mu$m. There is a slight overshoot in the filtered BPM reading (curve `F_out`), and the gradient set value decreases slowly, reflecting so the exponential drift behaviour of the cavities (curve `PID_out`).

To check the step and disturbance response, the parameters were varied in different ways and under different conditions, so to say energies (see Fig. 5). Attention was paid here also on minimizing the overshoot of the gradient set value, which has not been discussed so far. As a result, an optimum P value was found to be off the calculated value by a factors of 2 to 3. The reason for that is first seen in adding up of errors in the calculation of the system gain and in beam misalignment (i.e. off-center passing of a quadrupole, yielding unknown deflections). Further, a couple of assumptions had been made, like zero horizontal displacement and momentum of the beam when entering the dipole or on crest operation of the cavity.

Conclusion and look-out

Drawing a line, we can state that the method is working properly and as expected and is definitely an upgrade in beam quality and operability for long term experiments requiring higher mean energy stability. Looking at the reproducibility of any aimed time behaviour, there have to be improvements in the future, although the robustness of the loop is acceptable. One could develop a more detailed model of the system, containing the elements that disturb the beam trajectories, but measures taken will be rather a self tuning algorithm for the controller (Fig. 6), combined with active horizontal position control and high resolution field measurement, being thus an absolute energy measurement. The necessary technologies are partly applied at ELBE [6], partly they have to be extended

(BPM system). In case of FEL operation, users are rather interested in the infrared wavelength than in the energy, so the intention is to use continuous spectrometry as input for the control loop.
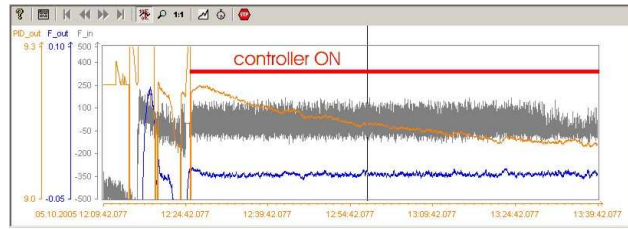
Fig. 4: *Operation of the energy stabilization loop. Gray: BPM measured value. Blue: BPM value filtered by 30. Yellow: gradient set value fo cavity 2 (controller output).*

Fig. 5: *Optimizing of the controller. (Green: Set Value with added step function).*
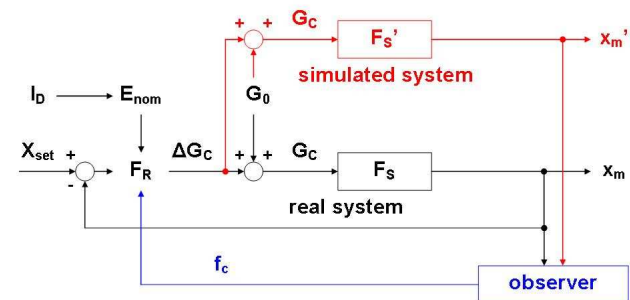
Fig. 6: *Proposal for self tuning control loop.*

[1] P. Evtushenko "Electron Beam Diagnostic at the ELBE Free Electron", dissertation submitted to the Technical University of Dresden, Rossendorf, 2004

[2] M. Justus et al. "Status and Development of the ELBE Control System", this report

[3] K. Wille "Physik der Teilchenbeschleuniger und Synchrotronstrahlungsquellen", B.G. Teubner, Stuttgart, 1996

[4] J. Rossbach, P. Schmüser „Basic course on accelerator optics", Proceedings of the CAS 5th General accelerator physics course, CAS 94-01 Vol.1, Geneva, 1994

[5] H. Lutz, W. Wendt "Taschenbuch der Regelungstechnik", Verlag Harri Deutsch, Frankfurt a. M., 2002

[6] U. Lehnert, NMR measurement, this report

Status and Development of the ELBE Control System

F. Herbrand, R. Jainsch, M. Justus, K. Leege

Abstract

Accelerator control design is started during the main design phase of a machine, but usually not finished when it is put in operation. Further improvement of operability, integration of diagnostic systems, changes in front-end design, keeping track with hardware and software upgrades and ? especially at ELBE ? continuous implementation of new beam line sections and experiments are the main tasks for the ELBE control group, supported strongly by the Department of Research Technology. Some contributions of this report are connected to this topic, while this one gives an overview of recent and ongoing work at the ELBE control system.

Control System Overview

The system architecture has been reported in the ELBE annual reports of 2001 and 2002 [1, 2], and it has not changed a lot in its basics. The scheme is given in Fig. 1, depicting the PC arrangement in a simplified way, and not showing data socket connections.

Right above field level, we run a system of SIMATIC PLC units (Programmable Logic Control, [3]), interconnected by two Profibus networks [4] applying the S7-communication protocol (formerly, Profibus FMS was used). The PLCs partly feature distributed I/O subsystems using Profibus-DP technology. Both electrical and optical transmission is used, creating a mix of bus architectures (line, ring, star).
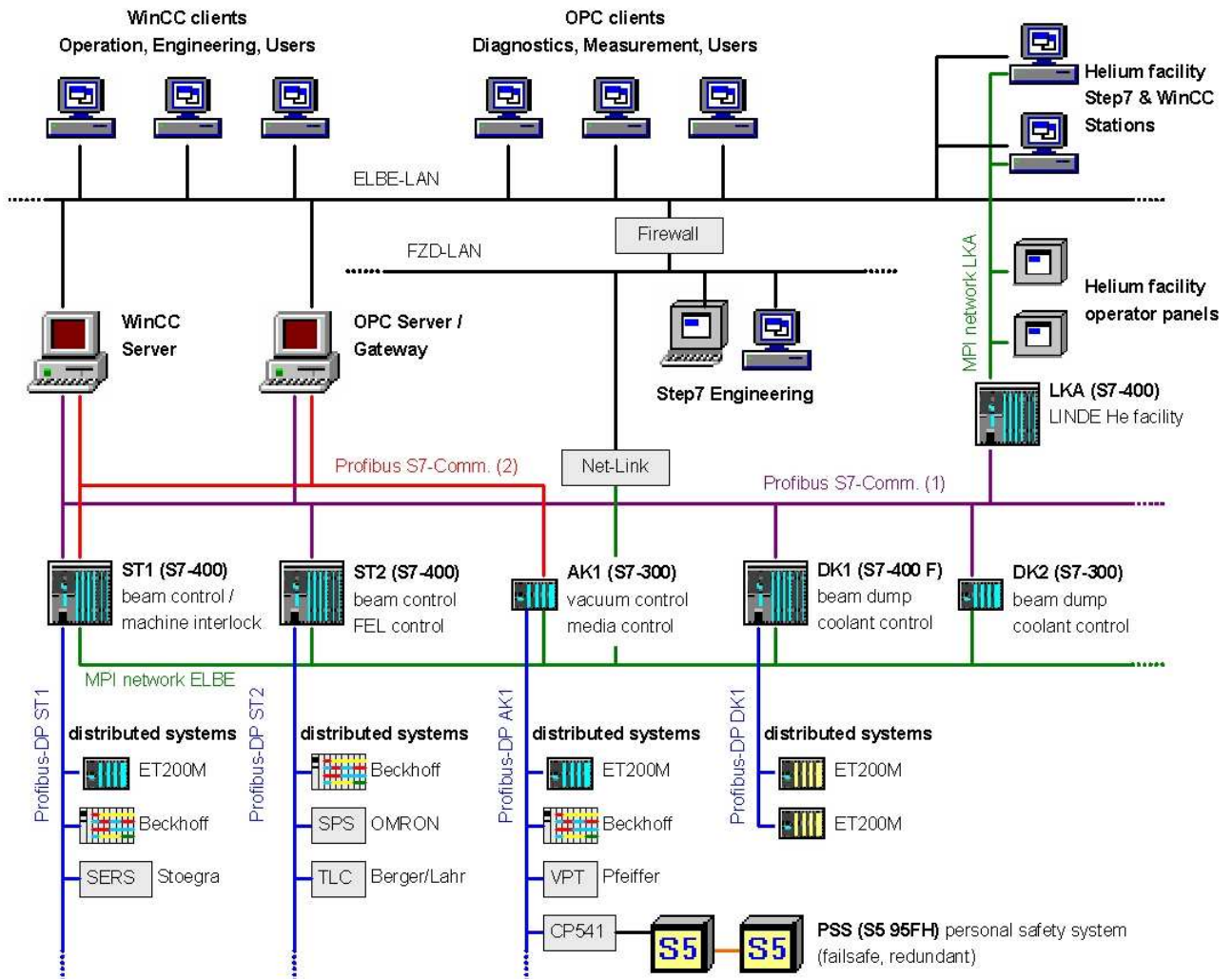

Fig. 1: *The ELBE control and visualization system architecture.*

Tab. 1: *Key parameters of the Simatic PLCs.*

PLC	PSS	ST1	ST2	AK1	DK1	DK2	LKA
technology	S5-95F failsafe redundant	S7-416	S7-414	S7-318	S7-414F failsafe	S7-314	S7-414
distributed I/O	none	13 clients	11 clients	19 clients	2 clients	none	none
serial DAQ	none	10 channels	12 channels	1 channel	none	none	3 channels
main tasks	personal safety system	beam steering, RF control, viewscreens	beam steering, FELs, IR beam lines	coolant, vacuum, climate, media, cryo	beam dump cooling systems (graphite)	beam dump and target cooling systems	helium liquifier control
interlocks	cave access, aeration, dose rates	diagnostics, beam loss, RF windows	diagnostics	coolant loss, overheating, vacuum loss	coolant loss, overheating	coolant loss, overheating	no direct interlocks

For visualization and operation, a SIMATIC WinCC server-client system (Windows Control Center, [5]) is connected to the Profibus networks. The software uploads and diagnostics are done via another interconnecting MPI network (Multi Point Interface), which is based on Profibus hardware, too. Data acquisition of industrial as well as in-house built instrumentation is managed by different types of serial communication. Computer based data acquisition (LabVIEW, LabWINDOWS) and data exchange with ELBE user applications (i.e. Lynx OS, Unix, LabVIEW) is done via OPC connections (OLE for Process Control [6]).

PLC system

Tab. 1 lists the Simatik S7 PLC units being in operation at the moment with their basic features and tasks. During 2005 and 2006, this system has been expanded to integrate data acquisition and control of the newer beam line sections. These are FEL2, the infrared laser beam guide (user labs), the FEL1/2 diagnostic station, a small section for electron energy measurement, and the proposed neutron and positron production targets. Detailed information on these projects can be found in numerous contributions of this annual report or in prior ones. Here, software integration means all aspects of beam steering and shaping, vacuum monitoring, cryogenics, media control, beam dumping and interlocks. Also, some parts of the diagnostic system are concerned. For the FEL2 optic components, an OMRON PLC is used [7]. In order to offer some statistics, Tab. 2 shows the progress in system integration summed up over all CPUs, excluding the Personal Safety System.

Tab. 2: *PLC system integration statistics.*

	Jan 2005	Jan 2007	increase
No. of CPUs	6	7	16,67%
Distributed I/O	29	45	55,17%
Serial Comm.	17	27	58,82%
Machine Code	544 kB	752 kB	38,24%
Data Points	2354	2779	18,05%

Quite a large step forwards has been made in improving the system documentation of Profibus networks, PLC hardware, electrical connections and parts of the software. The results are stored in the new documentation manager provided by the Department of Research Technology. Also, a fraction of the existing software was revised in terms of reasonable naming conventions and sufficient commenting.

Current efforts focus on the integration of the SRF Gun with its diagnostics beam line and laser system, as well as the infrared beam line connecting the Dresden High Field Laboratory to ELBE. Further, for the experimental setup of i.e. the neutron laboratory, S7-PLCs with standalone visualization have been delivered by contractors. They might be integrated into the PLC environment, too. The PSS is being revised in the near future to meet the safety requirements of connecting ELBE and the neutron laboraty. Coming to integration of industrial devices, we focus on solutions innately equipped with Profibus client interfaces or the use of cost-efficient integrated functionality (i.e. Beckhoff bus terminals for stepper control [8]).

Upgrades of the visualization system

By the end of 2005, the ELBE WinCC project was migrated to version V6.0, bringing with it some major improvements and enhancements that can be recognized in the design of the user interface now. The dominating issues are the change of the internal database system from Sybase SQL Anywhere to Microsoft SQL Server 2000. This simplifies the external database access for the users of OPC communication and database OLE methods by use of the standard interface WinCC Connectivity Pack. Further improvement concern the graphical display of stored machine data and their analysis.

Keeping track with the physical and software implementation of new parts of the facility (ref. the above standing section on the PLC system), the required desktop pages for the operators have been generated or extended, respectively. They have become more user-

friendly in some parts, but also more complex, satisfying the increased operating experience of the ELBE team. For ELBE users, some more complex procedures have been automated on the WinCC level to make e.g. scanning procedures more efficient.

Web-based provision of machine parameters has undergone some improvements, too, allowing the visualization now to be accessed from outside ELBE by authorized personnel. This was only possible because of the dedicated measures taken to enhance the system safety and availability by a separate domain controller and firewall for ELBE, as well as a cold server redundancy. Detail on this can be found in [9].

OPC based measurement and control

With a PLC based watchdog and a redesign of the PC based control programs a necessary monitoring functionality was build to detect software or communication malfunctions. Now the operator gets informed about these in real time.

By replacement of the wired serial communication link between the LB111 readout system and the PLC AK1 by OPC, the reliability of dose rate logging was improved.

Further, a set of easy to re-use software sources was deployed to ELBE-Users in order to simplify the communication between their specific user software (i.e. a undulator gap scan software at the FELBE facility)

and the control system via the ELBE OPC gateway in an approved range. The OPC gateway itself was optimized for fast and deterministic response by insertion of a second network adapter for data exchange with a dedicated set of computers.

[1] W. Gläser et. al. "The ELBE control system". Annual Report of the Institute of Nuclear and Hadron Physics & Radiation Source ELBE, Rossendorf, 2002

[2] A. Wagner et. al. "An Interface for Online Beam Parameters at ELBE", Annual Report 2003/2004 of the Radiation Source ELBE, Rossendorf, 2005

[3] SIMATIC Automation Systems, Siemens AG, Munich
http://www.siemens.com/simatic

[4] SIMATIC NET Industrial Communications, Siemens AG, Munich
http://www.automation.siemens.com/net

[5] SIMATIC Operator Control & Monitoring Systems, Siemens AG, Munich
http://www.siemens.com/simatic-hmi

[6] The OPC Foundation, Scottsdale, AZ, USA
http://www.opcfoundation.org/

[7] P. Michel „PLC-based Control System fort he U100 Optical Cavity", this report

[8] Beckhoff Bus Terminals, Beckhoff Automation GmbH, Verl, Germany
http://www.beckhoff.de/

[9] A. Schamlott et. al. "Improvement of the Reliability of the PC Cluster on ELBE", this report

Improvements in Machine Setup and Beam Operability of ELBE

M. Justus, U. Lehnert, K.-D. Schilling

Abstract

One of the main difficulties in running a multi-purpose electron beam source as ELBE is one in its now advanced state of commissioning, is the permanent switching between experiments and beam specifications within short timescales. Further, user demands in beam quality naturally increase after having made first experiences with ELBE. After the first 18 months of ELBE operation, when the basic experience in performance and interaction of all systems was collected, aspects of operability and beam quality improvement have come more and more to the fore.

Scaling of magnetic beam guide settings

Difficulties in switching the beam energy. Talking about Bremsstrahlung or X-ray production at ELBE, the experiment is carried out with a definite electron beam energy that has to be provided quickly after starting up the accelerator. In FEL operation, the main parameter of interest is the infrared wavelength, which can be adjusted using the electron beam energy as well as the undulator gap, implying that we are more independent from the electron beam energy here. But as often the overall laser power is to be maximized, he machine setup will tend towards small gaps and higher energies. Especially while carrying out gap scan experiments, the FEL operation will start at the smallest possible gap, which makes it necessary to adjust the wavelength by changing only the beam energy. Machine development time for preparation of settings is very limited, and the manual magnet-by-magnet beam alignment is a time consuming procedure. From the operating point of view, we experience that the lifetime of machine settings is limited, due to changes in the injection beam line or rearrangements of one or the other magnet.

Scaling routine. To meet these difficulties, a tool was developed that enables the operator to linearly extrapolate the magnetic field settings of dipoles, quadrupoles and steering coils of an existing machine setup to a different nominal beam energy. The beam line is therefore divided into two sections that can scaled by different factors, F_1 and F_2, which refer to the aimed contribution of both accelerating modules to the total change in energy.

$$F_1 = \frac{E_{new,1}}{E_{setting}}, \quad F_2 = \frac{E_{new,2}}{E_{setting}} \quad (13)$$

It is a decision up to the operator, which cavity will provide the change in beam energy, depending on the actual situation. Non-homogeneity, non-linearity and residual magnetism effects of the lenses are neglected, as this tool is developed for small scaling steps that have to be verified by the operator. Thus, the DC current of an element is simply calculated by multiplying with the appropriate factor:

$$I_{new} = F_i \cdot I_{setting} \quad (14)$$

The scaling routine is run simultaneously in both beam control PLCs (ST1 and ST2, see system overview in [1]). It is a sequence, calling a scaling function for each magnetic element that performs the selection cross check, the multiplication and the error check. The function is locked if the electron beam is on.

Operator interface. The WinCC interface (see Fig. 1) is designed to give the operator the opportunity to select the beam path and the type of magnets. To keep track with the actual beam energy when scaling in small steps, one can store the initial energy as a test value for each section. An error sum for each PLC indicates if one or more magnets have not been scaled, i.e. when the scaled value exceeds the operating range of the current supply. The latest scaling step can always be undone. After a successful step, the beam energy has to be adjusted, and the overall alignment is to be checked and corrected. In practice, the tool has been proven to perform very well even in ranges of 10 to 20 percent of energy for the NP and RP beam lines, being thus a quick calculator. In FEL operation, small steps of $1\ldots 2$ % are preferred to maintain the FEL lasing conditions from one step to the other [2].
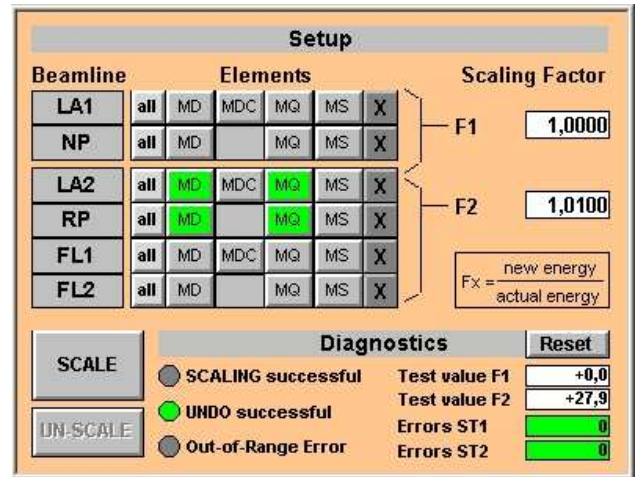
Fig. 1: *WinCC interface for magnetic field scaling beam line sections are LA1: behind LINAC 1, NP: nuclear physics, LA2: behind LINAC 2, RP: radiation physics, FL1: U27, FL2: U100.*

Cycling of dipole and quadrupole magnets

. Reproducibility of beam line settings. Occasionally, operators have to change the energy two to three times within one shift in a range that would require several

steps of scaling by the above described procedure. For that reason, but also being advantageous for any machine start up, we should be able to prepare magnetic settings for different beam energies during machine development time and be able to quickly reproduce those during user shifts.

Remanence effects of ELBE magnets. The main problem for reproducibility is the magnetic remanence of the dipoles and quadrupoles, which are usually equipped with a construction steel frame (ST37) and a stainless steel yoke (XC6 or XC10) [3]. Fig. 2 shows the magnetization curve drawn from manufacturing inspection data of a typical 45° dipole magnet with a current range of $0 \ldots 160$ Amperes, having a remanence of $0.26\,$mT. Additionally, a measurement series has been repeated four times, using a time structure for the dipole current as shown in Fig. 3a, where also the remanences measured after each magnetization by a hall probe are drawn. Looking at different currents (step 7 and forth), they show to be in the sub-mT range, too, which is three orders of magnitude below the maximum design field of $723\,$mT at full current. Between the four series, the dipole was magnetized stochastically, leading to large differences of the initial remanences (step 2).
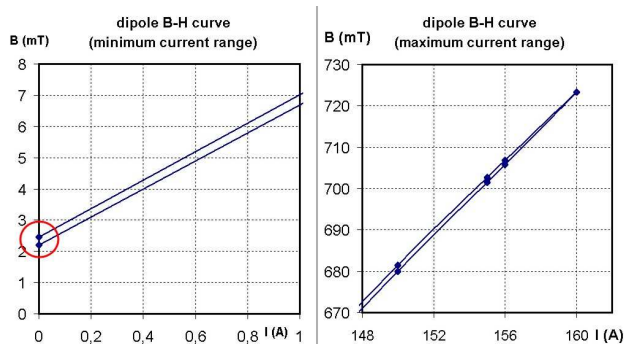
Power supplies for dipoles and larger quadrupoles ($I > 10\,$A) used at ELBE are unipolar current sources of the DANFYSIK® 8000/8500 system, type 55 [4]. Dipoles with a 0°-exit have an additional coil for remanence compensation. For small quadrupoles we use in-house built unipolar current drivers with polarity switch for 5 A or 10 A, where some zero-offset can occur. Thus, remanence compensation by field measurement will be very cost-intense, as one would have to equip all magnets both with appropriate field measurement and with an additional power supply for the compensation windings. The decision was made to use a cycling algorithm to bring the remanence not to zero, but to a defined and reproducible value in order to minimize the setup time for the machine.

Demagnetization. The basic mechanisms of magnetizing ferromagnetic material (shift of Bloch walls, reorientation of magnetic domains, paramagnetism) and are not discussed here to explain remanence, but can be studied in numerous books dealing with electromagnetism [5, 6]. If we were able to reach saturation in both polarities, a complete demagnetization would be possible by AC propagation with slowly decreasing maximum of the current for several hundreds of cycles, as illustrated in Fig. 4a.

Fig. 2: *Magnetization curve of a 45° ELBE dipole [3].*
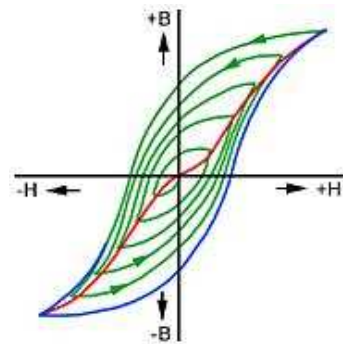
Fig. 4a: *Demagnetization by AC propagation [7].*

Fig. 3: *Magnetization sequence with measured residual field (4 data rows).*
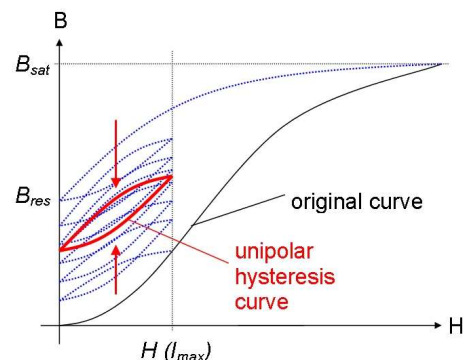
Fig. 4b: *Cycling of a unipolar, non-saturable magnet.*

However, the effect is – summed up over a whole beam line – critical enough to prohibit to loading an already used setup and immediately pass the beam to the target. Adjustment of nearly all magnetic components is required.

Due to the two facts that at ELBE none of the used dipole or quadrupole yokes reaches saturation and that we only have one direction of magnetization, it is obvious that the remanence is an absolutely non-predictable measure, as the history of magnetization is unknown. Also, the mentioned microscopic pro-

17

cesses underlay some uncertainty, like the Barkhausen effect. This can only be overcome by magnetizing up and down the material with the full available range of field strength several times, further called "cycling". So the unipolar, partial hysteresis we have to deal with will settle in a certain reproducible state. This is illustrated in Fig. 4b. The accuracy of this process is depending on the number of cycles.

The cycling scheme. It has been experimentally obtained in a consecutive series of cycling and magnetization that for ELBE dipoles the repeatability difference of the remanences as well as the top fields can reach less than 10^{-4}, when the dipoles are ramped up and down three times (see Fig. 5). From this, a cycling regime has been defined according to Fig. 6, where all dipoles are cycled within a 30 time scheme. Existing correction windings are cycled contrary to their magnetization direction for normal use, so that their field adds up to the field of the main windings. The in-house built power supplies are faster in ramping up the current, so quadrupoles are cycled to positive and negative maximum of the current for five times within a 10 s time scheme. They are separated into two groups to stress the DC converters less. A test series similar to the above described for the dipoles delivered results in the same order of magnitude for the field and remanence repeatability.
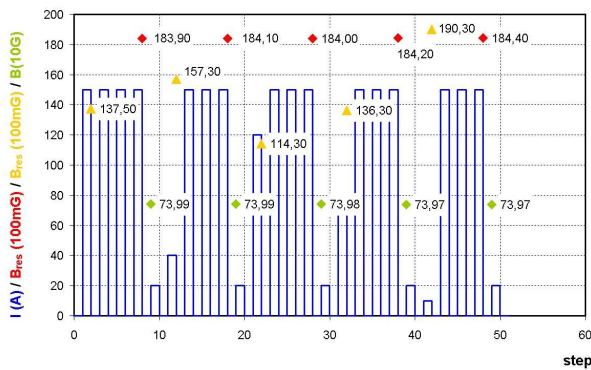

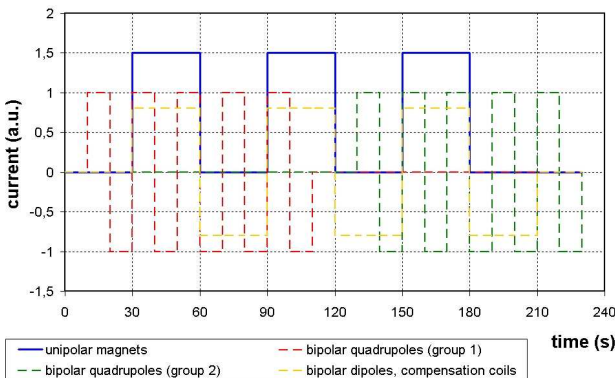**Fig. 5:** *Verification of magnet cycling using a dipole .*

Fig. 6: *ELBE magnet cycling scheme.*

The software routine is implemented similar to the scaling tool. It is a function block run in both beam control PLCs for each dipole or quadrupole, containing a beam line and cycling group cross check, the cycling sequence an error check, i.e. to detect failure of a power supply. Cycling is allowed only if the electron beam is off. During the 240 s running time of the procedure, any manipulation on magnets is blocked for the operator or other software tools.

Operator interface. For the operator, a WinCC interface (Fig. 7) has been developed that allows him to select and deselect magnets of the current beam path before starting the routine. The error detection gives intrinsic information on any magnet.

Experiences. Magnet cycling has become a standard part of machine setup by now. The basic procedure for the operator is to cycle all magnets of the beam path, load a setting and start fine adjustment. This means of course that preparing the settings requires an iterative procedure of cycling and beam adjustment for at least two or three times to achieve high reproducibility. Tests of the routine in U27 FEL operation, which is quite sensitive, proofed that the lasing conditions are preserved, when different magnetic settings have been loaded to the machine in between running it with a specific energy, or wavelength, respectively [2].

[1] M. Justus et al. "Status and Development of the ELBE Control System", this report

[2] ELBE electronic logbook, 2006
https://www.fzd.de/db/elbe.logbook.daten

[3] DANFYSIK, product information on ELBE dipoles and quadrupoles, Jyllinge (Denmark),1998-2006

[4] http://danfysik.dk

[5] L. Bergmann, H. Gobrecht "Lehrbuch der Experimentalphysik" Bd.2, Walter de Gruyter, Berlin / New York, 1987

[6] J. D. Jackson „Classical Electrodynamics", Wiley New York, 1999

[7] Schulzentrum Utbremen (professional & secondary school for technical assistants in physics), lectures on magnetism, University of Bremen, 2004
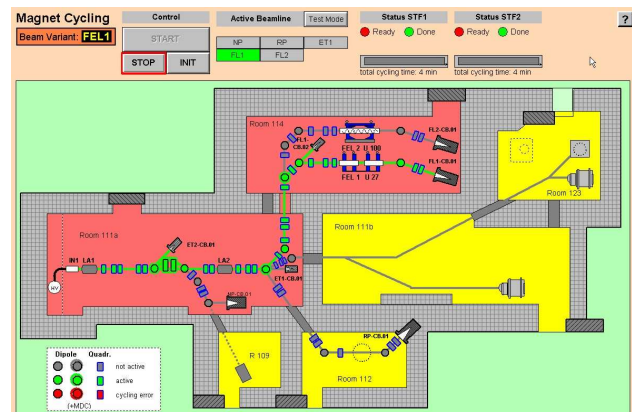http://www.szut.uni-bremen.de/bildungsgaenge/ PhyTA/h-feld4.htm

Fig. 7: *WinCC interface for magnet cycling.*

Operation of the ELBE Low-Level RF-System

H. Büttig, A. Büchner, C. Caspar, F. Gabriel, H. Langenhagen, U. Lehnert, P. Michel, J. Teichert, R. Schurig

The analog low-level RF system

The ELBE low-level RF System (LLRF) is designed as an analogue and direct converting (without IF) system. Each cavity is controlled individually by separate amplitude- and phase controllers. The operating frequency is 1.3 GHz, phase-locked to a 13 MHz clock. This decision on a 13 MHz clock was made because of the 13 MHz FEL excitation frequency. The architecture of the system is redundant for each of the 4 superconducting cavities and the 2 normal conducting bunchers. Fig. 1 shows the schematic diagram of one LLRF system. In the block diagram, the 1.3 GHz input signal is fed via the system phase shifter (trombone-type with dc-servo motors) in the controller. This remote controlled "system phase shifter" is used to vary the RF phase of a cavity against the beam phase. Inside the controller the signal is split in two paths. The "lower path" drives a high level mixer (+17dBm) used as phase detector, the "upper path" is connected to the voltage controlled phase shifter (phase controller:

working range 60 deg) and the amplitude modulator (voltage controlled attenuator).

After passing the RF switch (RF on/off) and the loop phase shifter (loop stability) the amplified signal (level: +4 ... 12 dBm) feeds the klystron driver. The input level requirement of the klystron rack is 0 dBm for +70 dBm (10 kW) output power. The feedback line from the fundamental pickup of the cavity to the controller is made of aged coax cable (Andrews FSJ4-50B) to perform best phase stability. Attenuators in front of the controller are used to match the input level, depending on the cable length. The phase dependency of the limiter in front of the phase detector is 4 deg within the dynamic range of the pickup signal (-2 dBm to +16 dBm). The limiter ensures phase detection independent from the amplitude of the cavity signal (because the mixer-type phase detector multiplies both input signals). All signals (settings, readings, switches) are controlled by a SPC (SIMATIC). The outputs of both detectors (amplitude and phase) are monitored.
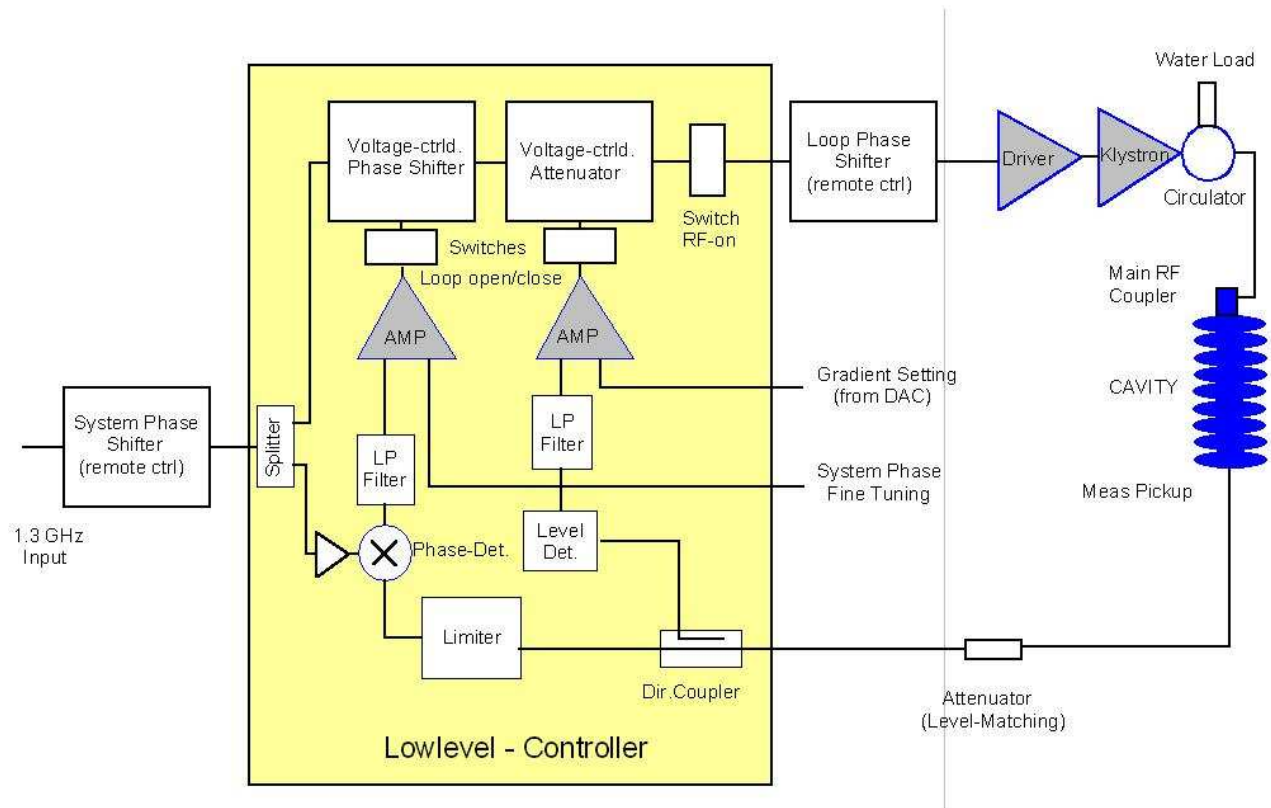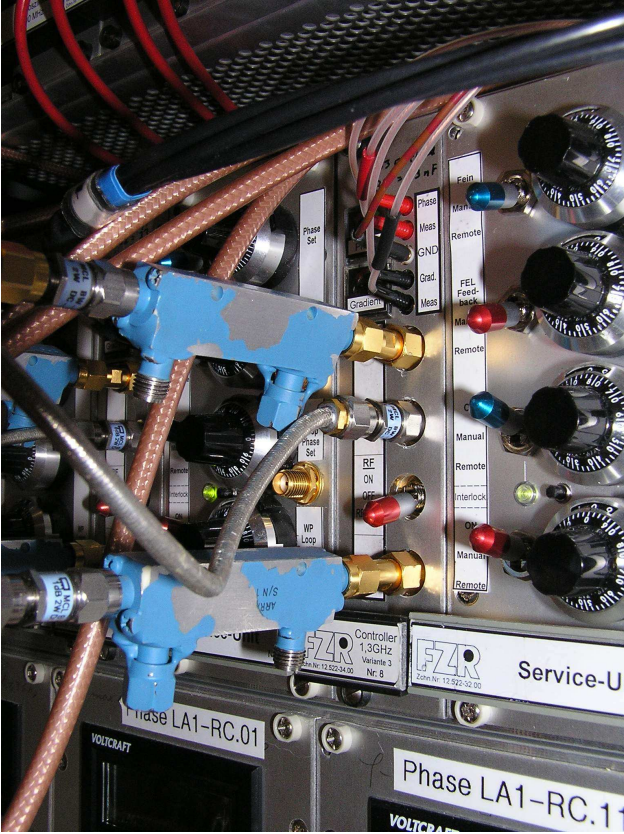

**Fig. 1:** *Block Diagram of one LLRF-System.*

Fig. 2: *One LLRF Controller and Service Unit.*

Performance of the LLRF System

To keep the energy spread of the accelerated electron beam below 10^{-3} the stability of the field amplitude has to be better than 0.5 % and a RF phase stability 0.3 deg (rms) respectively. The energy spread of the beam measured at ELBE is between 20 and 40 keV, depending on the setting of the machine. The measured stability of the field amplitude at ELBE is typically $2 \cdot 10^{-4}$ rms. The RF phase stability of the closed loop is 0.02 deg (rms). A proper adjustment of the gain of the control loops is needed as well as the minimization of all disturbances affecting the performance of the control loops. For the loop amplifiers very fast low noise OPA's are used to obtain a high gain bandwidth product. The RF bandwidth of the controller is between 5 and 10 MHz, the loop gain is adjustable between 10 and 100. The overall 3 dB bandwidth of the RF system (without cavity) is limited by the klystron, Fig.3.

The RF system is controlled by 13 MHz MASTER oscillator. The 13 MHz master oscillator is housed in a temperature controlled, double shielded quartz oven. The long time stability is better than $1 \cdot 10^{-8}$ per year. The 13 MHz clock signal is distributed via buffers to synchronize the 260 MHz and 1.3 GHz PLL's. Fibre links with temperature stabilized IR-light transmitters and receivers are used to distribute the clock signal within the labs and to the -250 kV terminal of the electron gun.
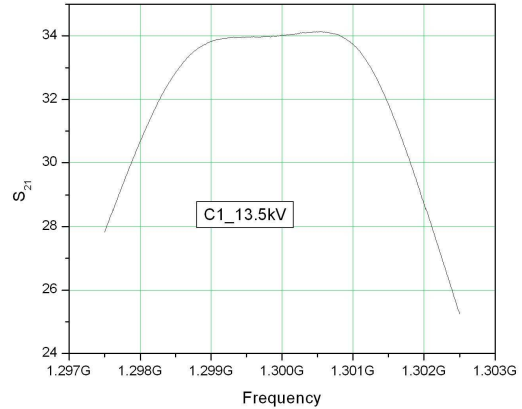
Fig. 3: *Measured Gain-Bandwidth Characteristics of the klystron VKL7811St (CPI), SN 1012.*

Much care was taken to provide "very clean" oscillator signals because the phase noise affects the energy spread of the accelerated electron beam directly. The excellent phase noise performance of the 1.3 GHz PLL, shown in Fig. 4, was obtained by implementing a temperature stabilized "high-Q" quartz oscillator (144 MHz) into the PLL design and by carefully optimized loop filters. Side band phase noise in terms of jitter (rms) is: 100 fs for the 13 MHz MASTER within 10 Hz to 10 kHz from carrier and 170 fs for the 1.3 GHz PLL within 10 Hz to 10 kHz from carrier [1].
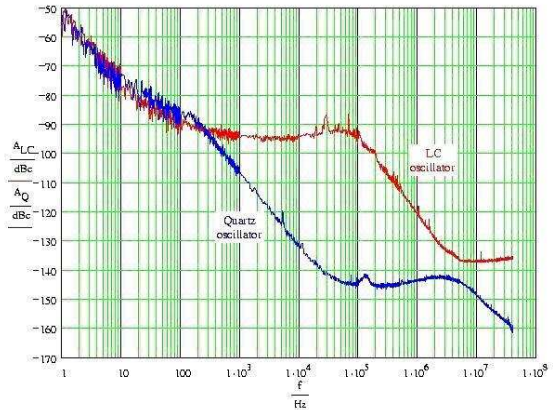
Fig. 4: *Phase Noise of the 1.3 GHz PLL-Oscillator Red: The early design using a standard-LC-oscillator, Blue: Quartz oscillator for 1.3 GHz (144.44 MHz).*

Disturbances affecting the stability of the control

Stability of the Helium pressure and microphonics
A lot of experimental work had been done to set the best working point for the machine and to study microphonics. The studies on microphonics are published in a separate paper. Assuming no helium pressure fluctuations the measured phase stability of the phase controller is 0.02 deg (rms). The working pressure of the He-plant at ELBE is 31 mbar. The pressure stability

is ±0.1 mbar. The frequency deviation of the accelerating π-mode caused by microphonics at 31 mbar He-pressure is between 20 and 30 z (Fig. 5).
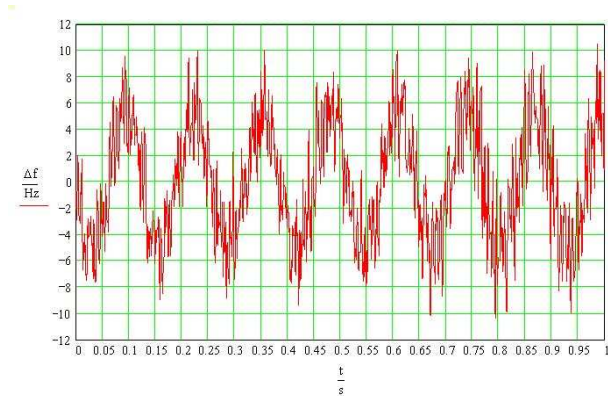
Fig. 5: *Frequency deviation (measured at cavity 4), He-pressure: 31 mbar.*

Lorentz Force Detuning
For CW-LINAC´s like ELBE Lorentz force detuning is an issue during ramping up the gradient during RF-pulsed operation. Operation with pulsed RF is used at ELBE to increase the gradient within the given limits (200 W @ 1.8 K) of the helium plant and to perform cavity training. The Lorentz force detunes the cavity according to $\Delta f = 2\pi K E_{acc}^2$ with $K = -1\,\mathrm{Hz/(MV/m)}^2$. To compensate for lorentz force the cavity tuners at ELBE are only manually

controlled to save lifetime of the tuner gears. During normal operation of ELBE tuner manipulations are seldom (depending on the experiment 1 to 5 times per shift).

Performance of the RF-System

Cavities:

Frequency	1.3 GHz ±5 Hz
Bandwidth (3dB)	114 Hz
Phase noise related microphonics	2...6 deg peak-peak

RF System:

Frequency stability	$<1 \cdot 10^{-9}$
Aging in 10 years	$<3 \cdot 10^{-7}$
Phase noise	<0.05 deg (rms)[1]

Measurements at 10 MV/m gradients without beam:

Phase stability	rms / <1 sec	0.02 deg
	per day	<1 deg
Amplitude stability	rms / <1 sec	$2 \cdot 10^{-4}$
	per day	$2 \cdot 10^{-4}$
LHe pressure stability	±0.1 mbar	

[1] A. Büchner, F. Gabriel, H. Langenhagen: Noise Measurements at the RF System of the ELBE Superconducting Accelerator; EPAC 2002, Paris, June 2002.

[2] A. Büchner et.al.: Pulsed RF System for the ELBE Superconducting Accelerator, EPAC 2006, Edinburgh, 2006

Test of Beam Deceleration at ELBE

U. Lehnert

For modern high-power FELs increasingly energy recovery linac (ERL) schemes are applied. The aim is to limit the necessary amount of RF power and to reduce the problems conected to dumping high-energy beams, thus, enabling higher beam currents. There is considerable interest about the behaviour of the RF control loop in a state where the beam is actually feeding power into the accelerator cavities. Accordingly, deceleration experiments were performed at ELBE to study this range of operation.

A 26 MeV beam was tuned and threaded through the switching magnet `LA2-MD.01` which was used as an energy spectrometer. Now, the phase of the cavity `LA2-RC.11`, the fourth and last one of the ELBE accelerator was varied over the complete available range. Fig. 1 shows the measured beam energy at very low beam current. This measurement allows to verify the phase settings and the gradient of the used cavity which amounts to 4.7 MV/m.
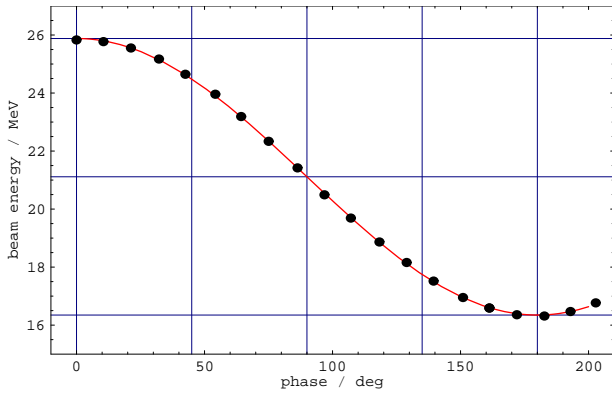

Fig. 1: *Beam energy measured when tuning the phase of the 4th (last) RF cavity of ELBE.*

In this case the cavity is not loaded by the beam but by the RF input coupler, only. The input coupler is designed for a matched transmission of the RF power at full beam loading - 800 μA at 10 MV acceleration voltage. In the unloaded case a considerable drive RF power is needed which is almost completely reflected at the coupler.

If now the beam current is increased the loaded impedance of the cavity decreases which influences the necessary drive power from the klystron amplifiers. The way the drive power is affected by this change depends on the phase of the beam induced currents with respect to the phase of the RF voltage. Fig. 2 shows the measured forward and reflected power in the case of a 180 deg phase shift between the beam induced

current and the cavity RF voltage. This corresponds to an on-crest deceleration of the beam.
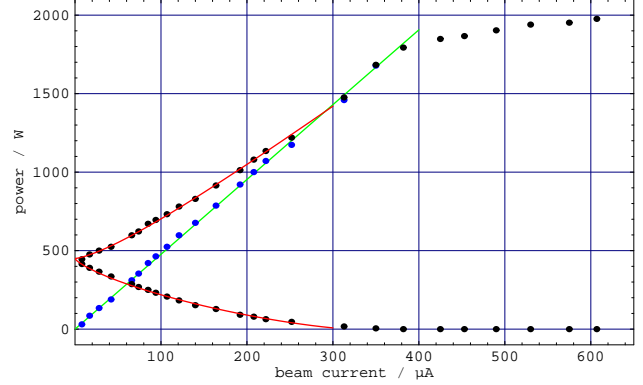
Fig. 2: *Forward and reflected RF power of an ELBE RC cavity set at 180 deg phase (on-crest decelerating) to an electron beam with varying current. The black dots are the measured values of the forward and reflected RF power with the red lines fitted by an analytical model. The blue dots indicate the difference of both and the green line shows the power loss of a beam decelerated by 4.7 MeV.*

As verified during the tests the beam energy is decreased by 4.7 MeV and shows no considerable change up to 300 μA beam current. At this point no forward power is needed to drive the cavity the 5 MV/m gradient is generated by the beam alone. The phase of the RF field still is on-crest decellerating. For beam currents beyond this point the control over the phase of the field is lost. Up to 380 μA the beam is still decelerated by $\approx$5 MeV but the cavity gradient increases so that the power can be tranfered into the transfer line load. Accordingly, the phase changes which shows in an increased energy spread of the decelerated beam. Above this load the beam generated power cannot be dissipated anymore, so the effective decelleration voltage drops.

The tests have shown that the ELBE RF system is suited to deceleration and ERL schemes as long as the cavity loading stays below the matching point, say als long there ist still some forward RF power needed to drive the cavity gradient. Beyond that the control over the beam parameters is lost and no stable operation is possible. This range will probably be greatly extended by the presence of a second beam which is accelerated at the same time, as the beam induced currents of both beams would be oposite in phase and (partially) cancel each other.

Operation of the VKL7811St Klystrons at the Radiation Source ELBE

H. Büttig, R. Schurig

Summary

Each of the 4 superconducting 1.3 GHz cavities of the ELBE Linac is individually driven by a RF-system including one VKL 7811St klystron (CPI). The first two systems became operational in May 2001. The operating time of the VKL7811St klystrons used for the two superconducting cavities in „Cryomodule-1" is nearly 8000 hours now. The „Cryomodule-2" was assembled and put into operation in January 2005. This paper describes the system and reports on experience during the operation.

General layout

The klystron VKL7811St (CPI Palo Alto, USA) is a 5-cavity tube with a permanent magnet system for focusing the beam (Fig.1). The typical gain characteristic is presented in Fig.2, the S_{21}-curve in Fig.3.

Specification:

|	
Filament Voltage:	8 V
Filament Current:	4 A
Beam Voltage:	-15 kV (cathode)
Beam Current:	1.9 A
Gain:	36 dB
RF-Output:	70 dBm
Input Connector:	N type
Output Connector:	WR650

Fig. 1: *Klystron VKL7811St at ELBE (1.3 GHz, 10 kW).*

Filament Power Supply

The filament power supply is an adjustable constant current source. This guarantees soft-start of the filament power. Hardwired interlocks are provided by door switches, water flow sensors, an air-stream sensor and a watchdog for the filament current (window-discriminator with optical link to the interlock card). If one interlock trips the high voltage is switched off promptly (hard wired).
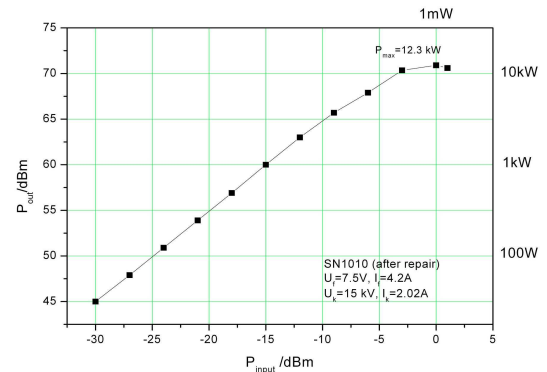
Fig. 2: *Transfer function of the klystron amplifier as shown in Fig.5 (including the driver).*
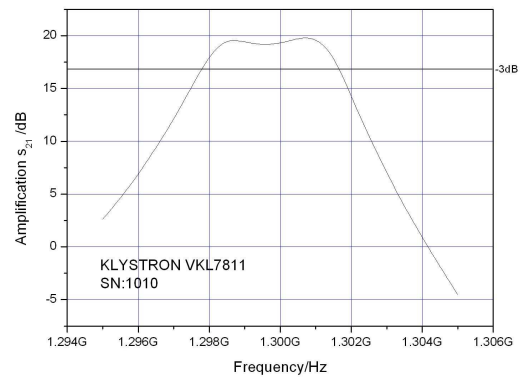
Fig. 3: *Gain- Frequency Characteristic (S_{21}-curve) of the klystron amplifier as shown in Fig.5.*

HV-Power Supply

The HV-PS (Fig.4) used for each klystron is a switched mode Power supply Model HCH 40000-15000 (FuG Elektronik GmbH Rosenheim/Germany). The maximum voltage is 15 kV and the maximum current 2.5 A. The HV-PS is remote controlled by a SIMATIC SPS, except the hard-wired interlock. For save operation of the klystrons the HV-PS can set to „stand by mode" (lower beam voltage) during longer beam-off time. The cable between HV-PS and the klystron is about 25 m long, representing a capacity of 1.6 nF. The sideband noise of the switched mode power supply on the RF signal is in the range of -70 dB and does not affect the beam quality.

Status 1/2004: each rack (smps) delivers 15kV, 2.5A

Fig. 4: *Klystron HV-Power supplies (FuG Rosenheim).*

Klystron rack

The block diagram of a 10 kW klystron amplifier is presented in Fig. 5. A 19-inch rack contains the klystron itself, and all hardware except the high voltage power supply. The control of the klystron amplifier as well as the power supplies is implemented into the ELBE control system using SIMATIC SPS systems.

Failures during operation

The overall availability of the RF system is good and comparable to other components of the accelerator. The VKL7811St klystron operation during the first six years was nearly free of tube related problems except klystron serial number SN1010:

Multipacting:
When measuring the S_{21}-characteristics of klystron SN1010 a power jump was detected. This was reproducible. (When increasing the drive power from -7 dBm to -6 dBm the output power jumped from 65.8 dBm to 68.3 dBm.) The problem was reported to CPI and was successfully cured following their instructions.

Vacuum Leak:
SN1010 failed after 3500 hours of operation by a vacuum leak on the cathode insulator. A major repair was necessary.
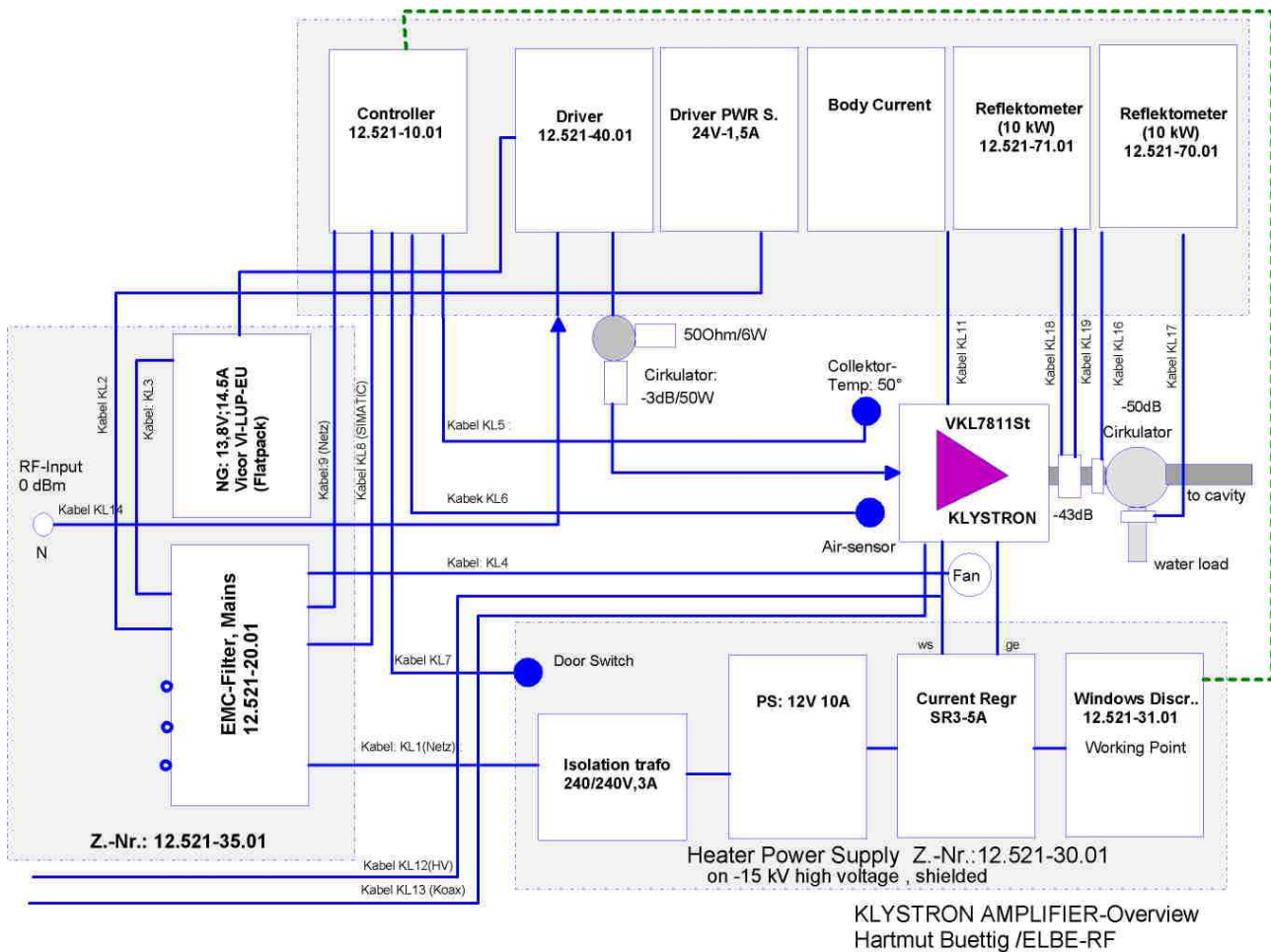
Fig. 5: *Block Diagram of the 10 kW Klystron Amplifier.*

24

Pulsed RF System for the ELBE Superconducting Accelerator

A. Büchner[1], F. Gabriel[1], H. Büttig, U. Lehnert, P. Michel, Ch. Schneider, R. Schurig

To increase the versatility of ELBE the RF system was modified to operate not only in cw mode but in pulsed mode too. With a pulsed mode RF system an easy in-situ conditioning of cavities and coupler windows is possible. So the system was designed for 4 operating modes:

- CW mode
- pulsed mode
- conditioning mode
- manual test mode.

For simplification the manual test mode will be omitted in the following. To use this modes the RF system, the macro-pulser and the control system software were changed.

Principle of operation for pulsed mode

The block diagram of the modified RF system is shown in Figure 1. The added parts in the controller are shown in green colour.

It is necessary to switch the RF on before the beam is switched on. The macropulser has to deliver an extra pulse which starts before the beam macropulse to give the RF system enough time to settle. With the beginning of this pulse a fixed amount of RF power (determined by the open loop gradient setting) is sent to the cavity and the system works open loop. When the gradient in the cavity gets near his final value (determined by the closed loop gradient setting) the control voltage in the amplitude loop comes into the working range of the loop. This is detected by a trigger which closes the loop. At the end of the macropulse the RF is turned off again.

The design bandwidth for the ELBE system is 114 Hz so a settling time of roughly 15 ms is needed to guarantee settling. The maximum klystron power of 10 kW could be used till settling. The minimum macropulser period is 40 ms given by the camera synchronisation for the beam diagnostics.
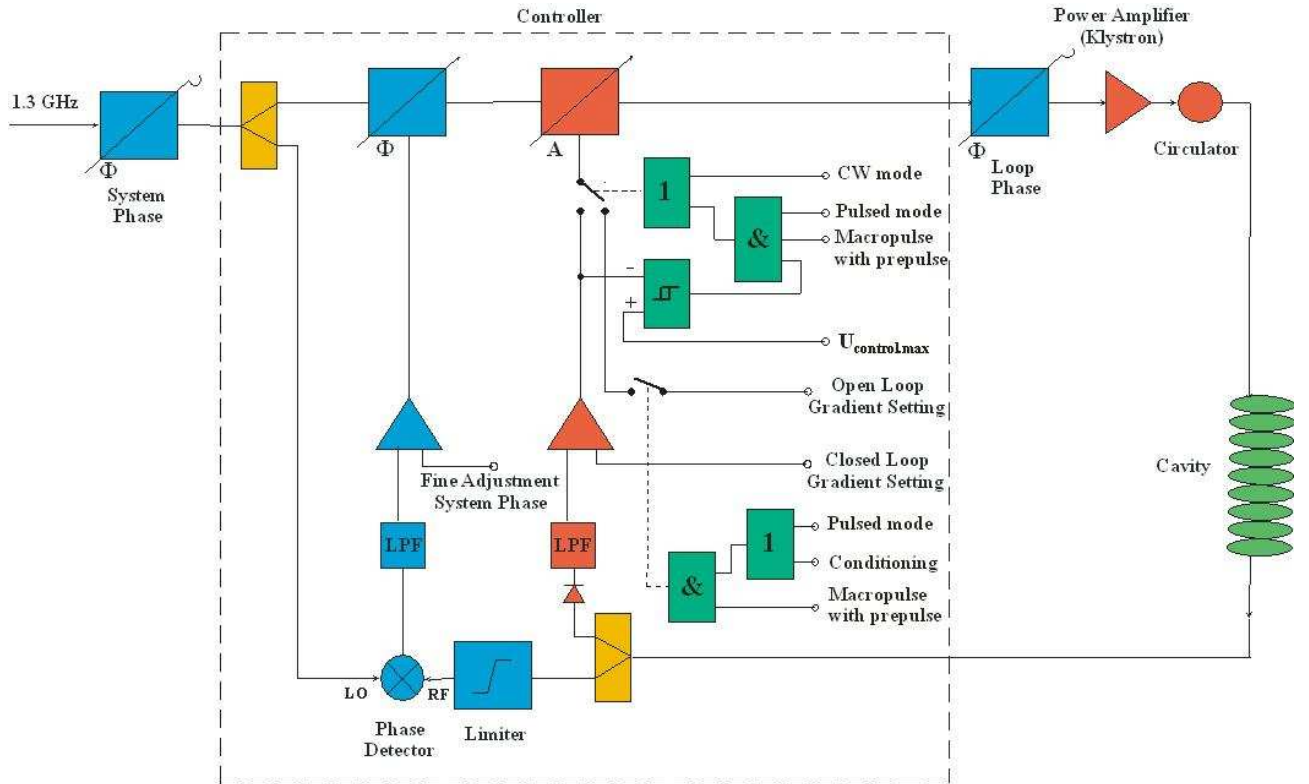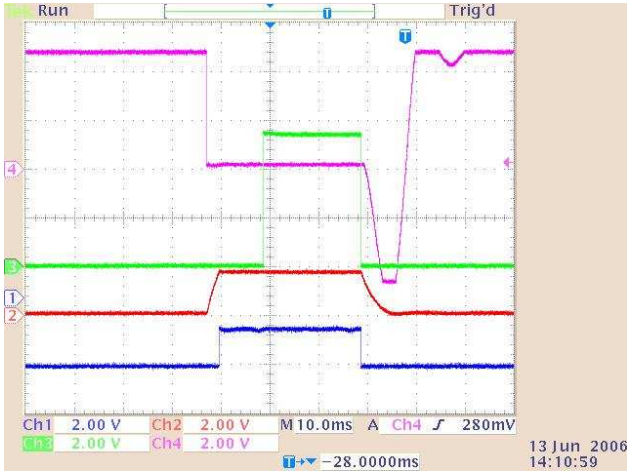

Fig. 1: *Block diagram of the modified RF system.*

Fig. 2: *Signals in the control loop:*
Blue: amplitude control signal
Red: measured gradient
Green: beam macropulse
Pink: measured phase signal.

Principle of operation for conditioning mode

In this case the RF system operates all time open loop. For ease the macropulse with prepulse is used for conditioning with roughly 20 ms duration and 280 ms period. After every 2 minutes the RF power is slightly increased by the control system till the maximum value of 10 kW when no interlocks occur. The control system checks for light, vacuum and temperature interlocks at the windows. If an interlock occurs the system continues conditioning after the interlock with the same power until no events are observed for 2 minutes.

In case of windows conditioning the cavity is completely detuned by the control system. So almost no gradient develops in the cavity and the power system works all time with full reflection.

In case of cavity conditioning the operator has to tune the cavity by hand to the maximum gradient. Because of the nonlinearity caused by Lorentz force detuning this gets a delicate task at high gradients.

Although the windows and the couplers are conditioned before they are installed an additional in-situ check is useful because it is inevitable to contact them with air during assembling.

Results

Cavity processing is possible till 15 MV/m. This is mainly limited by the klystron power. For this gradient the effect of Lorentz force detuning comes in the range of 2 times the bandwidth. Operation at these gradients requires a very stable helium pressure and tuning becomes more difficult. Till now the cavities were operated in cw with beam at 10 MV/m maximum. In pulsed mode stable accelerator operation is possible with 14 MV/m for the cavities. No significant increase of the beam energy spread was observed.

A Pulsed-RF High-Power Processing Effect
of Superconducting Niobium Cavities
Observed at the ELBE Accelerator

A. Büchner[1], H. Büttig, F. Gabriel[1], U. Lehnert, P. Michel, Ch. Schneider, R. Schurig

Introduction

The ELBE accelerator utilizes two cryomodules each containing two 9-cell TESLA cavities. Though the design and production tests show that at least a 15 MV/m accelerating gradient should be reached we were never able to drive any of our cavities much beyond 10 MV/m. This limit is given by the onset of field emission which leads to an excessive heat load and instability introduced into the helium supply system.

Heat Load Measurements

The helium supply system of the ELBE cryostats is designed to minimize pressure fluctuations in the helium vessel. This is necessary because the helium pressure influences the tuning of the accelerator cavities. Any fluctuations lead to changes in the resonance frequency of the cavities. The low-level RF system cannot fully compensate for the resulting phase jitter of the accelerating field which leads to energy fluctuations of the accelerated beam.

A constant pressure can best be realized with a constant gas flow. Therefore, we keep the fill valve which determines the flow of liquid helium into the cryostat at a constant setting slightly above the expected consumption. The extra helium fed into the cryostat is evaporated by a heater which is controlled to keep the helium level constant. Rapid changes of the set accelerating gradient are compensated with a feed-forward control acting on the heater.

This control scheme now easily allows a readout of the heat load introduced from the RF field. It is is just the difference between the heater power with the accelerator cavity at gradient or off. The feed-forward control can be switched off for that purpose. This type of measurement of the helium consumption is stable and reproducible as the whole liquefier remains at a steady operation point and only the load is distributed between the heater and the RF losses.

Cavity Behaviour in CW Operation

In addition to the heat load measured by the helium consumption we measure the radiation dose rate generated by the accelerator cavities. Typically, we use the room monitor for this measurement. Therefore, in most cases the dose rate cannot be quantitativly compared between different accelerator modules due to the differing geometry. For any single cavity it is, however, reproducible and yields significant insight in the origin of the RF losses.
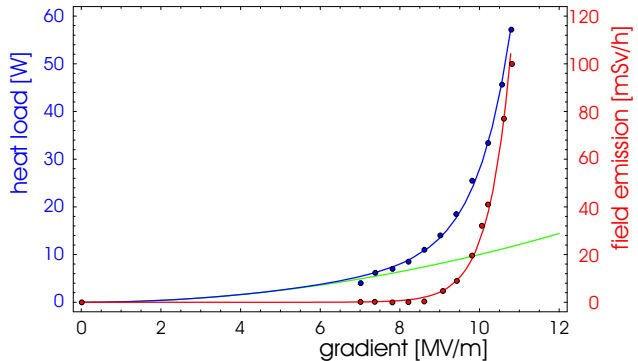

Fig. 1: *Typical data for heat load and field emission generated by our cavities in CW operation. The green line shows the ohmic RF losses, the blue line is a fitted qudratic-plus-exponential model. The field emission is well fitted by a single exponential.*

One typical measurement is shown in Fig. 1. From the residual resistance of the superconducting niobium cavities results a heat load that depends quadratically on the accelerating gradient. But this relation holds for low gradients, only. At a certain level of the accelerating gradient we observe the onset of field emission, seen both in the radiation dose rate as in the helium consumption. The heat load and the instability of the field emission limit the gradients that can be used in CW operation to 10 MV/m, typically.

Pulsed-RF Operation

To overcome the otherwise stringent gradient limit for special experiments we have tried to operate our accelerator modules with pulsed RF. One example is shown in Fig. 2 below. The RF feed is switched on with a fixed forward power approximately 12 ms before the actual beam pulse starts. Depending on the cavity tuning it takes a few miliseconds until the gradient reaches the preset value. At this time the control loop kicks in and stabilizes the RF field at the desired amplitude and phase. For a detailed description see [1].

With this mode of operation we were able to drive our cavities up to 15 MV/m. The gradient is mainly limited by the Lorentz force detuning. The mechanical tuner is set to be within the resonance bandwidth at the final gradient which is required for the control loop to work properly. However, the cavities are far-off detuned at the beginning of the RF pulse, so, the coupling of the feed RF to the cavities is very weak and the field amplitude rises only slowly.

---

[1] FZD, FWF
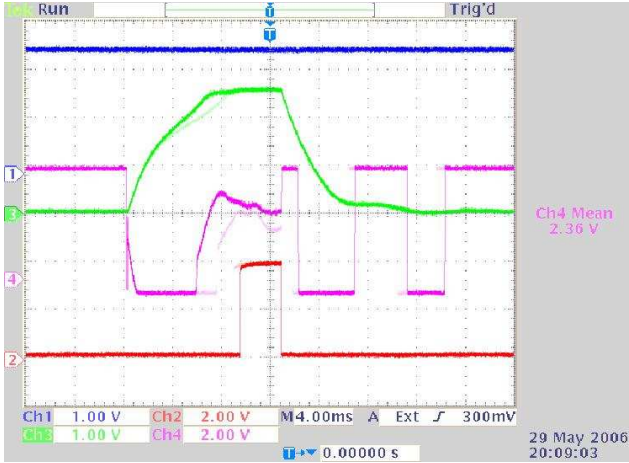
Fig. 2: *Pulsed-RF operation of an accelerator cavity. The green trace shows the gradient, the red one is the loop-lock signal and the pink trace shows the signal of the phase control loop.*

A first beam test of this pulsed-mode operation was run in May, 2006. In this test the first accelerator module was still operated in CW. Both cavities of the second module were, however, operated in pulsed mode. It showed that both cavities would stabily hold 15 MV/m with the field emission an helium consumption reduced by the duty cycle. The beam quality did not show any degradations with respect to the CW operation that would indicate a reduced stability of this operating mode.

RF-Processing Effects

During the tests with the pulsed-RF system a reduction of the radiation dose rate around the cryomodules was observed. We attribute this behaviour to an RF-processing of the cavity surface which burns off field emitters. This observation is in contrast to previous tests which did not show major training effects for cavities operated for several hours at the maximum gradient they would hold in CW operation.

To verify this observation both cavities of the first ELBE cryomodule were trained with pulsed high gradients up to 15 MV/m. This gradient is about 40%

above the maximum that could be reached in CW operation. The result was a significant reduction in field emission as shown in Fig. 3. This now allows an operation of both cavities at gradients that are about 2 MV/m higher than previously reached with the same heat load (see Fig. 4) and stability. Later tests showed a slight degradation of the effect with the major part of the gradient increase still usable.
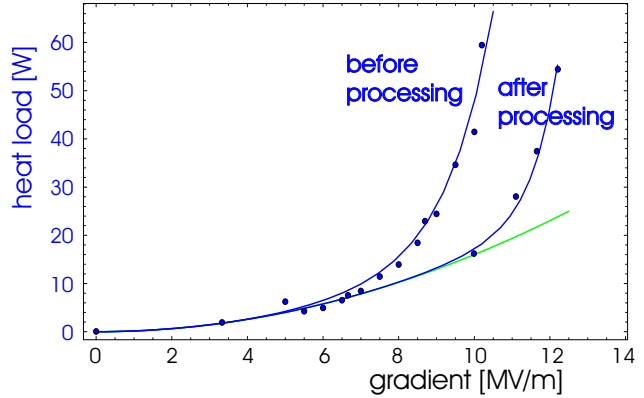
Fig. 3: *After a high-gradient pulsed-RF training run the onset of field emission occurs at much higher gradients.*
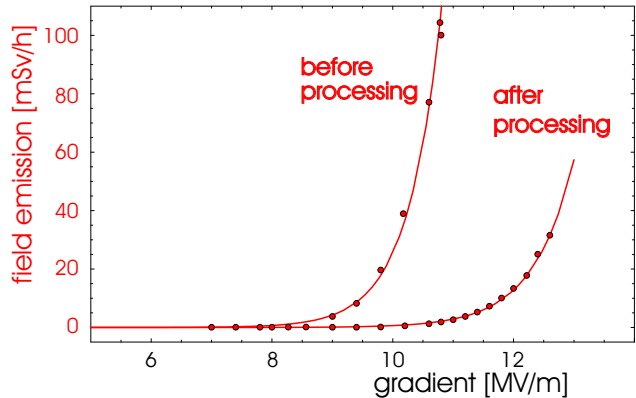
Fig. 4: *After a trining run with pulsed RF the helium consumption is considerably reduced in CW operation as well.*

[1] A. Büchner, EPAC'06, Edinburgh, June 2006, MOPCH151.

# A Resonant Ring for High-Power Tests of RF Couplers and Waveguide Windows

H. Büttig, A. Büchner, M. Krätzig

Motivation

Based on the experience at DESY a coupler test stand was developed and built at ELBE in 1999. All RF couplers and waveguide windows used at ELBE and for the current SRF-gun project at FZD were conditioned before assembling. The maximum available RF power delivered by the klystron VKL7811 (CPI) is 8.5 kW (at 1dB saturation). A sliding short at the end of the waveguide allows tests at all phases. Thus the maximum power in standing wave mode is 34 kW. Within the framework of the EUROFEL project and for the present SRF-Gun project at FZD higher power limits for coupler components are required. A resonant ring for 1.3 GHz and a power up to 100 kW has been designed, build and put into operation by Marko Krätzig in the context of his diploma thesis.

Genaral layout

A resonant ring, or travelling wave resonator, is a closed waveguide loop which can amplify apparent power through the coupling of waves at its input. The length of the ring must be equal to an integer number of guide wavelengths (32 cm for 1.3 GHz and WR650 waveguide) to ensure resonance. Figure 1 shows the basic resonant ring. At resonance the waves coupled to the ring through the directional coupler add constructively. This generates a power gain in the ring. The resonance can be tuned using a 360 deg waveguide phase shifter. In the straight section for insertion devices waveguide windows or other components, like rf-couplers can be inserted. The phase shifter ensures resonance.
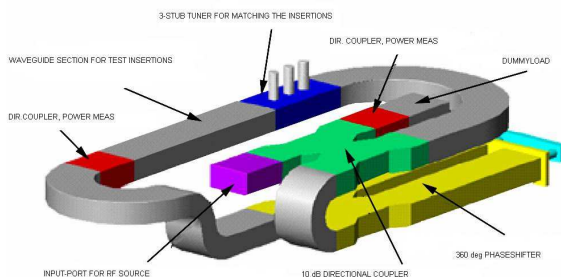
Fig. 1: *Basic Resonant Ring (CAD). The RF-power is fed through the input-port to the 10dB-directional coupler and further to the dummy load. The -10dB section of the coupler is part of the resonant ring. To save space, a folded design was used.*

Simulation

The behaviour of the ring was simulated with CST-Microwave Studio. As an example the electric field strength component in this travelling wave resonator is shown in Fig. 2.
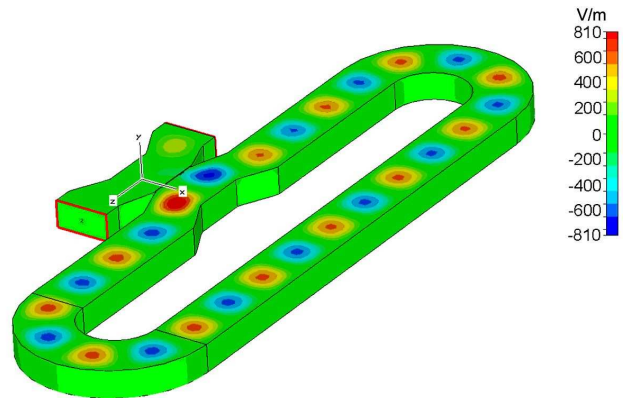
Fig. 2: *Magnitude of the Electric Field in the Resonant Ring.*

The achievable gain depends on the directivity of the directional coupler used (Fig. 3) and the sum of the losses in the ring (Fig. 4).
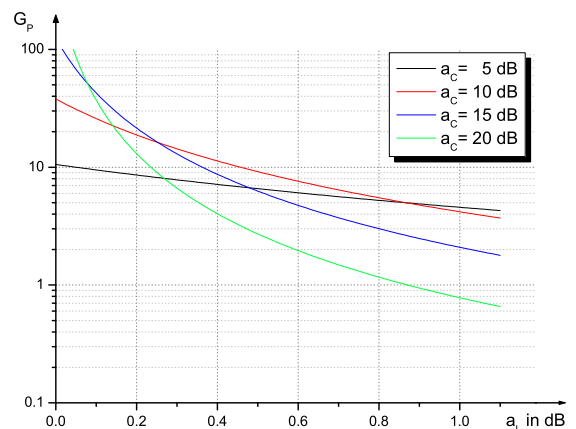
Fig. 3: *Achievable Power-gain of the ring for different directional couplers (calculated).*
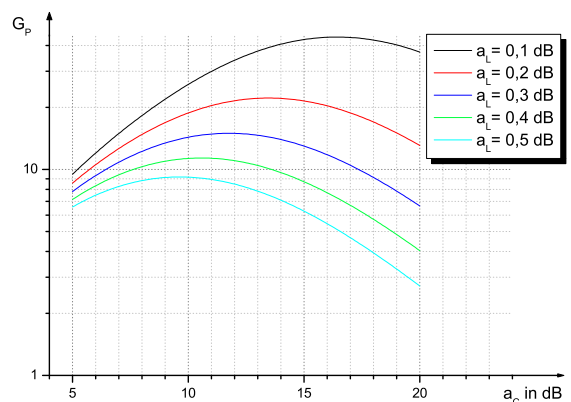
Fig. 4: *Achievable Power-gain of the ring, depending on the sum of the attenuation in the ring The ring itself behaves like a resonator (Fig. 5).*

Fig. 5: *Resonance curve (measured) of the resonant ring.*

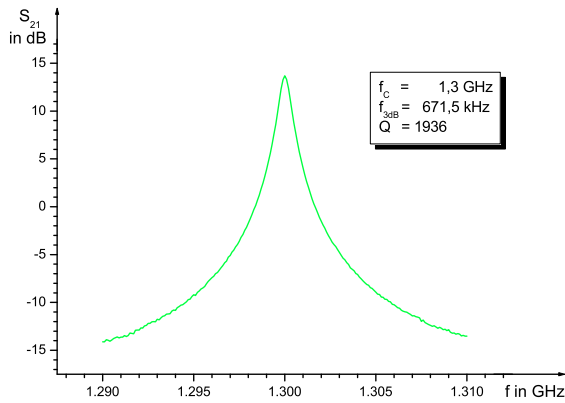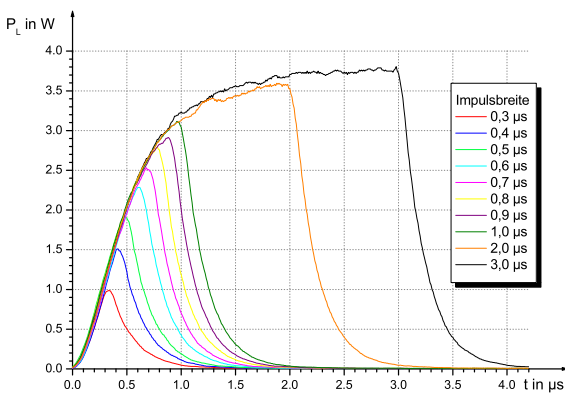The resonance can be studied using pulsed RF. One can see how the resonant ring get filled (Fig. 6). A 10 kW klystron amplifier (1.3 GHz klystron VKL7811St (CPI)) was used to operate the resonant ring. The measured RF-power in the ring is shown in Fig. 7.

Fig. 6: *Filling of the ring using pulsed RF-power.*
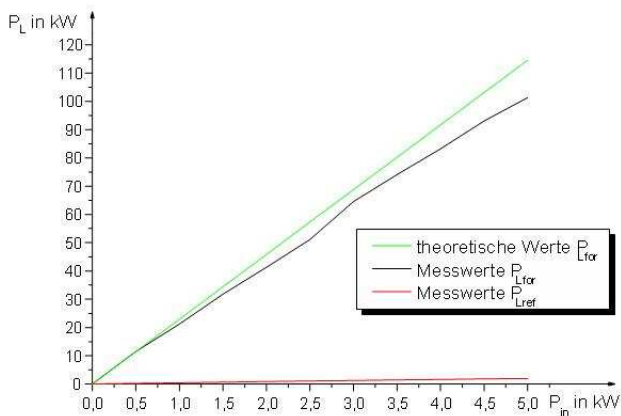
Fig. 7: *Power characteristics of the resonant ring black: forward power, red: reverse power.*

Setup

The resonant ring is pictured in Fig. 8. This setup was used to test WR650 waveguide windows. The polyethylene WG-windows (Rexolithe) were tested up to 100 kW.
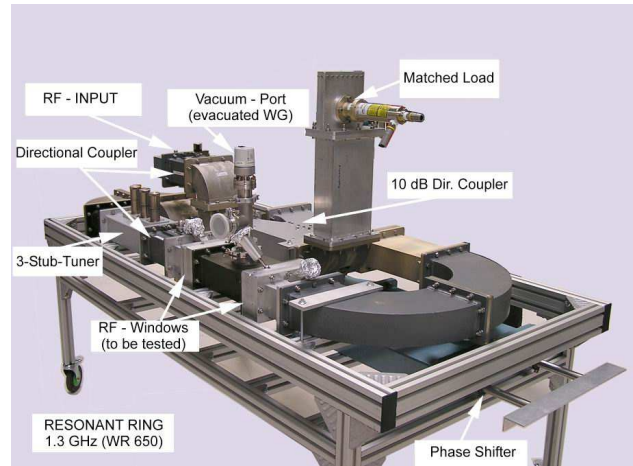
Fig. 8: *Setup of the resonant ring for 1.3 GHz.*

A first test of a ceramic window has shown a dramatic temperature raise because of its high loss factor (Fig. 9).
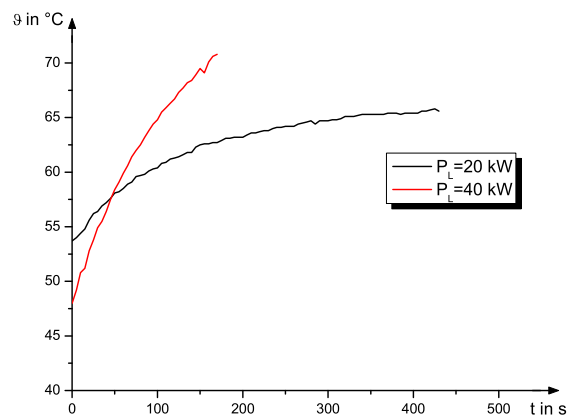
Fig. 9: *Temperature on the surface of a ceramic waveguide window being tested in the resonant ring.*

[1] Krätzig, M.: „Aufbau und Optimierung eines resonanten Ringes aus Hohlleiterbau-elementen", Diplomarbeit, HTW-Dresden, Oktober 2005

[2] Veshcherevich, V.: Resonant ring for high power tests of RF couplers. Cornell University, Ithaca-NY, USA, ERL03

[3] Büchner, A.; Büttig. H.; Stephan, J.: RF Window Diagnoses and Training, HPC2002, Workshop on High Power Couplers, J.-Lab., Newport News,USA, 2002.

Simple Universal Wide Range Waveguide to Coax Transition

G. Staats

Abstract

For application on TESLA cell cavities used for beam acceleration coaxial input couplers needed. These couplers have to transfer high RF power from a feeding waveguide to a cavity through a vacuum window. For ensuring high operating stability of an accelerator it is advantageous to test such couplers before using it. Therefore coupler test stands are needed.

In contrast to the later using of the couplers in the coupler test stand a transition from a rectangular standard waveguide WR650 to the coaxial line of the coupler are requested. This is usually of course not a design problem, also for 100kW of rms input power. But in conjunction with the wide spectrum of coupler tip lengths needed for different coupling factors in the later application of the couplers the design of the transition is not easy, especially for a simple robust solution.

Design

The design is based on a rectangular standard waveguide WR650 with a circular mounting flange on the top for the coaxial coupler and a rectangular waveguide flange for the output. For the given couplers it has been found that the maximum possible length of the coupler tip inside the waveguide should be used, therefore the circular flange on the input is an integral part oft the waveguide top.
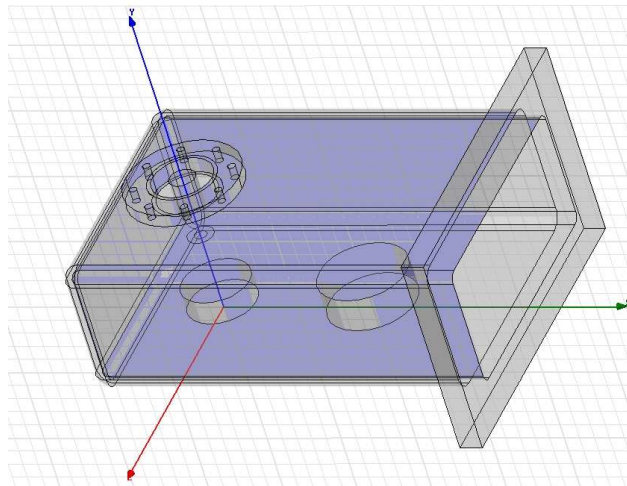

Fig. 1: *Design of the coax to waveguide transition.*

Furthermore it must be mentioned that no variations of the tip of the coupler are allowed, for testing the coupler the same tips should be used as in the later application with the TESLA cavity. This is the main problem of the design. Together with the length variations from 30.2mm up to 43.2mm this lead to the reported design which are shown in Fig. 1 for 36.2mm

coupler length.

By variation of diameter, high and position of the cylinders this design was capable to adapt all the mentioned tip lengths of the different couplers which should be tested. For calculating the S-parameters and also for determine the optimum parameters HFSS was used.
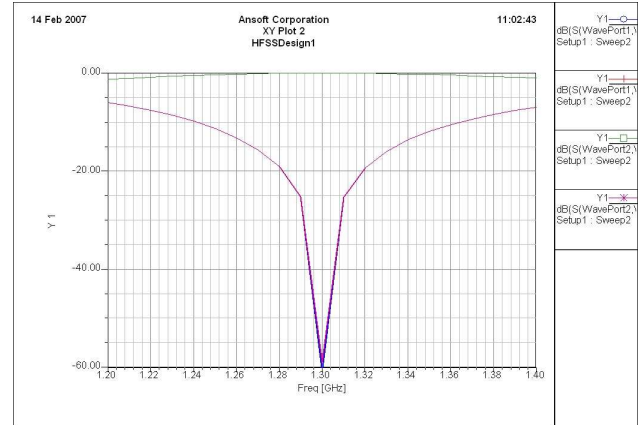
Fig. 2: *Transmission and reflection of the design for 33.2mm tip at 1.3GHz (RL=61.05dB, IL=0.0030dB).*

Fig. 2 shows the transmission and reflection characteristic of the design for 33.2mm tip length. By optimization it was no problem to reach 50dB return loss even for the minimum (30.2mm) and also for the maximum (36.2mm) tip length used at FZD. Also with the 43.2mm tip length which was used at CCLRC in maximum it was possible to reach 30dB return loss. Of course these values are pure theoretically, as a statistic analysis with 1% uniform distribution of design parameters has been shown. Considering this values of about 30dB return loss are more realistic.
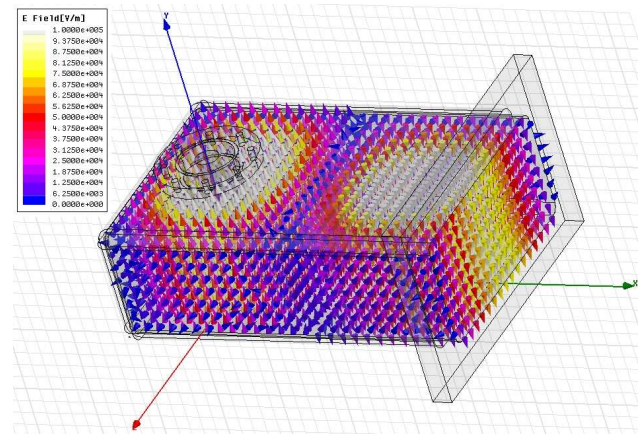
Fig. 3: *Electric field distribution of the design.*

Fig. 3 shows the electric field distribution inside the rectangular waveguide for 100kW rms input power. The maximum electric field strength is in the range of 400kV/m. For better seeing in Fig. 4 the electric

field strength in the near of the tip is shown. This is the most critical area.
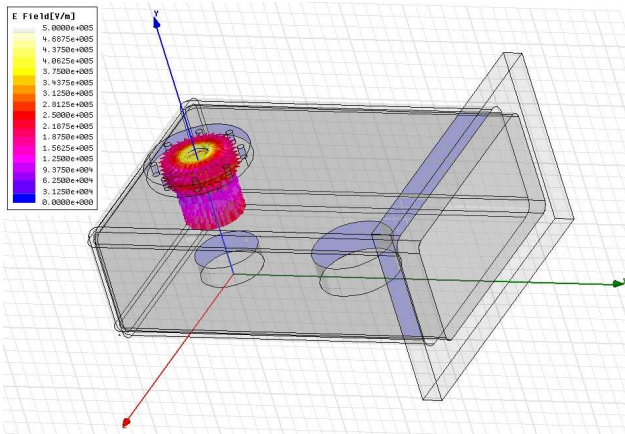
Fig. 4: *Electric field distribution at the tip of the coaxial input coupler.*

Also interesting is the magnitude and the vector of the electric current density inside the rectangular waveguide, pictured in Fig. 5.
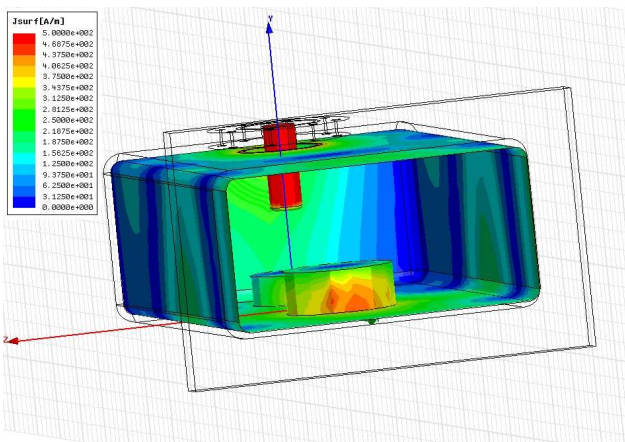
Fig. 5: *Magnitude of the electric surface current density inside the rectangular waveguide.*

In Fig. 6, 7 and 8 the results of the optimization process for the main tip lengths of 30.2mm, 36.2mm and 43.2mm are shown. In practically design of the waveguide transition these values for the different tip length are easy reached by changing the two cylinders inside the waveguide. No further mechanical parts are needed, which is advantageous in respect to the high electric current density inside the waveguide and also to the different vacuum in- and outside the transition.

Conclusions

An simple, robust and easy to adapt coaxial to waveguide transition for using on coupler test stands has been designed.
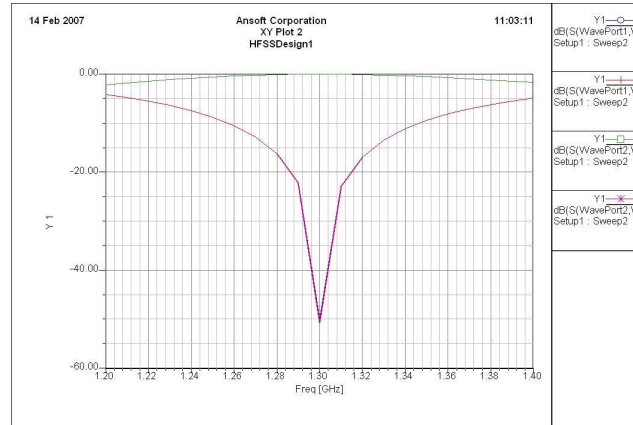
Fig. 6: *Transmission and reflection of the design for 30.2mm tip at 1.3GHz (RL=50.32dB, IL=0.0036dB).*
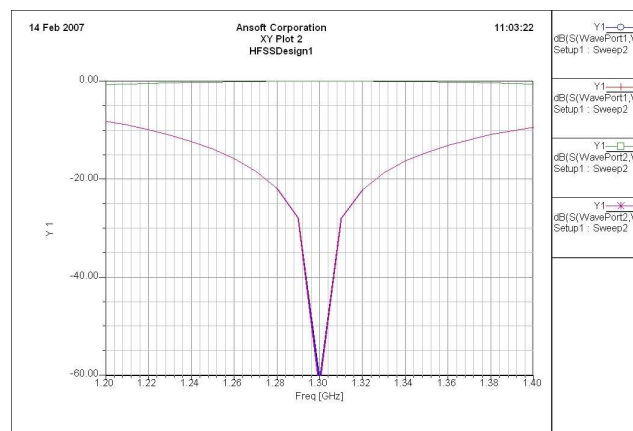
Fig. 7: *Transmission and reflection of the design for 36.2mm tip at 1.3GHz (RL=60.72dB, IL=0.0027dB).*
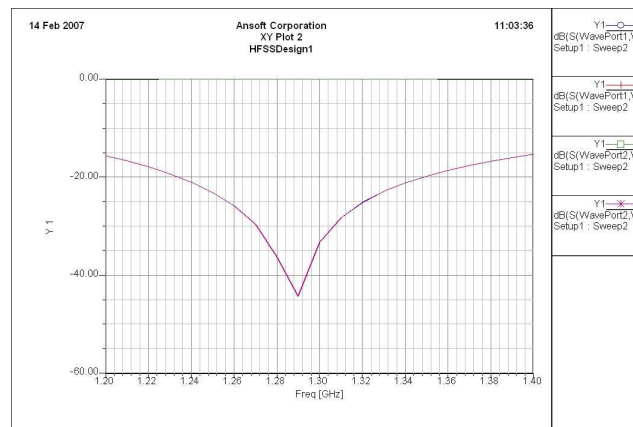
Fig. 8: *Transmission and reflection of the design for 43.2mm tip at 1.3GHz (RL=32.24dB, IL=0.0044dB).*

[1] C. Balanis: "Antenna Theory, Analysis and Design", pp.352-388, 2nd ed., John Wiley and Sons, New York, 1997.

[2] G. L. Matthaei, L. Young, E.M.T. Jones: "Microwave Filters, Impedance-Matching Networks and Coupling Structures", pp. 255-353, Artech House, Norwood, 1980.

Zweikanaliger HF-Leistungsmesser für gepulste HF-Signale

H. Büttig, P. Piede

Neue Controller für die Amplituden- und Phasen-regelung erlauben an ELBE neben CW-Betrieb die Tastung der HF-Leistung, um bei der zur Verfügung stehenden Heliumleistung die Cavities mit höheren Beschleunigungsgradienten betreiben zu können. Die vorgestellte universelle Baugruppe entstand im Rahmen einer Diplomarbeit /[1].

Technische Daten

Aus-/ Eingänge:

- 2 HF-Leistungseingänge (Pi / Pr)
- Triggersignaleingang (optisch/ TTL-Pegel)
- Reset

- 2 Analogausgänge (0…10V)
- 2 Digitalausgänge (Schwellwerttrigger)
- Messbereichsanzeige extern umschaltbar (100W, 1kW, 10kW)

Kenndaten:

- Versorgungsspannung: 24V
- Frequenz : 1,3 GHz
- Leistungsbereich: -20 dBm … +10 dBm
- Max. Abtastfrequenz: 1,5 kHz
- Min. Pulsbreite: 60μs
- Messfehler 0,5% bezogen auf +10dBm Eingangspegel
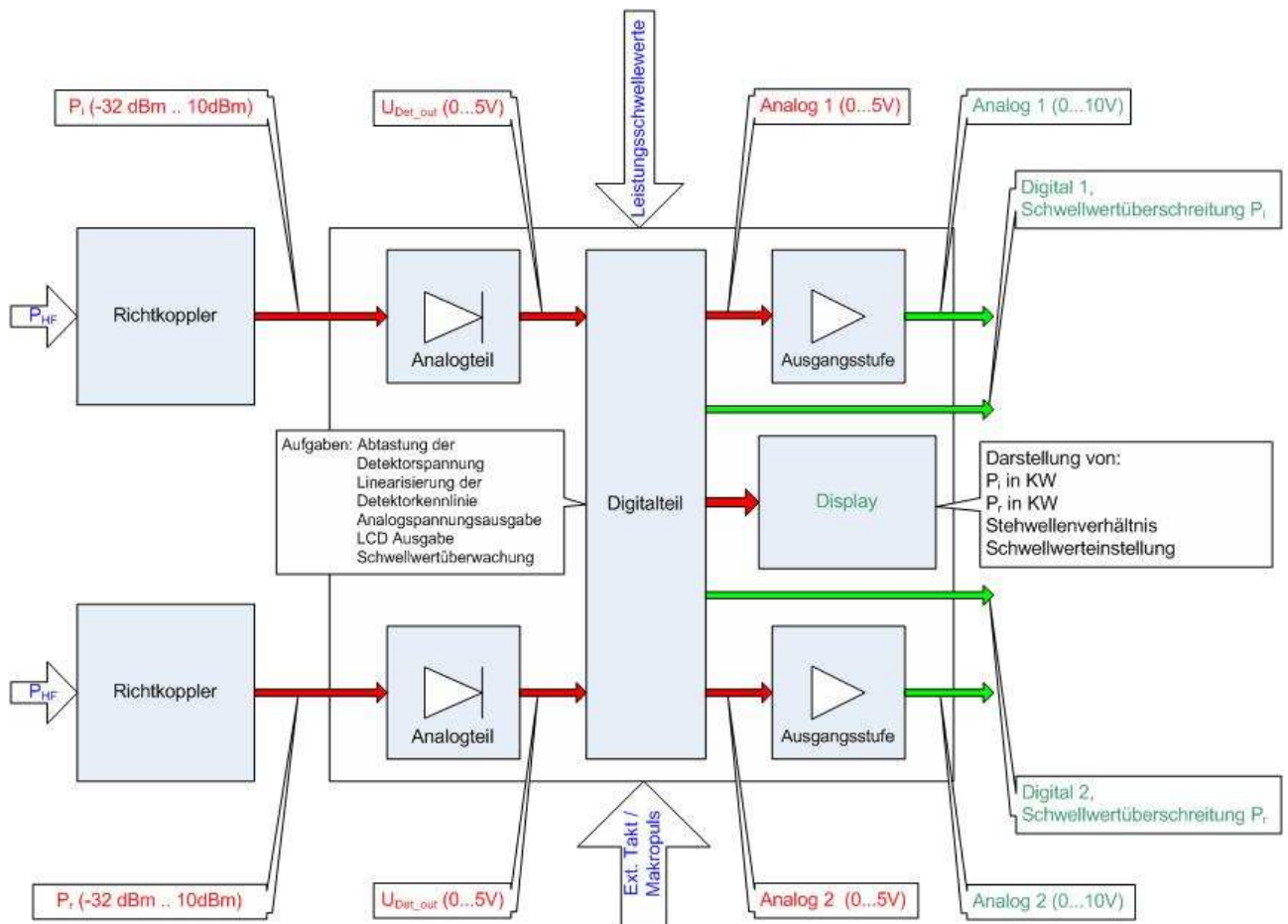
Fig. 1: *Blockschaltbild mit Pegelplan.*

Hardware

Die eingesetzten Detektoren LTC1055 (Linear Technology) geben bei +10dBm am Eingang eine Ausgangsspannung von +5V ab. Die Demodulationsbandbreite ist auf 10 MHz mittels Tiefpassfiltern begrenzt. Die beiden Detektorsignale werden je einem ADC-Eingang des Prozessors (ATMEGA 32-12) zugeführt, der nach intern folgende Funktionen realisiert:

- Signalverarbeitung mit ATmega 32 Controller (Atmel)
- ADC
- Sampling,

- SWR - Berechnung,
- Schwellwertüberwachung,
- Leistungsbereichsumschaltung
- Kommunikation mit dem Displaycontroller
- PWM-Signalerzeugung zur DAC.
- Analogsignalausgänge zur SPS (Simatic) mittels DAC,
- Digitalausgänge (Optokoppler) für Leistungsschwellwerte
- Externe Synchronisierung der Baugruppe durch ELBE – Makropuls,

[1] Ph. Piede: Entwicklung eines zweikanaligen Leistungsmessers für gepulste HF-Signale mit Digitalanzeige, Diplomarbeit HTW-Dresden 2006

Fig. 3: *Gerätefoto (Baugruppeneinschub 3HE).*
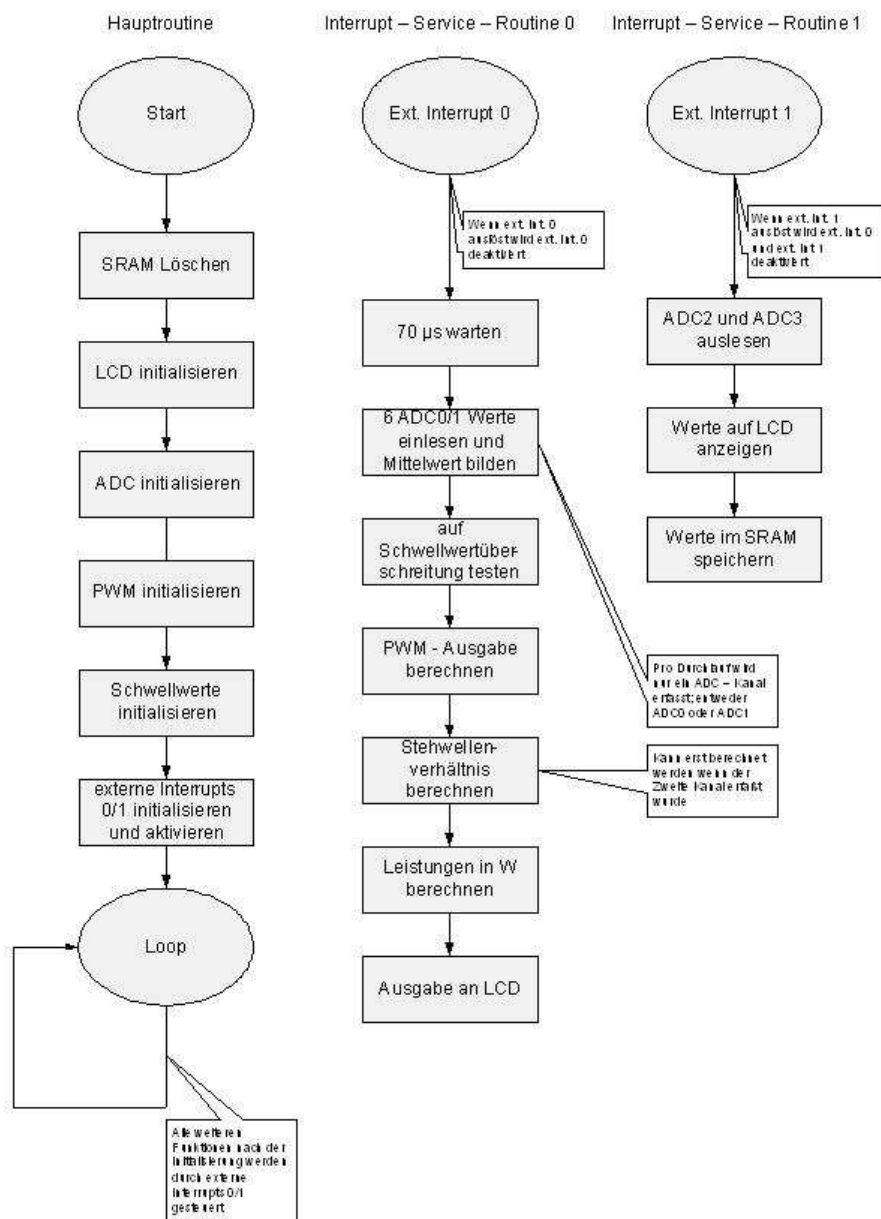
Fig. 2: *Programmablaufplan.*

Microphonics Measurements at the ELBE Accelerator

G. Staats

Introduction

Microphonics measurements at the ELBE accelerator were already made in 2002 and published in [1]. The widespread use of the Rossendorf accelerator module which is manufactured in license by ACCEL and the recent development of energy recovery Linacs created new interest in microphonics measurements. With the further completion of the ELBE accelerator significant changes were made. In 2002 only one cryomodule with 2 cavities was in operation. The measurements in 2002 were done with the second cavity. Now we did qualitative measurements for all 4 cavities.

Measurements of phase controller signal

During the measurements the RF feedback signal of the phase lock loop was recorded with a PXI-6115 analog to digital converter board in a PXI-1042 main frame. Using a LabView application it was possible to record the data in the time domain or to do a real time transform of the data in the frequency domain (power spectrum, power spectral density, integrated power spectral density and automatic peak search). For the later evaluating of the data however we prefer to record the signal in time domain for longer duration to make the fourier transformation for lower frequencies possible.

Measurements are taken in the time domain for about 10 minutes and thereafter transformed in the frequency domain. The Sampling rate was chosen to 20 kSample/s equal to an upper frequency limit of 10 kHz, the amplitude resolution of the PXI-6115 card has been chosen to 12 Bit. The phase controller signal was in the range of 0...5 V.

Furthermore it was found a strong dependency for the RMS- and peak-values of the microphonic signals for all 4 cavities at gradients above 8.5 MV/m, caused by the heavier cooling load of the helium machine due the higher losses in the cavities, as shown in Fig. 1.

The already known difference in microphonics properties between the 2 modules has been found also in this measurements, the microphonics of module 1 with cavity 1/2 is much lower than the microphonics of module 2 with cavity 3/4, as shown in Fig. 2.

By peak search the resonances in Tab. 1 are identified. It has been found that cavity 1/2 and also cavity 3/4 has very similar resonances. Furthermore the resonances agree not with the frequencies given in [2]. Therefore the assumption is, that the measurements have shown the resonances of the modules 1/2 and not of the cavities.

Measurements of body sound

To find the sources of microphonics measurements with a body sound sensor (geophon, sensitivity was about 30 mV/mm/s) are carried out. For recording the data the already described LabView application was used again. In Fig. 3 some of the results are shown. Very strong sources of microphonics are the He-compressors, cooling water pumps and also the air-condition.

(a) RMS (b) Peak
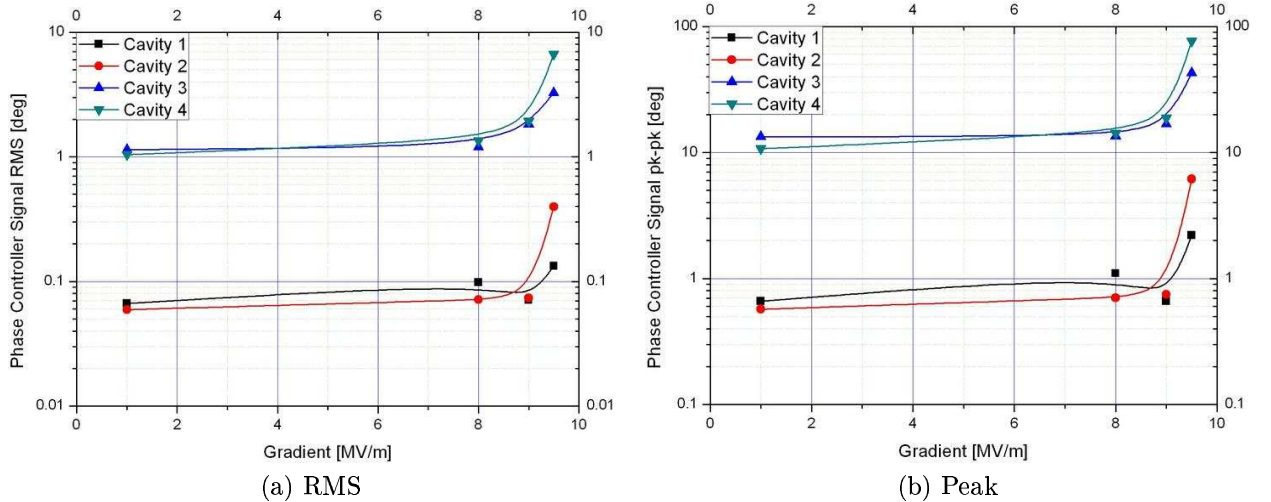
Fig. 1: *Variation of RMS- and Peak-values of phase controller signal with the gradient for all cavities.*
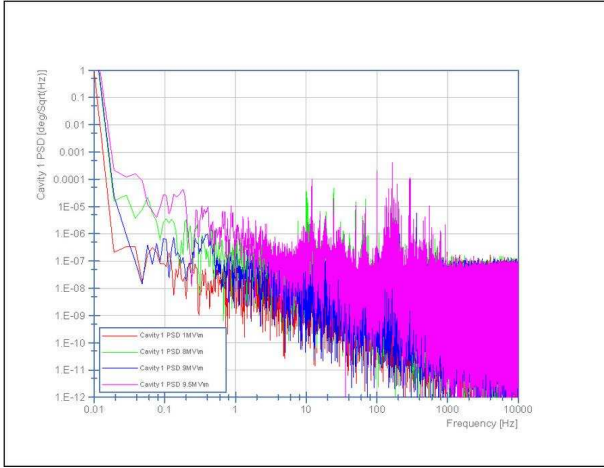
(a) Cavity 1.
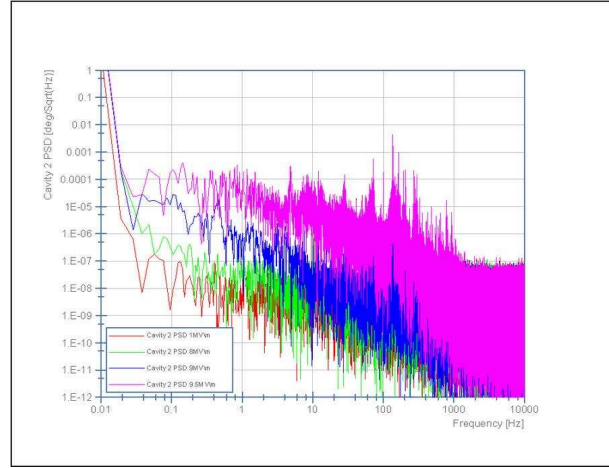
(b) Cavity 2.
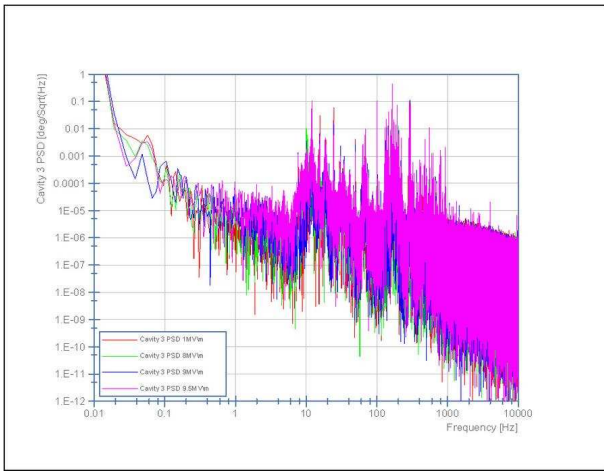
(c) Cavity 3.
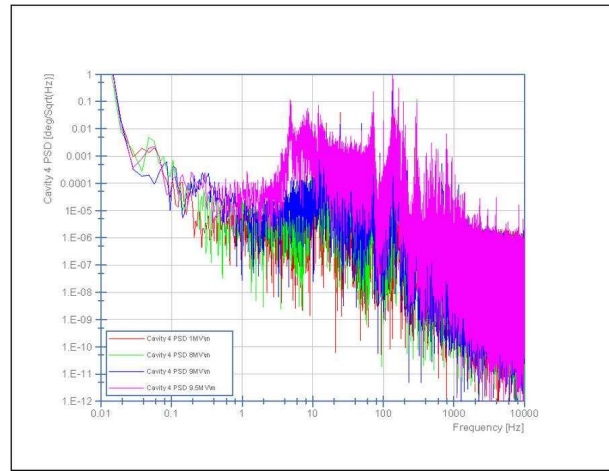
(d) Cavity 4.

Fig. 2: *Variation of power spectral density of phase controller signal for cavities 1 to 4 at gradients of 1, 8, 9 and 9.5 MV/m.*

Conclusions

Cavity 1/2 and also cavity 3/4 have very similar peaks. The peaks are not corresponding to calculated values for the self resonances of the cavities [2] without housing. In Module 2 a significant component at 7.7 Hz could be observed. It would be useful to reduce this to the levels of module 1 and to reduce the hum components at 50 and 100 Hz. Module 1 has shown a much lower microphonic signal than module 2. The microphonic level of both modules increases strong a gradients above 8.5 MV/m.

Tab. 1: *Resonances of Cavity 1 to 4.*

Number	Cavity 1	Cavity 2	Cavity 3	Cavity 4
1	24.6	24.4	7.7	7.0
2	69.5	69.6	49.0	49.2
3	74.2	75.6	73.3	73.2
4	99.9	100.1	259.7	259.7
5	132.2	132.2	292.4	292.0
6	164.2	164.2	–	–
7	169.6	169.2	–	–
8	193.5	193.5	–	–
9	300.1	300.1	–	–

[1] Büchner, A.: Noise Measurements at the RF System of the ELBE, Superconducting Accelerator, EPAC 2002, Paris, June 2002

[2] Schilcher, T.: Vector Sum Control of Pulsed Accelerating Fields in Lorentz Force Detuned Superconducting Cavities, DESY, Hamburg, August 1998 (98-20)
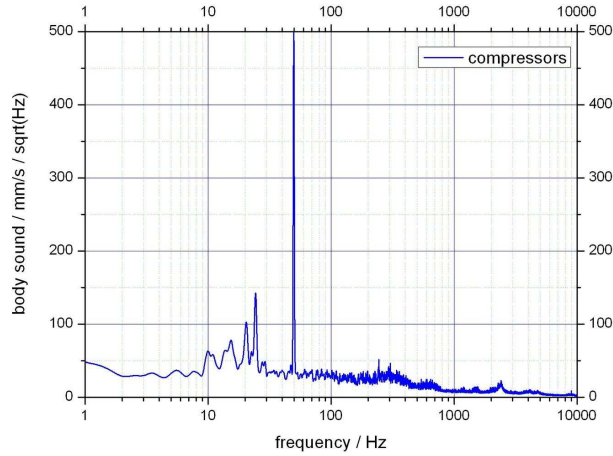
(a) Compressors.
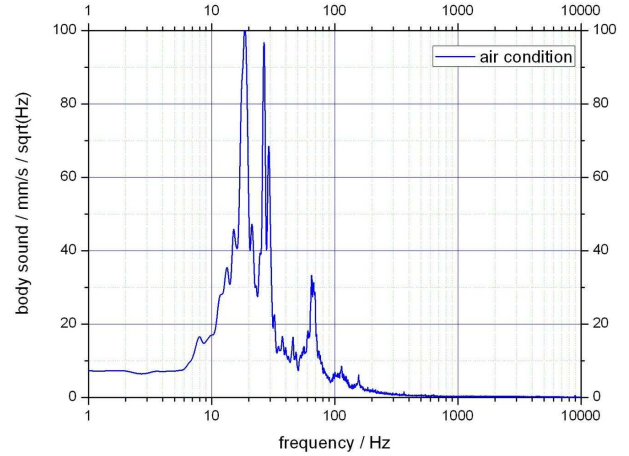
(b) Air Condition.
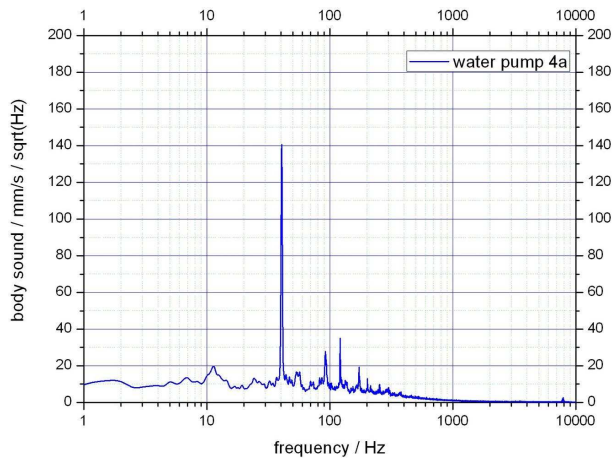
(c) Cooling water pump 4a.
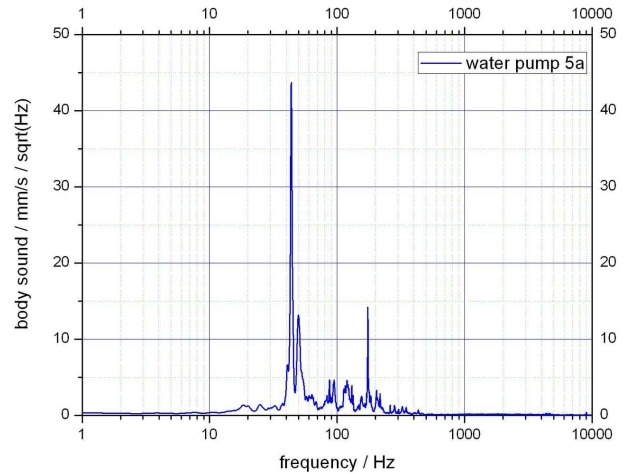
(d) Cooling water pump 5a.

Fig. 3: *Some power density spectra of body sound sources at ELBE.*

Control of BPM Data Acquisition at Low Micro-Pulse Rates

D. Pröhl, R. Schurig, P. Evtushenko

For the nondestructive measurement of the beam position, the accelerator ELBE is at several points equipped with $\lambda/4$ strip line Beam Position Monitors [1]. For signal processing they have an analog electronics which operates at the fundamental frequency of the accelerator (1.3 GHz) and a logarithmic detector [2]. The logarithmic detector has a bandwidth of about 10 MHz and conv$n$ (n=2, 4, 8, 16, 32, 64, 128, or 256). Due to the bandwidth of the RF to DC converter at small micro pulse rates the analog output signal of the analog BPM electronics is not a DC value as for micro pulse rates like 260, 26, or 13 MHz, but is a separated pulse for each single electron bunch from the gun. Therefore the analog electronics was equipped with a sample and hold amplifier [3], [4]. For the exact time alignment of the signals at the different BPM positions each BPM electronics board (contains for channels of one BPM) has a delay line for the compensation of the different times of arrival of the electron bunch. It was necessary to develop a synchronization electronics which makes it possible to adjust the switching time of the sample and hold circuit, the ADC clock phase, and the start of data acquisition with the timing of the electron bunches from the gun by computer control. The reference time is derived from the GUN clock, which is delivered from the output of the frequency divider situated in the electronics section of the gun. The GUN clock is a division of the 26 MHz oscillator, which is synchronized by the 13 MHz master oscillator of the accelerator. The overview of the general scheme of the electronics is shown in Fig. 1. The control of the delay and width of the trigger pulse (start of ADC

data acquisition), the division factor and the different phase shift for the ADC clock and the sample/hold signal for the analog electronics will be carried out via the digital interface of the PXI ADC modules by software. The adjustment can be done in steps of 76.9 ns (one period of the 13 MHz master clock). The frequency of ADC clock and sample/hold signal is in all cases 101.5825 kHz only in the case of a clock ratio 26 MHz/256 it has to switch down to 50.78125 kHz. The logic necessary for these functions was developed and is comprised in a field programmable gate array circuit (FPGA) in an electronics module, which is situated in the same crate as a number of the BPM analog electronics modules. There are two BPM synchronization modules each for one of the two PXI data acquisition complexes consisting of a crate with BPM electronics boards and an accompanying PXI crate with ADC boards. The adjustment of the parameters was then done by watching the BPM output signals, the sample/hold, and the ADC clock using a scope. The parameters are stored in the control software. In the result the BPMs deliver now the right beam position also at lower micro pulse rates then 13 MHz.

[1] P. Michel at el. Proceedings of EPAC 2002 Paris, 2002
[2] R. Schurig ,Wissenschaftlich- Technische Berichte, FZR-341, April 2002
[3] P. Evtushenko, R. Schurig, Proceedings of DIPAC 2003 Mainz, 2003
[4] P. Evtushenko, "Electron Beam Diagnostics at the ELBE Free Electron Laser", PhD thesis, presented at the Technical University Dresden, 2004
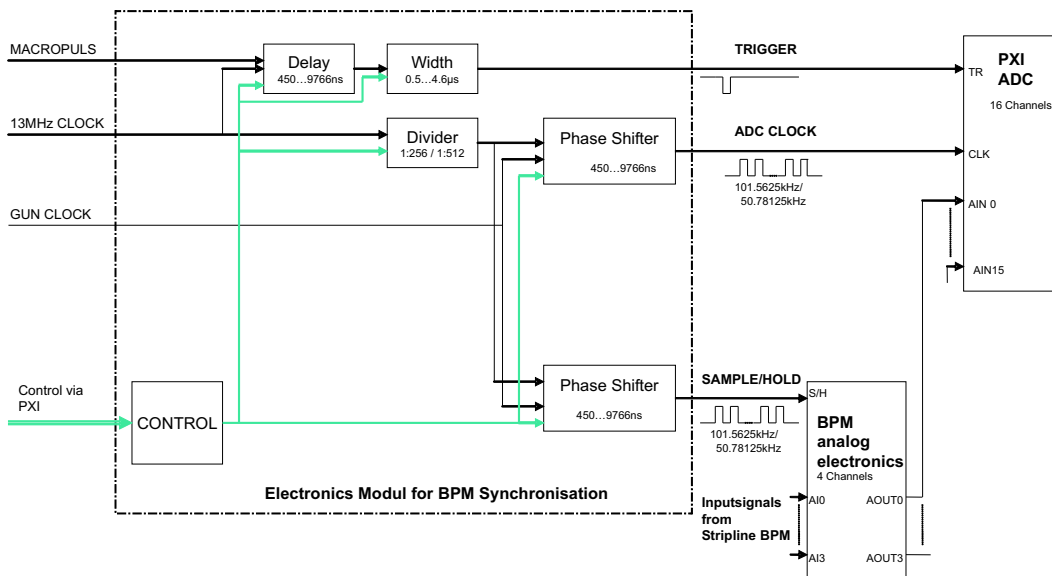
Fig. 1: *Scheme of BPM Synchronization.*

Wartungszustand der Beschleunigeranlage ELBE

M. Freitag

Die Wartung- und Instandhaltungsarbeiten an der Beschleunigeranlage ELBE werden möglichst parallel zu den Reinigungsarbeiten der Heliumanlage durchgeführt. Weiterhin besteht die Möglichkeit aller 4 Wochen Montags während der Frühschicht Wartungsarbeiten direkt am Beschleuniger durchzuführen. Die Planung und Koordination aller Wartungsarbeiten erfolgt entsprechend den Zuarbeiten der Gruppenleiter durch den Betriebsingenieur „Aufbau und Wartung". Der momentane Zeitrahmen für Wartungsarbeiten ist ausreichend wobei zu beachten ist, dass die entsprechende Arbeitskapazität auch zur Verfügung steht. Mit dem weiteren Ausbau der Beschleunigeranlage und dem zunehmenden Alter einzelner Anlageteilen ist in der Summe mit einer Zunahme an Wartungsarbeiten zu rechnen. Die Übernahme der erforderlichen Dokumentationen von der Zentralabteilung Forschungstechnik ist noch nicht abgeschlossen.

Hauptaufmerksamkeit muss dem Betriebszustand der Heliumanlage gewidmet werden. Auf Grund technischer Unzulänglichkeiten ist es erforderlich, die Anlage in regelmäßigen Abständen zu reinigen. Hierbei müssen ausgefrorene Gasverunreinigungen durch Aufwärmen der Anlage abgepumpt werden. Durch die Kollegen der „Kältegruppe" wurden im vergangenen Jahr umfangreiche Diagnosearbeiten durchgeführt und sehr erfolgreich mit der Behebung dieser Fehler begonnen. Die Wartung der Kühltürme wird durch die Gruppe „Betriebsdienst" der Abteilung „Standortmanagment" in Abstimmung mit der ELBE-Mannschaft regelmäßig durchgeführt.

Die gesamten Vakuumelemente unterliegen einem festgelegten Wartungsrhythmus. Hierbei zeigt es sich, dass die Vorgaben der Hersteller unbedingt eingehalten werden müssen. So müssen die Pumpsysteme des Isoliervakuums der Beschleunigermodule bzw. der Heliumtransferleitungen regelmäßig nach rund 9000 Betriebsstunden einer umfangreichen Wartung unterzogen werden. Die eingebauten Ionengetterpumpen sind auf Grund des guten Vakuums innerhalb des Strahlrohrsystems so gut wie Wartungsfrei. Die dazugehörigen Steuerteile weisen dagegen eine relativ hohe Defektrate auf. In Zusammenarbeit mit dem Hersteller wird an der Verbesserung der Zuverlässigkeit gearbeitet. Durch den Einbau getrennter Vor- und Hochvakuummessröhren konnte der Ausfall einzelner Vakuummesssysteme reduziert werden.

Alle Wartungsarbeiten an den Kühlwasseraufbereitungsanlagen obliegen der Gruppe „Betriebsdienst" der Abteilung „Standortmanagment". Diese Arbeiten erfolgen in Abstimmung mit den entsprechenden Kollegen der ELBE- Mannschaft.

Die im Pneumatiksystem verwendeten Kunststoffschläuche und Verbindungselemente wurden teilweise gegen strahlenbeständigeres Material ausgetauscht. Der Austausch der entsprechenden Teile wird auch in der Zukunft fortgesetzt. Dies gilt auch für die verwendeten Kühlwasserschläuche aus Kunststoff.

Durch die Gruppen „Elektro" und „HF" wurden alle routinemäßigen Wartungsarbeiten an den Klystronschränken sowie den Netzteilen durchgeführt. Auf Grund des Standortes auf den Gängen der ELBE-Halle waren hier insbesondere Reinigungsarbeiten und der Austausch von Lüftern notwendig. Es hat sich gezeigt, dass die Durchsicht der FUG- Netzteile mindestens einmal im Jahr durchzuführen ist. Durch den Austausch der wassergekühlten 1,3 GHz-Buncherverstärker gegen eine luftgekühlte Variante konnte eine höhere Zuverlässigkeit dieser Baugruppe erreicht werden.

Alle Personensicherheitssysteme werden im Monat einmal routinemäßig durch die verantwortlichen Betriebsingenieure und der Abteilung Sicherheit und Strahlenschutz überprüft und die entsprechende Wartung der Strahlenschutzmessgeräte veranlasst. Die im Gebäude installierten Sauerstoffmangelanzeigegeräte sind sehr störanfällig. Hier wird durch eine beauftragte Firma an einer Lösung gearbeitet. Alle überwachungspflichtigen Anlagenteile der Gebäudeinfrastruktur (Krananlage einschließlich Anschlagmittel, Feuerlöscheinrichtungen usw.) werden durch beauftragte Firmen regelmäßig überprüft und gewartet. Ein Nachweis über diese Prüfungen erfolgt ordnungsgemäß und konnte bei den anstehenden TÜV- Überprüfungen vorgelegt werden.

ELBE Medienversorgung

J. Claussner, B. Eppendorfer

Die Übersicht der Arbeiten bezieht sich auf die Leistungen zum stabilen Strahlbetrieb, auf Erweiterungen zum Projekt ELBE und der Unterstützung von Versuchsaufbauten. Sie beinhalten die Bereiche Kühlwasser, Pneumatik und Stickstoff-Gas. Die nachfolgend aufgeführten Arbeiten erfolgten in Zusammenarbeit von B. Eppendorfer (FWKE) und J. Claußner (FWFM). Kühlwasserseitig sind die Aufgaben eng mit dem Standortmanagement von FKTM verbunden.

Bereitstellung der Kühlwasserversorgung für den Beschleunigerbetrieb

Durch zwei getrennte Kreisläufe wird Kühlwasser für die Geräte des Beschleunigers bereitgestellt. Diese Kreisläufe und Unterkreisläufe bedürfen der Kontrolle und Nachregulierung. Hauptparameter sind Druck, Volumenstrom, Temperatur und Leitfähigkeit. Weiterhin sind die Kreisläufe auf Leckagen und Materialveränderungen an den Rohrleitungen, Verbindungen und Schläuchen zu prüfen. Auffälligkeiten werden je nach Möglichkeit sofort oder in einer folgenden Wartungsschicht beseitigt. Ein besonderes Augenmerk bei den Prüfungen bedürfen die Beamdumps. Diese Komponenten sind sicherheitsrelevant und in ihrem Aufbau sehr komplex.

Pneumatikversorgung

Der überwiegende Teil aller Viewscreens in der Strahlführung werden pneumatisch gesteuert. Die Kombination aus elektropneumatischen Ventil und Pneumatikzylinder wird über Drosselventile eingestellt und ist in seiner Funktion zu kontrollieren. Schlauchleitungen und Verschraubungen unterliegen einer Strahlenbelastung und müssen turnusmäßig geprüft und gegebenenfalls ersetzt werden.

Stickstoffversorgung

Entlang der Beamline werden Zapfstellen für Stickstoffgas bereitgestellt. Diese können bei Wartungsarbeiten zur Flutung der Beamline und zum Abblasen mit der Blaspistole genutzt werden. Diese Leitungen unterliegen analog den Pneumatikleitungen einer entsprechenden Strahlenbelastung und sind turnusmäßig zu überprüfen.

Turnuswartungen in der strahlfreien Zeit

Kühlwasser:

- Ein- und Nachregulierung der Räume und der einzelnen Teilkreisläufen.
- Kontrolle der Durchflüsse.
- Kontrolle und Austausch von Komponenten.

- Neueinregulierung von Kreisläufen nach Komponentenwechsel.
- Kontrolle und Reinigung von Filtern.
- Überprüfung von Leckmeldern
- Prüfung der Danfysik Schränke. Anschlüsse erneuert.
- Austausch von Komponenten in Bereichen mit hoher Strahlenbelastung
- Austausch von Patronen zur Wasseraufbereitung an Beamdump's
- Bereitstellen der Proben für die Überprüfung der Kühlwasserzusammensetzung.
- Austausch und Entsorgung von Kühlwasser

Pneumatik- und Stickstoffversorgung:

- Überprüfung der pneumatischen Komponenten (Druckregler, Schlauchleitungen usw.)
- Überprüfung und Abgleich der Pneumatischen Antriebe

Arbeiten zur Verbesserung der Stabilität der Anlage

- Anschlüsse am Bunchereinschub erneuert.
- Einsatz von strahlenbeständigeren pneumatischen Verschraubungen.
- Konzeptionelle und Gerätetechnische Erneuerung der Kühlwassernachspeisung für die Kreisläufe Sekundär 1, Sekundär 2 und Kälteanlage. Mit der Realisierung konnte die Konstanthaltung des statischen Druckes der Kreisläufe erheblich verbessert werden.

Erweiterungen der Medienversorgung

- Raum 111a (Kühlwasser):
  Erweiterung der Hauptanschlüsse für die Kühlwasserversorgung SRF- Gun. Verbunden damit war ein Konzeption, Ablassen und Entsorgung des im Raum befindlichen Kühlwassers, Koordinierung der Montagefirma, Befüllung, Entlüftung und Einregulierung des Raumes
- Raum 114 - FEL 2:
  Installation von Kühlwasser, Pneumatik und Stickstoff für die Komponenten FEL 2. Inbetriebnahme und Einregulierung aller betroffenen Komponenten. Inbetriebnahme und Einregulierung des Beamdups. Überprüfung der Signalisation und Verriegelungsbedingungen im WinCC.

- Raum 111b:
Konzeption, Betreuung der Installationsarbeiten, Befüllung und Abnahme der Kühlwasserversorgung Raum 111b. Montagebetreuung und Abnahme der Kühlung für das Projekt EPOS. Installation von Kühlwasser, Pneumatik und Stickstoff für die Komponenten der Beamlines im Raum 111b.

- Raum 123:
Konzeption, Betreuung der Installationsarbeiten, Befüllung und Abnahme der Kühlwasserversorgung Raum 123. Montagebetreuung und Abnahme der Kühlung für das Projekt BleiLoop. Vorbereitung der Installation von Kühlwasser, Pneumatik und Stickstoff für die Komponenten der Beamline im Raum 123. Überprüfung der Signalisation und Verriegelungsbedingungen im WinCC.

- Kühlwasseranpassung zur Umsetzung Danfysik Schränke Raum 106a zu Raum 200:
Demontage der Kühlwasserverbindung der im Raum 106a befindlichen Schränke. Konzept der Kühlwasserversorgung und Integration in den Sekundärkreislauf 1. Ablassen und Entsorgung des in den Rohrleitungen befindlichen Wassers zur Schaffung der Montagefreiheit. (ca. 450 l). Betreuung der Bauarbeiten am Kühlwasserkreislauf. Anschluss der Schränke an den Kreislauf. Befüllung und Entlüftung der Anlage. Einregulierung des Kreislaufes 200 mit dem Sekundärkreislauf 1.

- OL4:
Konzeption, Installation und Inbetriebnahme der Pneumatikkomponenten der Beamline OL4.

Sonstiges

- Blei-Loop:
Unterstützung und Bereitstellung der Medienversorgung für den Versuchsaufbau der Blei-Loop. Kühlwasser wurde durch eine Kopplung mit einem Umlaufkühler bereitgestellt und die pneumatischen Komponenten wurden mit Druckluft versorgt.

- Kopplerversuchstand:
Bereitstellung von Kühlwasser und Anschluss der Komponenten. Integration in den laufenden Anlagenbetrieb.

- Kühlung Heliumanlage :
Ersatzbeschaffung und Austausch einer Pumpe im Kühlsystem der Heliumanlage. Integration eines Durchflussmessers zur besseren Anlagenführung.

- Raum 112:
Integration eines Produktionstargets in den Kühlwasserkreislauf des Raumes 112

- IOT:
Beschaffung eines Umlaufkühlers mit hoher Kühlleistung für die geplante Versuchseinrichtung.

- Allgemein:
Material und Ersatzbeschaffung

Störungen

- Hauptursache für Störungen sind Spannungsschwankungen im Landesnetz bzw. Blitzschläge, welche zum Ausfall der Kreislaufpumpen oder der dazugehörigen Steuerung führen.

- Nicht rechtzeitig erkannte Strahlenschäden an Schläuchen und pneumatischen Verschraubungen.

- Ausfall einer Pumpe im Kreislauf Heliumanlage. (Ersatz)

- Sequentielle Falschanzeige mit Schwellwertüberschreitung des Temperatursensor Kühlwassertemperatur Kälteanlage. Fehler konnte noch nicht klar lokalisiert werden.

Möglichkeiten für weitere Verbesserungen

- Wartung:
In der strahlfreien Zeit müssen Zeiträume für die planmäßige Wartung geschaffen werden. Nach der Betriebszeit sollten die Komponenten der Kühlwasserkreisläufe den Räumen überprüft werden. Nach der Überprüfung sollte eine Einmessung, Einreguliert und Funktionskontrolle zum WinCC erfolgen.

- Dokumentation von Wartung und Installation:
Durch die Schaffung einer einheitlichen Dokumentation der Wartung und Installation können Problemlösungen gezielter gefunden werden.

- Rohrleitungsnetz:
Besteht die Notwendigkeit zur Erweiterung der Kühlkreisläufe, müssen die in der ELBE Halle befindlichen Hauptstränge bis zum Pumpenraum vom Durchmesser erweitert werden. Damit kann der über den Rücklauf anfallende Druckverlust gesenkt werden und die Anlage stabiler betrieben werden.

- Hardware:
Überprüfung der im Jahr 2002 eingebauten Durchflussregler durch den Hersteller.

- Dokumentenverwaltung:
Integration von Anlagendokumentation in die Dokumentenverwaltung FWF

In der Zentralabteilung Strahlungsquelle ELBE eingesetzte Beamdumps und deren Kühlung

J. Claussner

In der Zentralabteilung Strahlungsquelle ELBE werden für die Abbremsung des Elektronenstrahles verschiedene Beamdumps eingesetzt. Die Unterscheidung der Beamdumps bezieht sich auf ihre konstruktive Ausführung, die maximale Leistung und die unterschiedliche Kühlung. Damit verbunden sind unterschiedliche Ausführungen der Kühlmittelbereitstellung, der Sicherheitssteuerung und der Verbindung zum Vakuumsystem.

Art der Kühlung des Beamdumps

Man unterscheidet grundsätzlich zwischen luft- und wassergekühlten Bemdumps. Alle derzeitigen Beamdumps mit einer maximalen Leistung größer 0.2 kW, werden mit Wasser gekühlt. Beamdumps mit einer Leistung von 5 kW und 20 kW werden direkt vom Kühlwassersekundärkreislauf 2 gekühlt. Alle Ausführungen der 50 kW Beamdumps werden mit separaten Kühlkreisläufen gekühlt. Diese Kreisläufe geben ihre Wärme durch einen Wärmetauscher an den Kühlwassersekundärkreislauf 2 ab. Die Ausführung dieser separaten Kühlkreisläufe unterscheidet sich nach der Bauform der Beamdumps.

Tab. 1: *Leistungsspektrum der Beamdumps.*

| Maximale Leistung	Zeichnungs- Nummer	Entwicklung bei
0,2 kW	12.218-51(3)	FWFM
5,0 kW	12.214(1)	FWFM
20,0 kW	12.215(1)	FWFM
50,0 kW	12.262(2)	FWFM
50,0 kW		FWS

Beamdump bis 0,2 kW

Der für den niedrigen Leistungsbereich konzipierte Beamdump besteht aus einem Kupferkörper, welcher von einem Axialventilator gekühlt wird. Über eine DN 40 CF Vakuumverbindung wird dieser direkt an das jeweilige Strahlrohr montiert. Mit Hilfe eines PT 100 Temperatursensors erfolgt die Messung der Kerntemperatur. Aus diesem Messwert erfolgt die Steuerung des 220 Volt Lüfters und die Ermittlung der maximal zulässigen Betriebstemperatur. Bei Überschreitung der Betriebstemperatur wird der Elektronenstrahl abgeschaltet. Der Einsatz des Beamdumps erfolgt vor allem im Diagnosebereich.
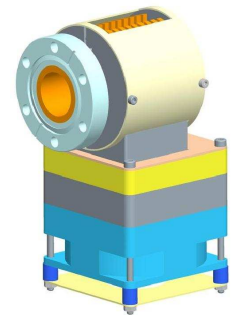
Beamdump bis 5 kW

Der für den Einsatz bei geringer Leistung konzipierte Beamdump wird in einer wassergekühlten Ausführung eingesetzt. Der Beamdump besteht im Grundkörper aus Kupfer. Über eine DN 114-63 CF Vakuumverbindung wird dieser direkt an das jeweilige Strahlrohr montiert. Mit Hilfe eines Temperatursensors erfolgt die Messung der Kerntemperatur. Aus diesem Messwert wird die maximal zulässige Betriebstemperatur zur Abschaltung des Elektronenstrahls abgeleitet. Der Beamdump hat einen Kühlwasserbedarf von 7 l/min und ist für einen maximalen Betriebsdruck des Kühlwassers von 10 bar zugelassen. Auf Grund seiner Konstruktion und seiner Temperatursteuerung kann der Beamdump direkt am Sekundärkühlwasserkreislauf 2 betrieben werden.
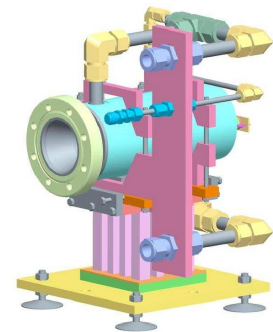
Beamdump bis 20 kW

Der für den Einsatz bei mittlerer Leistung konzipierte Beamdump wird in einer wassergekühlten Ausführung eingesetzt. Der Beamdump besteht im Grundkörper aus Kupfer. Über eine DN 200-156 CF Vakuumverbindung wird dieser direkt an das jeweilige Strahlrohr montiert. Mit Hilfe eines Temperatursensors erfolgt die Messung der Kerntemperatur. Aus diesem Messwert wird die maximal zulässige Betriebstemperatur zur Abschaltung des Elektronenstrahls abgeleitet. Der Beamdump hat einen Kühlwasserbedarf von 28 l/min und ist für einen maximalen Betriebsdruck des Kühlwassers von 10 bar zugelassen. Auf Grund seiner Konstruktion und seiner Temperatursteuerung kann der Beamdump direkt am Sekundärkühlwasserkreislauf 2 betrieben werden.
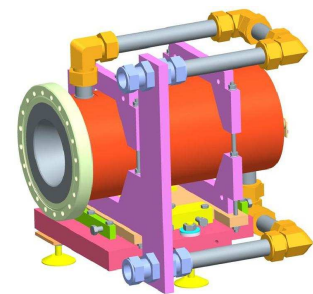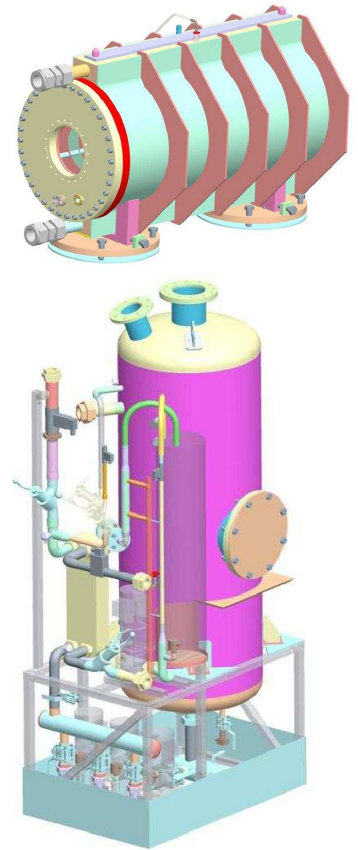
Beamdump bis 50 kW

Der für den Einsatz bei hoher Leistung konzipierte Beamdump wird in einer indirekt wassergekühlten Ausführung eingesetzt. Der Elektronenstrahl trifft im Inneren des Beamdumps auf einen Grafitkern. Dieser bremst den Elektronenstrahl ab und wandelt in dabei in Wärme um. Die entstehende Wärme des Grafitkörpers wird durch Wärmestrahlung an die innere Behälterwand des Beamdumps abgegeben. Das an der Außenseite der Wandung fließende Wasser des Kühlsystems transportiert die Wärme ab. Der Innenraum mit dem auf Keramikstutzen stehenden Grafitkern stellt einen eigenen Vakuumbereich (p<1 mbar) dar. Über einen Flansch an der Vorderseite erfolgt die Verbindung zu einem Berylliumfenster. Das Berylliumfenster trennt die Vakuumbereiche von Beamdump und Strahlrohr. Mit Hilfe von PT 100 Temperatursensoren erfolgt die Messung der Wasser- und Flanschtemperatur. Aus diesem Messwert wird die maximal zulässige Betriebstemperatur ermittelt. Bei Erreichen der maximalen Betriebstemperatur erfolgt die Abschaltung des Elektronenstrahls. Der Beamdump wird mit einer speziellen Kühlung in der Bauart eines „offenen Kreislaufes" betrieben. Durch einen Wärmetauscher erfolgt zusätzlich die Trennung von Beamdumpkreislauf und den Sekundärkühlkreislauf 2 ELBE. Aus sicherheitstechnischer Sicht, wird durch eine redundante Anordnung der Kreislaufpumpen und einer USV- gestützten Stromversorgung, ein sicherer Betrieb ermöglicht. Bisher wurden die Beamdumps des Typs im Raum 111a/112 und zweimal im Raum 114 eingesetzt.

Beamdump bis 50 kW

Der für den Einsatz bei hoher Leistung konzipierte Beamdump wird in einer direkt wassergekühlten Ausführung eingesetzt. Der Elektronenstrahl tritt am Ende des Strahlrohres aus dem Berylliumfenster des Strahlrohres aus, durchquert einen mit Stickstoff gespülten Bereich und tritt in das Berylliumfenster der Targetkammer ein. Der Beamdump ist direkt mit der Vakuumkammer des Targets verbunden. Der Elektronenstrahl wird in dem aus Aluminium bestehenden Körper abgebremst und in Wärme umgewandelt. Die im Aluminiumkern befindliche, Kühlwasser durchflossene, Rohrwendel führt die entstehende Wärme direkt an das Kühlsystem ab. Mit Hilfe von PT 100 Temperatursensoren erfolgt die Messung der Wasser- und Flanschtemperatur. Aus diesem Messwert wird die maximal zulässige Betriebstemperatur ermittelt. Bei erreichen der maximalen Betriebstemperatur erfolgt die Abschaltung des Elektronenstrahls. Die Kühlung des Beamdumps erfolgt durch einen speziellen Kühlkreislauf. Dieser Kühlkreislauf wird als „geschlossenen Kreislaufs" mit einem statischen Druck von 5 bar betrieben. Über einen Wärmetauscher erfolgt zusätzlich die Trennung von Beamdumpkreislauf und den Sekundärkühlkreislauf 2 ELBE. Bisher wurden die Beamdumps des Typs im Raum 111b/123 aufgebaut. Es bestehen derzeit noch keine Betriebserfahrungen.
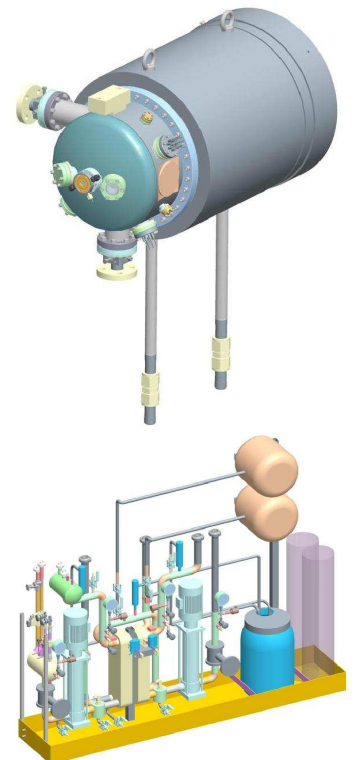
Investigation of Impurities in the Helium plant

Ch. Schneider, J. Weiske, A. Winter, U. Wünsche, Ch. Haberstroh[1]

Impurity Problem of the HE-Plant

The start of the accelerator operation with the first cryomodule in 2001 at ELBE shows up a serious problem with the operation time of the cryogenic plant. The operation time was limited to duration of around three month. During the operation time characteristic phenomena like an ongoing pressure drop in front of the turbines, a shift of specific cold box temperatures and a level shift towards higher opening angels of the far away joule Thompson valves in the distribution box in the accelerator hall could be observed. The impurity levels observed in all characteristic points of the plant are smaller than 1 vpm for N_2 and H_2O and smaller than 4 ppb for oil and therefore within the specification of the producer. In 2005 two findings could be achieved one concerning the water and one the nitrogen content in the system which brought some understanding to the mentioned problem.

Water contamination of the plant

From at least the year 2000 on water could be found in the cold box in the maintenance periods. The location of the water is mainly in the first heat exchangers of the cold box, what is to be expected if the water comes in with the warm helium gas. In the first years we have determined the quantity of water in the maintenance by flushing the coldbox with dry nitrogen gas and measuring the humidity with a dew point meter. The water content could be recalculated from the known nitrogen flow. In the first heat exchangers of the cold box we evaluate the water content to around 50 ml of water in every maintenance. In 2005 we have changed the method because of the inaccuracy of the nitrogen flushing method described above and try to measure the water content more precisely by collecting the water in a cold trap. This method is much more precise and efficient and extracts the water in approximately one or two days from the cold box. In the 3rd maintenance 2005 we have collected a quantity of 260 ml water from the coldbox, see Fig. 1. This leads to the idea to investigate the water content in the compressor oil. The analysis shows around 60 ppm in the used oil and around 3500 ppm in the new oil. The difference has therefore been extracted into the coldbox and the big charcoal adsorber over time. In the next maintenance we have still found 150 ml in the coldbox, see Fig. 1 maintenance 2006/1. Only after the replacement of the old charcoal in the adsorber no water could be found in the coldbox.
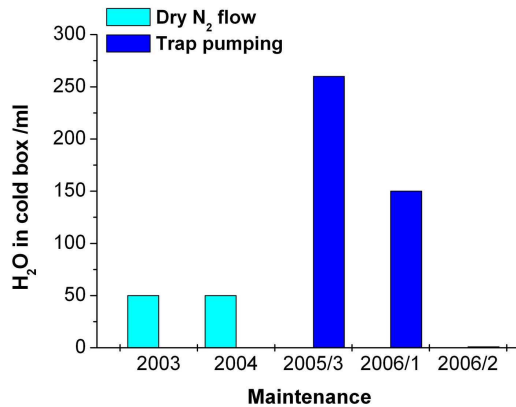
Fig. 1: *Water content found in the coldbox in specific maintenance. The method of flushing the coldbox with dry nitrogen determines only around 50 ml of water (2003, 2004). Pumping over a cold trap yields 250 ml water (2005/3). Replacement of the charcoal yields 0 ml water (2006/2).*

The mechanism we found is therefore: the new (not dried) compressor oil brings in a small content of water over time, small enough not to be alarmed by the multi component measurement. As a difficulty the charcoal adsorber between the compressor system and the cold box acts as an unpredictable water buffer.

Air leakage into the warm helium cycle

Pumping the high-pressure cycle of the helium plant without the coldbox connected leads to a steadily increase of the nitrogen contents measured with the multi component detector, see red curve Fig. 6. The leakage analysis of the compressor stations in static conditions has brought no findings. Therefore the rotary seal, separating the pure helium in the compressor from the outside air, could be a potential leakage system during compressor operation. We build therefore a provisional second shield in front of the rotary seal, which could be flushed with helium gas and acts then as a sealing gas buffer, see Fig. 2 and Fig. 3. The result is shown in Fig. 4, over the operation time of around 12 hours no measurable contamination of the compressor cycle with air (N_2) could be found.

---

[1] TU-Dresden
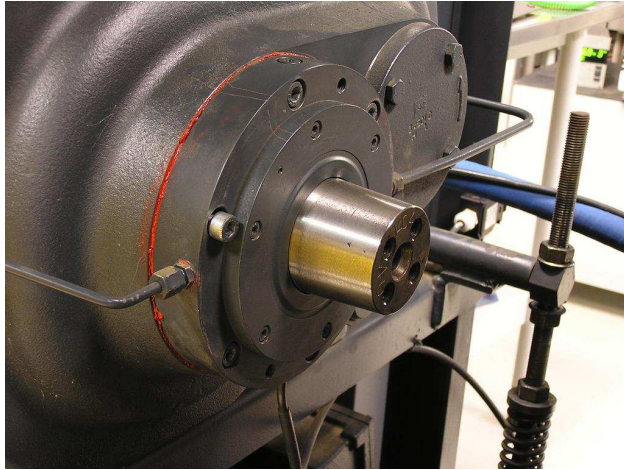
Fig. 2: *Picture of the front section of a screw compressor block without drive wheel.*
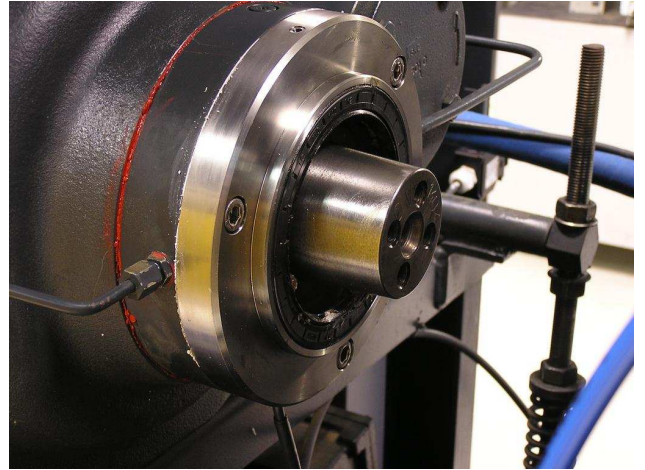
Fig. 3: *Now an additional shield is fixed in front of the rotary seal of the compressor, which can be flushed with helium sealing gas.*
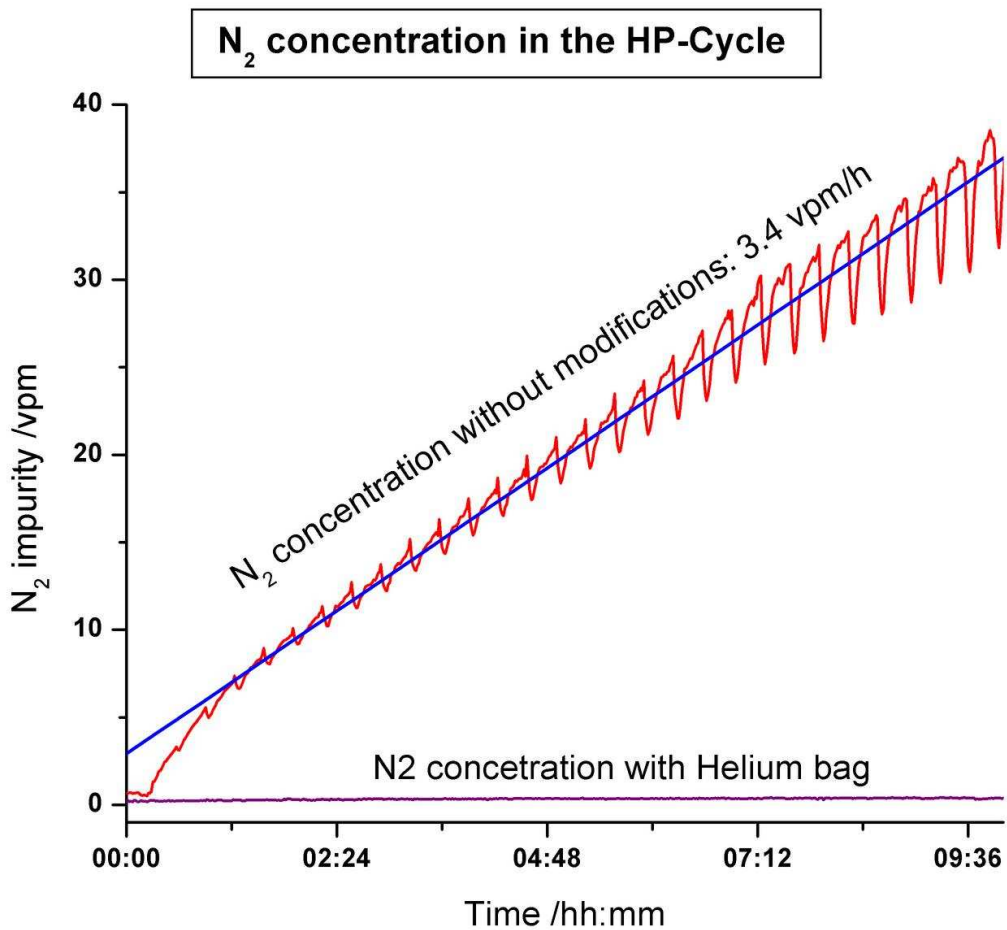
Fig. 4: *N_2 concentration in the high pressure (HP) compressor cycle, if it's operated without connected coldbox. The red curve shows the normal increase of the N_2 concentration with time. The not increasing violet curve shows the operation with helium sealing gas in front of the rotary seals of the compressors.*

Modifications in the Injector High-Voltage Region

J. Hauser[1], F. Herbrand[1], D. Pröhl[1], J. Teichert

Due to experiences in the operation of the injector with a grid-pulsed thermionic gun at ELBE [1] a requirement did arise for improvements of the HV-divider. The HV-divider delivers the middle electrode voltage of the gun (see also Fig.1). This voltage should be half of the operation voltage of the cathode (minus 250kV). In the case of a leakage current from the middle electrode to the cathode or to ground the voltage of the middle electrode will be shifted. A too large shift can cause a flashover between middle electrode and ground or cathode. The voltage shift is depending on the leakage current and the resistance of the HV-divider. To reduce this effect the resulting resistance of the HV-divider was reduced by using new resistors with lower resistance and the current was increased to 2 mA. This increases the power dissipation of the HV-divider to 500 W, and did demand a new design with a suitable air cooling for the resistors.

Fig. 1: *HV circuit at the ELBE thermionic gun.*

In the scheme in Fig. 1 is shown in principle the wiring of the HV circuit with the current measurement points. Another point to improve was the HV-training procedure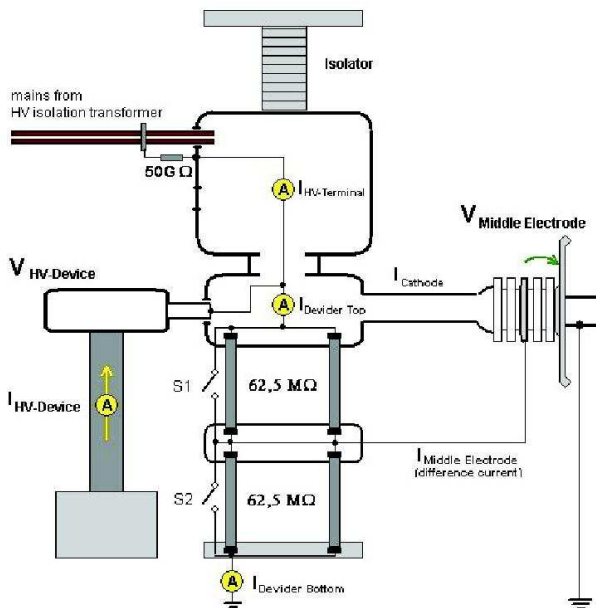 of the gun which is necessary before the operation of the accelerator starts, especially after longer shutdown periods. A switch gear was designed, which makes it possible by remote control to connect the middle electrode either with the HV-platform or with ground directly (at normal operation the connections shown as switches S1 and S2 in Fig. 1 are open). The connection will be done by a motor driven wire in connection with a nylon cord. By limit switches it will be controlled, that the cord will be stopped in the ap-

propriate position. In this way it is now possible to perform the HV-training of the gun for both sides separately.

To automate the training procedure a program was written, which increases the high voltage and monitors the pressure in the vacuum system of the gun. If the pressure is rising above a settled value the raising of voltage will be stopped until the pressure is fallen to the usual value. Then the procedure will be continued until the end voltage for the formation is reached.

In a second step the whole arrangement of the gun HV region had to be reconstructed to make room for the installation of the photo RF gun. At first it was necessary to take the HV isolation transformer for the mains supply of the gun electronics (situated on the HV platform of the gun at minus 250 kV) out of the accelerator room.

To connect the transformer with the HV platform a pair of new longer coaxial HV cables is used. The cables are on their ends to the so called "Hamburger" fitted with heat shrinkable sleeves, which incorporate a low conductivity to control the electrical field on the end of the cables. The sleeves cover the last 1.5 m of the cable and have an overall resistance of 60GΩ. This arrangement replaces a chain of discrete resistors used at the old cables. The other end of the cables reaches into the oil filled container of the 300 kV insulation transformer. To avoid high electrical field strength there, the shorted outer conductor of the coaxial cables was equipped with a funnel shaped elongation and cast with epoxy resin.

Another measure to gain more space was to fasten the "Hamburger", which contains the gun electronics, to the ceiling above the HV-divider. The HV-device is furthermore placed beside the HV-divider and now mounted on a sliding support to give way to carry the parts of the photo RF gun through, without to dismantle parts of the equipment. After the reconstruction the whole system is working without problems. A photograph of the new arrangement is shown in Fig. 2. In the foreground the Glassmann high voltage power supply is visible. Behind it the new voltage divider is arranged and above the HV platform. The electron source, hidden by the metal wall, is on the left side.

[1] FZ-Dresden, FWF

Fig. 2: *The gun region after reconstruction.*

After reconstruction, the operation voltage of 250 kV was reached without any difficulties. The following parameters were measured:

divider resistance, upper	55.9 MΩ
divider resistance, lower	60.9 MΩ
resistance of the shrinking tubes	60 GΩ
spray current at 250 kV	ca. 6 μA
total current at the HV power supply at 250 kV (beam switched off)	2135 μA

The reconstruction changed the distance between the electron source and the HV platform in which the electronic pulse formation unit is placed. The longer RF cable causes a phase shift and influences the pulse amplitude in dependence on the pulse repetition frequency. The phase shift could easily corrected in the low level RF control system but the pulse amplitude effect required a series of test measurements in which the optimum cable length was determined. Fig. 3 presents the results of these measurements. In addition to the necessary RF cable length, pieces of different length were introduced and the electron current was measured for pulse frequencies between 26 MHz and 0.8125 MHz. An optimum was found with an extension cable length of 26 cm. In that case the pulse amplitude variation was less than 10% for pulse frequencies $\leq$13 MHz.
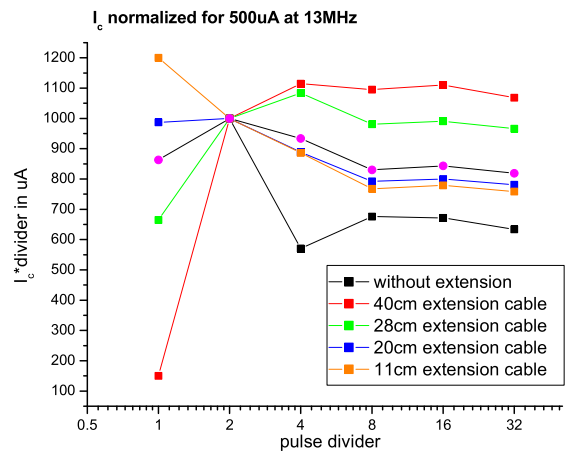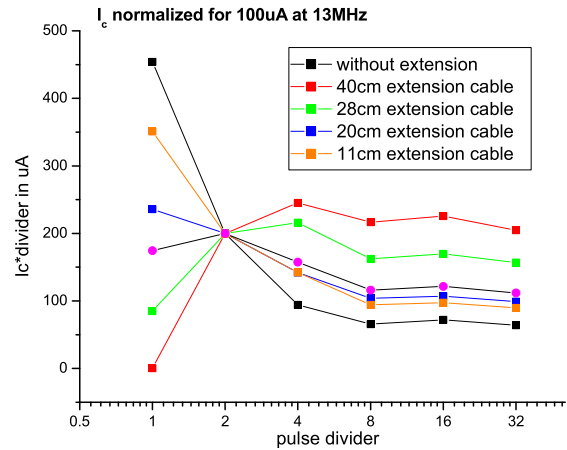
Fig. 3: *Normalized electron current as a function of pulse frequency with different extension cable length for 100 μA (top) and 500 μA (bottom) electron current. In the ideal case the measurement point should form a horizontal line.*

[1] F. Gabriel et al., Projekt Strahlungsquelle ELBE, Design Report FZ Rossendorf (1998)

Neue Elektroinstallationen an der Strahlungsquelle ELBE

J. Erber

Zusammenfassung

Die Strahlungsquelle ELBE ist seit Mai 2001 in Betrieb. Seitdem wurden parallel zum Nutzerbetrieb neue Anlagenteile installiert, neue Experimente in Betrieb genommen und dafür Strahlführungssysteme und Instrumentierungen erweitert. Dieser Bericht gibt einen Überblick über Elektroinstallationen, die in den letzten beiden Jahren realisiert wurden.

Realisierung Neuer Projekte

Hierzu zählen:

- Erweiterung und Umsetzung der Steuerschränke (DANFYSIK) für Dipole und Quadrupole (Fig.1)
- Aufbau einer Undulator-Steuerung für den langwelligen FEL mit dem Undulator U-100 (Fig.2)
- Aufbau eines Steuerschrankes für die Dipolsteuerung (Fig.3)
- Projektierung und Aufbau eines Steuerschrankes für die Kathodenpräparation für die Supraleitende Photo HF Gun, (SHF-GUN) (Fig.4)
- Aufbau der gesamten Steuerelektronik für den FEL 2
- Instrumentierung der Beamline für die Neutronenphysik und die Positronenphysik (Fig.5)

Fig. 1: *Neue Installation der DANFYSIK Netzgeräte.*

Instandhaltung und Prüfungen elektrischer Anlagen

Sowohl die Betriebsführung von elektrischen Verteilungsanlagen als auch deren Instandhaltung erfordert fundiertes technisches Know-how, kompetentes Personal und Einsatz von einwandfreiem Material. Die Instandhaltung und permanente Wartung der elektrischen Anlagen sind für eine hohe Verfügbarkeit der

Strahlungquelle ELBE unerlässlich. Der Grund für das Auftreten von Mängeln liegt in der Tatsache begründet, dass sich elektrische Anlagen im normalen Betrieb kontinuierlich verändern. Dabei können diese
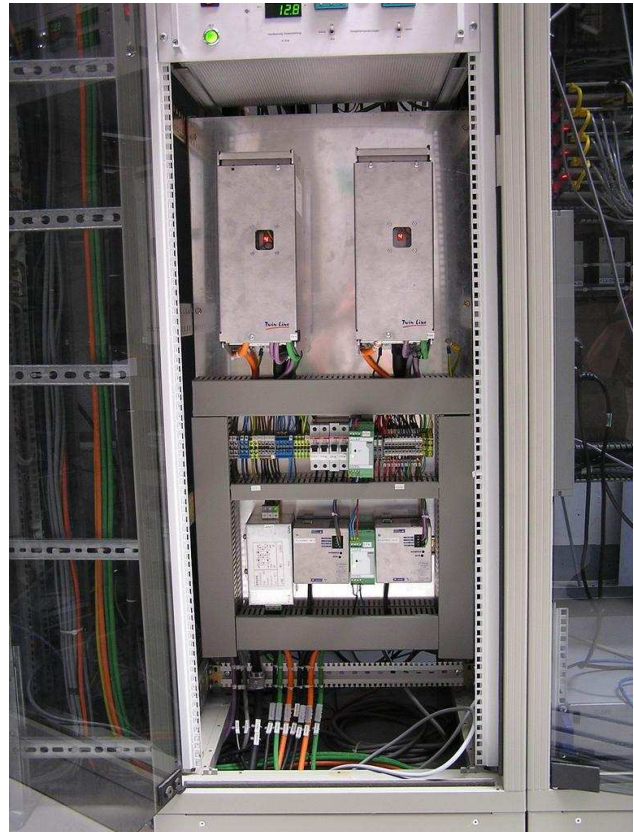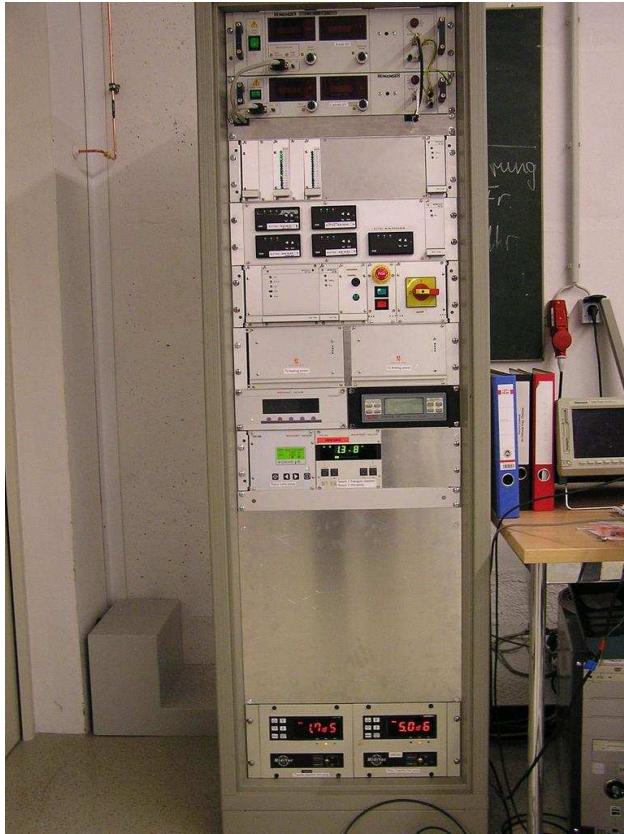

Fig. 2: *Undulator-Steuerung für U-100.*

Fig. 3: *Steuerschrank für Dipolsteuerung.*

Fig. 4: *Steuerschrank für Kathodenpräparation für die SHF-Gun.*

Fig. 5: *Installationen für die Neutronen- und die Positronen-Beamline im Raum 111b.*

Veränderungen sowohl aktiv durch äußere Eingriffe herbeigeführt werden, als auch passiv durch den normalen Verschleiß auf Grund von üblichen Betriebsvorgängen (z.B. Steuervorgänge und kurzzeitige Überlastung).

Der Unternehmer hat dafür zu sorgen, dass die elektrischen Anlagen und Betriebsmittel auf ihren ordnungsgemäßen Zustand geprüft werden, und zwar vor der ersten Inbetriebnahme als auch nach einer Änderung oder Instandsetzung. Diese Prüfung wird durch eine Elektrofachkraft oder unter Leitung und Aufsicht einer Elektrofachkraft und in bestimmten

Zeitabständen durchgeführt. Insbesondere werden alle E-Anlagen an ELBE in einer Watungsfrist für ortsfeste Anlagen aller 4 Jahre gewartet. Die Prüfung der Anlagen wird dokumentiert.

Dokumentation

Die Dokumentation der elektrischen Anlagen an Elbe ist eine Grundvoraussetzung für den bestimmungsgemäßen Betrieb, für die Wartung der Anlage und für eine effektive Reparatur. Hier zeigt sich, dass für bestimmte Anlagen noch die Dokumentation insbesondere die Stromlaufpläne erstellt werden müssen. Für diese Arbeiten steht nun das Softwarepaket: „Elektroplaner E-Plan" zur Verfügung. Zukünftig werden alle elektrischen Anlagen mit dieser Software geplant und erweitert. Des weiteren wurde ein Fehlertagebuch als Exel-Datei erstellt, das zu statistischen Zwecken als auch zur Unterstützung bei Reparaturen dient.

Weiterbildung

Im Zeitalter der enorm anwachsenden neuen Technologien ist die ständige Weiterbildung der Elektrofachkräfte unabdingbar. Durch die Firma Knobloch GmbH Großharthau werden sehr gute elektro- Fachseminare und Fachvorträge gehalten. Diese beinhalten unter anderem: Rechtliche Anforderungen für Erst- und Wiederholungsprüfungen an elektrischen Anlagen (Betr SichV, BGV A3, GUV-V A3), Erst - und Wiederholungsprüfungen elektrischer Anlagen nach DIN VDE 0100 und DIN VDE 0105, Nachweisführung der Prüfungen, umfangreiches Messpraktikum an Netzmodellen zur Befähigung des gefahrlosen, richtigen und rationellen Messens.

Sicherheit von elektrischen Anlagen

Für elektrische Anlagen gelten bestimmte Sicherheitsgrundlagen. Im FZD werden elektrische Anlagen in großem Maße in Eigenregie projektiert und aufgebaut. Hierzu werden vom FZD Sicherheitsvorschriften (Gabusnachweis) vorgegeben. Dieser beinhaltet wichtige Gesetze und Richtlinien, anzuwendende Regeln, Information und Grundsätze der Unfallkassen , Sicherheitsnachweis, Gefährdungsanalyse, Strahlenschutz und die Eigenherstellerbescheinigung. Für Klystronsteuerschränke, Netzteile und den Schaltschrank für die Kathodenpräparationsanlage wurden positive Abnahmebescheide erteilt. Für viele weitere Geräte besteht noch Abnahmebedarf. Die Prüfungen der elektrischen Anlagen gemäß DIN VDE 0751 (neue Fassung, gültig vom 1. Oktober 2001) DIN VDE 0702 , BGV A2 dürfen nur von speziell ausgebildete Personen durchgeführt werden, die einer ständigen Aus- und Weiterbildung unterliegen. Weiterhin dürfen nur für diese Prüfungen zugelassene, geprüfte und kalibrierte Messgeräte zum Einsatz kommen.

Improvement of the reliability of the PC cluster on ELBE

U. Hofmann[1], R. Jainsch[2], U. Konrad[1], K.-W. Leege[2], A. Schamlott

The controlling of the linear accelerator ELBE is hierarchically developed and based on three columns [1]:

- Process level: machine control and interlock are based on PLC (SIMATIC S5/S7)
- HMI and data archiving are based on PC by means of Siemens WinCC software
- Diagnostics, data acquisition (BPM's, BLM's, dose meters), videograbber / videomux, FEL control, data analysis, machine logbook [2] – are also based on PC using standard software (e.g. Origin, Excel) as well as software custom-made (by means of LabVIEW, Oracle)

The connection of the PLCs among themselves and to the control level takes place by means of Profibus (process level: optical fibers as medium). The computers and a number of other data terminals (COM server, scopes) are networked over Ethernet. Primarily they were a normal part of the campus network. Apart from local failures of individual computers above all two scenarios are possible, which can compromise a smooth operation of ELBE:

- Viruses and other malicious software, which can compromise the ELBE computers
- Disturbances in the campus network, which interrupt the connection to the domain controllers. The WinCC software queries periodically the authentification of the clients and stops if the answer is missing.

Thus the safe operation of the accelerator is not impaired (all safety-relevant procedures run on the PLC), however the human machine interface (HMI) is affected so that it is impossible to control the machine by an operator.

An aggravating factor is further that the client server operation of WinCC does not get along with the virus scanner Sophos used at the campus. The communication of the WinCC clients with the server is substantially obstructed by running this virus scanner.

In order to protect the ELBE cluster against attacks from the network and to increase the availability, a set of procedures was implemented. An own subnet was configured for the ELBE computers at first. Also a hardware firewall was installed for safeguarding this netsegment (model: Nokia IP 265). All ELBE computers as well as data terminals necessary for the operation of ELBE are behind the firewall. The ELBE computers in principle do not have access to the Internet, access to central components on the campus (file server, web server) are regulated by firewall policies. For certain computers, which are outside of the Firewall inside the FZR domain, access options on ELBE computers (VNC) are furthermore regulated by firewall policies. Additionally the use of diskettes/ USB sticks/ CD is strongly restricted. By means of these measures a sufficient protection from harming software is ensured.

An own domain controller was furnished behind the firewall to protect against technically caused disturbances in the campus network. All ELBE computers get their authentification from there. On this domain controller runs a DNS server and a WINS server. Thus an autonomous working of the ELBE PC cluster is possible.

A technical difficulty consisted in the fact that the measured data have to be made available to certain users over an OPC gateway, which also runs on an ELBE computer. The synchronisation of these data with the machine data however is time-critical. By the longer running time of the data due to the firewall there were frequently problems. The OPC gateway therefore was equipped with a second network adapter which is localized in the same network segment as the data acquisition computer (VME Crate).

Moreover measures like UPS for important components of the cluster, harddisk images of all computers with special function as well as a partial hardware redundancy were taken for the coverage of an unobstructed operation of the IT technology at ELBE. Thus a special procedure was compiled and tested for the substitution of the primary WinCC server by the secondary server (the active WinCC server must always have the same network name and IP address, the project and the measured data have to be the same on both servers for instance).

Naturally restrictions arise in the users comfort (e.g. Internet access) or in case of an access to the ELBE computers from outside as a result of this structure (a firewall policy has to be added for each computer which comes along).

The cluster works successfully in this configuration since January 2006. The configuration selected for the ELBE network serves as a reference solution for networks with high availability and safety requirements at the campus.

[1] F. Gabriel et al, "Maschinentechnisches Konzept (Designreport) Strahlungsquelle ELBE", Rossendorf 1998
[2] C. Ruecker, A. Schamlott, "A web based electronic logbook for ELBE", Annual Report 2003/2004 Radiation Source ELBE, FZR-428, Rossendorf 2005, p.50

[1] FZD, Department of Information Technology (FKTI)
[2] FZD, Department of Research Technology (FWF)

ELBE Live Display

P. Auerbach, A. Schamlott

For the operation of the linear accelerator ELBE there is a set of parameters, which delivers information about the mode of operation (type of the used secondary radiation, pulsed or continuous (cw) beam, beam current, energy) and the operating condition (beam on / off). These operating parameters are important not only for the personnel, who runs the accelerator, but also for the users and observers of the beam time. The secondary radiation is used by different users for research purposes. In the case of breakdown or short intervals they have to be informed about the status of the machine. Furthermore different institutes and scientists from all over the world are interested in the status of ELBE. For this purpose a web based live display was sketched, on which at each time the current operating conditions are readable.

The live display is based on a PHP script, which works with all PHP versions starting from PHP4. The data for the live display are stored by the ELBE control program (WinCC) on the WinCC server. The script selects it there, writes it into the file history.txt and produces a diagram for the cathode current and the beam paths from the information of the last 24 hours. On the live display you can find the parameters acceleration gradients, beam energy, type of secondary radiation, cathode current and beam mode (quasi cw mode or macro pulse mode). Moreover a color bar is presented where different colors indicate the type of secondary radiation which was produced in the last 24 hours. Furthermore there is a diagram which displays the cathode current over the last 24 hours as well as the beam mode (quasi cw mode or macro pulse mode). The live display is accessible to all prospective customers via the Internet.
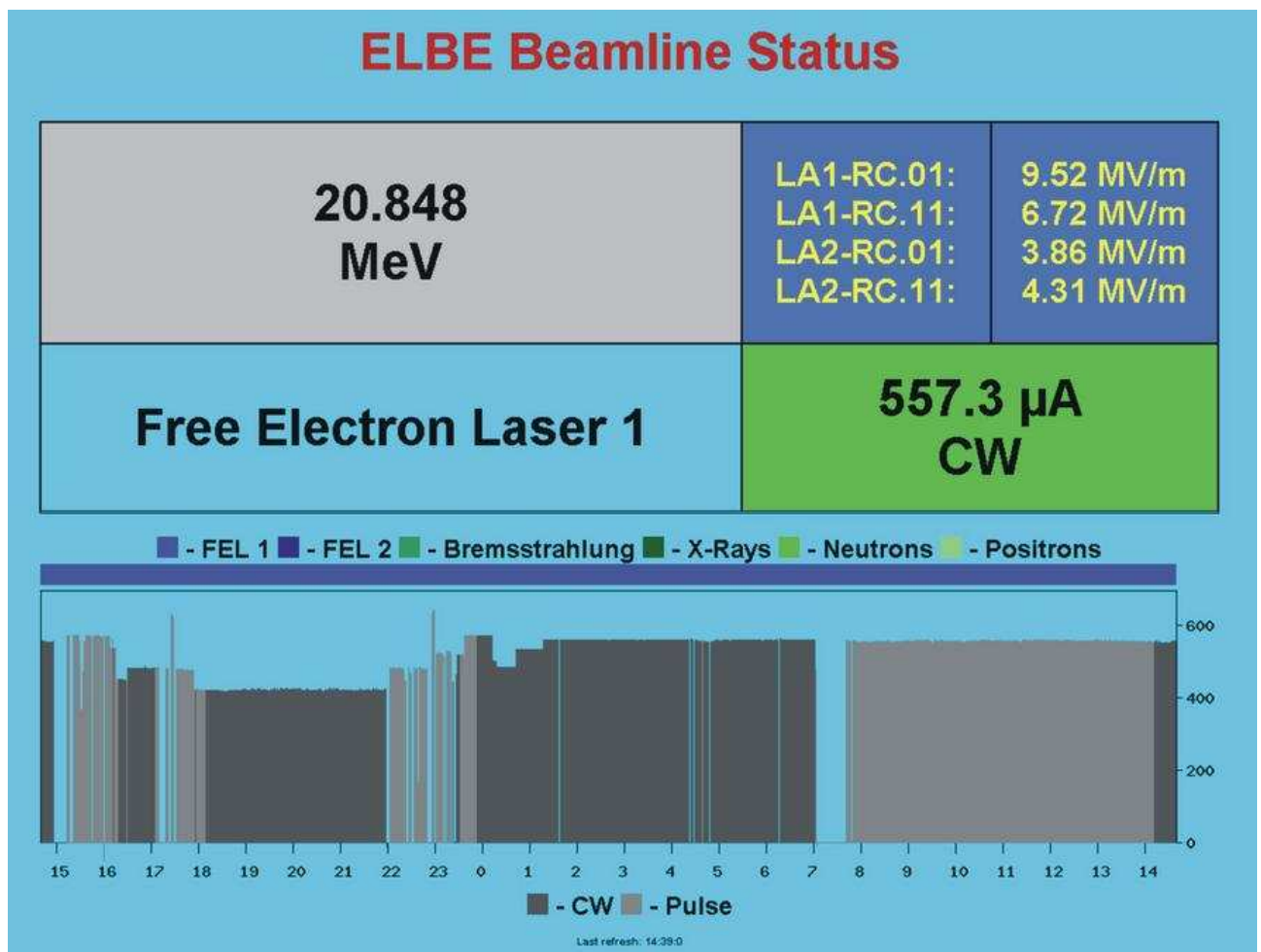

Fig. 1: *Screenshot of the ELBE live display.*

Neutron Beam Characteristics, Collimator Design and Detector Simulations for ELBE-nToF

J. Klug, E. Altstadt,[1] C. Beckert,[1] R. Beyer,[2] H. Freiesleben,[3] M. Greschner,[3] E. Grosse,
A.R. Junghans, D. Légrády,[1] B. Naumann,[4] K. Noack,[1] S. Schneider,[5] K. Seidel,[3] A. Wagner, F.-P. Weiss[6]

The neutron time-of-flight (nToF) system at ELBE uses the electron beam to produce neutrons in a liquid-lead neutron radiator. The neutron energies that can be used for nToF measurements range from 70 keV up to 10 MeV when ELBE delivers a beam repetition rate of 0.5 MHz. In this energy interval there is a need for neutron cross section data relevant for transmutation and for testing materials of fission and fusion reactors [1]. In addition, energies in the 30–70 keV range, accessible with a reduced repetition rate, can be utilized for nuclear astrophysics experiments.

By using the neutrons emitted from the radiator perpendicular to the direction of the electron beam a high suppression of the forward-peaked bremsstrahlung photons is obtained. The neutrons will be shaped by a collimator into a beam entering the experimental site in the adjacent room.

Monte Carlo simulations were performed using MCNP4C3 [2] to characterize neutron and photon intensities at the sample position, time and energy distributions, and resolutions. The main parameters determining these are the radiator dimensions, the energy of the beam electrons, the beam current, and the length of the neutron flight path. Tab. 1 shows a compilation of predicted source strengths and fluxes at the measuring position 3.9 m from the radiator, for different electron energies.

**Tab. 1** *Simulated neutron source strength and flux at the measuring position (electron beam current $I_e = 1\,mA$).*

Electron energy / MeV	Radiator source strength / s^{-1}	Flux / cm^{-2} s^{-1}
20	$7.9 \cdot 10^{12}$	$4.3 \cdot 10^6$
30	$1.9 \cdot 10^{13}$	$1.0 \cdot 10^7$
40	$2.7 \cdot 10^{13}$	$1.5 \cdot 10^7$

It was found that only the radiator gives significant contributions to the neutron flux at the measuring position—almost 92 % stem directly from the lead in the radiator, while about 8 % of the neutrons were created or scattered in the molybdenum channel confining the lead. A very small fraction ($< 0.1\,\%$) was scattered in the steel housing accommodating the radiator.

A further objective of the simulations was to optimise the geometry and material composition of the collimator and of a beam filter. This aimed at (i) eliminating neutrons and photons scattered or produced in the collimator, thereby creating a well-defined beam of unscattered neutrons, having a minimal background of both neutrons and photons outside the beam, and (ii) minimizing the component of slow neutrons coming directly from the radiator, overlapping into the next beam pulse and creating measurement ambiguities.

Fig. 1 shows five examples of investigated collimator compositions placed in the wall consisting of 1.2 m concrete and 1.2 m of heavy concrete (seen from left to right). Dark-coloured collimator insertions are made from lead and light ones from borated polyethylene (CHB), while uncoloured regions do not contain any material. The neutrons travel from left to right, and the lead insertions are placed behind the CHB sections in order to absorb photons created in (n,γ) reactions. An additional 10 cm thick lead shield is placed after the wall.
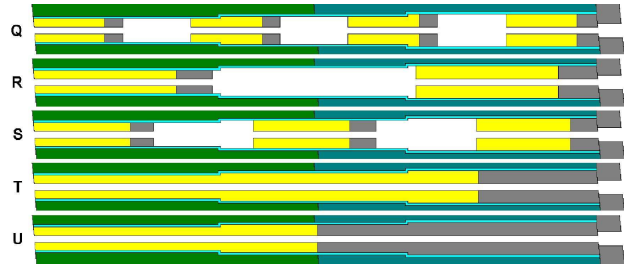
Fig. 1 *Examples of investigated collimator designs. Dark sections: lead; light sections: borated polyethylene.*

Collimator types Q, R and S have the same thickness of CHB and lead in the axial direction, but distributed mainly in 4, 2 and 3 groups, respectively. Types T and U are completely filled; the former with the same ratio between materials as the types mentioned first, and the latter with 50 % each of CHB and lead. All collimators have an opening (beam diameter) of 3 cm, and increasingly larger outer radii of 5, 6 and 7 cm, defined by a stainless steel tube with 1 cm thick walls.

The neutron beam profile for the different collimators is shown in Fig. 2, given by detectors at an axial distance of 3.9 m from the radiator (50 cm after the collimator opening), and at increasing radial distances from the beam center. All collimators shape a neutron beam with a sharp edge, indicated by the intensity drop between $r = 1.5$ cm and $r = 2.0$ cm. At larger distances, the intensity is four orders of magnitude less than in the beam. A similar trend has been shown for photons.
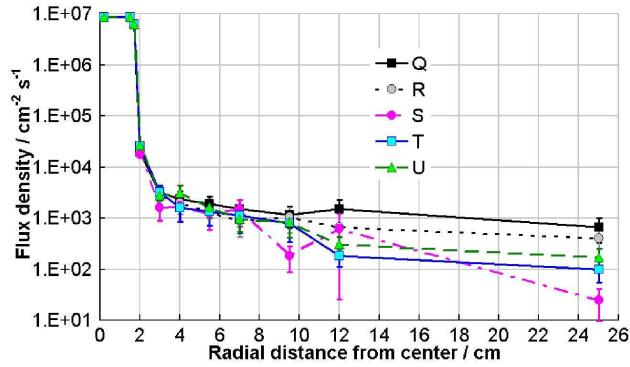
[1] *FZ Rossendorf, FWS*
[2] *also Friedrich-Schiller-Universität Jena*
[3] *TU Dresden, Institut für Kern- und Teilchenphysik*
[4] *FZ Rossendorf, FKT*
[5] *FZ Rossendorf, FWF*
[6] *TU Dresden, Institut für Energietechnik*

Fig. 2 *Neutron fluxes after the collimator (3.9 m from the neutron radiator), at different distances from the beam center ($E_e = 30\,MeV$ and $I_e = 1\,mA$).*

A close inspection of the fluxes at points with small errors (at $r = 1.7$, 2, and 3 cm) shows that collimators not fully filled (i.e., Q, R, S) produce less neutron background outside the beam than those without air gaps. Among these, the S-type collimator shows the best performance. In addition, it was found that a conical beam channel (with a smaller entrance diameter) improves the beam profile even more.

With an accelerator repetition rate of 13 MHz, most of the neutrons will overlap into the following pulses, making unambiguous measurements impossible. This problem can be overcome by lowering the repetition rate to 0.5 MHz and by placing a filter in the beam. The intensity loss due to a lower rate will be compensated for with a superconducting RF photo electron injector being developed, allowing for a beam current of 1 mA at a repetition rate of 0.5 MHz [3]. The effect of different filters is shown in Fig. 3.
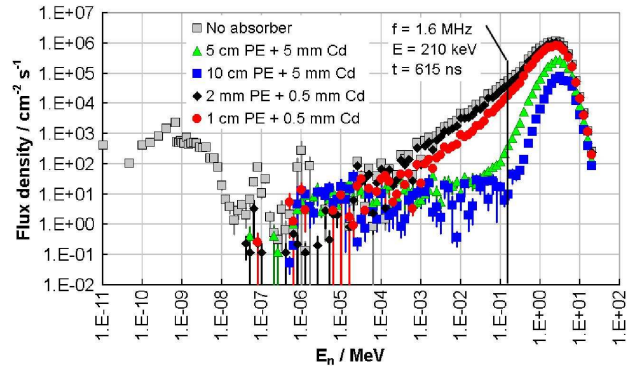

Fig. 3 *Neutron fluxes with different absorbers placed in the collimator entrance. Neutrons with $E_n < 210\,keV$ should be prevented from creating background in subsequent beam pulses.*

With a frequency of 1.6 MHz, the next pulse comes 615 ns later (indicated). Thus, neutrons with $E_n < 210\,keV$ must be suppressed. With a 5 cm thick slab of polyethylene and a thin disc of Cd placed at the collimator entrance (triangles), the neutron flux below

210 keV drops two orders of magnitude, compared to the situation with no filter (light squares).

The cost of using the filter is a decrease in peak intensity by a factor of 5, but the relative background reduction is considerable—up to two orders of magnitude. The correlation between neutron kinetic energy and time of flight, as well as the energy resolution shown earlier [4], is preserved.

Lithium-glass detectors (diam. 46 mm, thickness 10 or 25 mm) and plastic scintillator stripes (cross sections of $11 \times 42\,mm^2$ or $22 \times 42\,mm^2$) were simulated to obtain neutron detection efficiencies, time spectra and energy resolutions. The share of events with lost timing information due to neutron scattering before detection was also determined. This is shown for different detectors in Fig. 4 (lowest histograms).
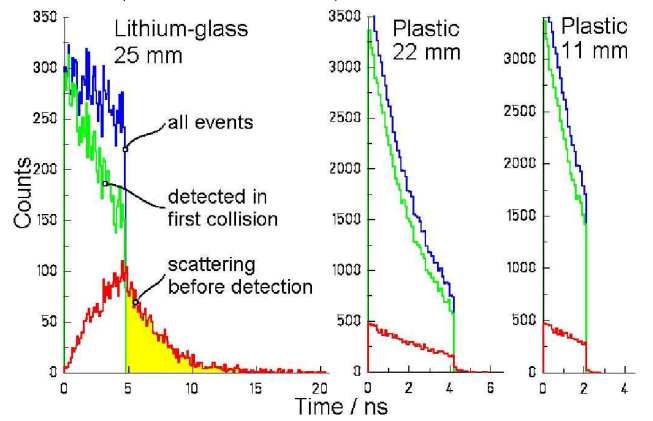
Fig. 4 *Simulated detector time spectra. $E_n = 144\,keV$.*

For Li-glass detectors, 34 % of all events have lost their timing information, and 16 % (shaded area) of all events lie outside the time range related to the detector thickness. These significantly worsen the energy resolution. For the plastic scintillators, a threshold of 5–10 keV can be applied by triggering in the single-electron peak and using a coincident readout with two photomultiplyer tubes [5], reducing the share of events with lost timing to 15 % and the fraction outside the detector thickness to below 1 %. The detection efficiencies are also in favour of plastic scintillators (60–80 %, depending on thickness) compared to Li-glass detectors ($< 5\,\%$).

[1] Long Term Needs for Nuclear Data Development, comp. M. Herman, INDC(NDS)-428, IAEA Nuclear Data section, Vienna, Austria (2001)

[2] MCNP—a General Monte Carlo N-Particle Transport Code (Report LA13709), ed. J. F. Briesmeister, Los Alamos National Laboratory (2000)

[3] J. Teichert, FZR, private communication (2005)

[4] E. Altstadt, C. Beckert et al., IKH Annual Report 2004, FZR-423 (2005) 19

[5] R. Beyer, E. Grosse et al., this report, p. 40

Testing the Performance of Timing MRPC Detectors at ELBE

F. Dohrmann, R. Kotte, L. Naumann, J. Wüstenfeld, Institut für Strahlenphysik

Multigap Resistive Plate Chambers (MRPCs) are potentially suited for cost-efficient large-area time-of-flight arrays needed for the identification of minimum ionizing particles (MIPs) in large-scale heavy-ion experiments [1-7]. Since the specific energy loss of 10-40 MeV electrons is quite similar to that of MIPs, a test setup is installed at the radiation source ELBE where scattered electrons are used to mimic the behaviour of MIPs within RPC detectors. Furthermore, the high precision of the accelerator RF signal allows for a well defined time reference. Therefore, no high-resolution start counter requiring an additional pulse-height correction (time slewing) is necessary. Electrons from ELBE are scattered (quasi) elastically off a thin (18 μm) Al target. Passive (Pb shielding) and active collimation (various scintillation counters) defines a small solid angle and hence sufficient background suppression. The test detector is positioned 2 m away from the target at scattering angle of 45 degrees. For the layout of the experimental setup, see ref. [8].

Here, we present results obtained with a 20 cm long prototype of a symmetric Multistrip MRPC (central anode with 16 strips of 2.5 mm pitch, six gas gaps of 250 μm, eight float-glass plates of 1 mm) developed for the FOPI experiment at SIS/GSI [4-7]. Moreover, we tested two identical six-gap MRPCs (called IKH-MRPC), with four readout strips of 1 cm pitch and 7 cm length using the same float glass of high resistivity of $\sim 10^{12}\,\Omega\,cm$. The IKH-MRPCs were built in the detector workshop of the Institute of Radiation Physics. The detectors were irradiated with 34 MeV electrons. The corresponding results are published recently [8].

The counters are operated with a gas mixture of 85 % $C_2H_2F_4$ + 10 % SF_6 + 5 % iso-C_4H_{10} at a flow of 1.8 l/h.

Typical results of time resolution measurements are summarized in figs. 1 - 4. Reproducibility is achieved within ±10 ps. Note that the given resolution values are corrected for the finite resolution of the time-to-digital-converter (TDC, here: CAEN V1290N) but not for any jitter of the RF signal and the front-end electronics (FEE, here: GSI development precursor with 4 channels, single-ended 50 Ω input, gain $\lesssim$ 250, bandwidth $\sim$ 1 GHz, threshold $\lesssim$ 100 mV [6, 7]).

The high-rate capability of MRPCs can be decisively improved by using low-resistivity glass. Thus, two four-gap MRPCs (called INR-MRPC) equipped with silicate glass plates showing a bulk resistivity of $\sim 10^{10}\,\Omega\,cm$ have been assembled at the Institute for High-Energy Physics and the Institute for Nuclear Research, Moscow, and successively tested at ELBE. Time resolutions of about 100 ps and efficiencies larger than 95% were obtained for rate densities

up to 20 kHz/cm² (cf. fig. 5) meeting the demands of experiments planned at the future Facility for Antiprotons and Ion Research (FAIR) in Darmstadt such as the Compressed Baryon Matter (CBM) experiment. These results will be published soon [9].

[1] P. Fonte et al., Nucl. Instr. Meth. A 443 (2000) 201
[2] P. Fonte et al., Nucl. Instr. Meth. A 449 (2000) 295
[3] A. Blanco et al., Nucl. Instr. Meth. A 485 (2002) 328
[4] M. Petrovici et al., Nucl. Instr. Meth. A 487 (2002) 337
[5] M. Petrovici et al., Nucl. Instr. Meth. A 508 (2003) 75
[6] A. Schüttauf, Nucl. Instr. Meth. A 533 (2004) 65
[7] A. Schüttauf, Nucl. Phys. B (Proc. S.) 158 (2006) 52
[8] R. Kotte, F. Dohrmann, J. Hutsch, L. Naumann, D. Stach, Nucl. Instr. Meth. A 564 (2006) 155
[9] V. Ammosov et al., to be published in Nucl. Instr. Meth. A
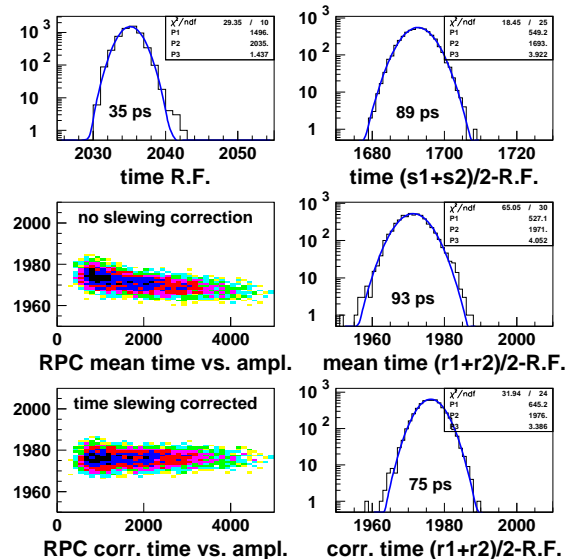
Fig. 1: *The time resolution, σ_t, of different measured quantities of the FOPI-MRPC prototype (full lines: Gaussian fits, TDC time slope 24.5 ps/ch). Upper left panel: The 13 MHz time reference signal of ELBE fed into two TDC channels (self-coincidence). For the resolution values given in the right side panels this TDC contribution is quadratically subtracted. Upper right: Mean timing $(t_{left}+t_{right})/2$ of a 2 x 2 cm² (5 mm thick) scintillator read out on two sides by XP2020 photo tubes. Middle (lower) left: Dependence of a similar mean timing of a RPC strip on integrated charge before (after) time slewing correction. The corresponding right panels show the projections onto the time axis. The RPC potential voltage was set to 8.2 kV and the corresponding rate was limited to 50 Hz/cm².*
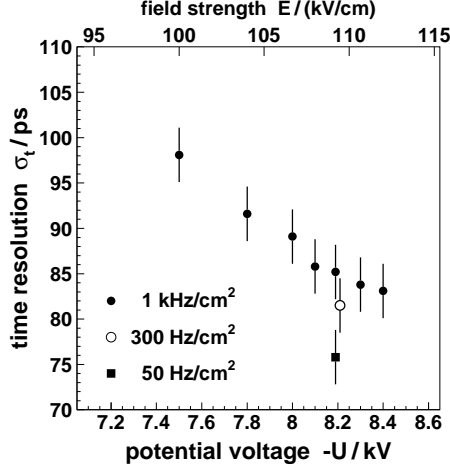
Fig. 2: *The time resolution vs. potential voltage applied to the FOPI-MRPC (bottom axis). The apparent field strength being the ratio of potential voltage over sum of gas gap sizes per detector half is provided as top axis. The various symbols indicate measurements taken at different count rates.*
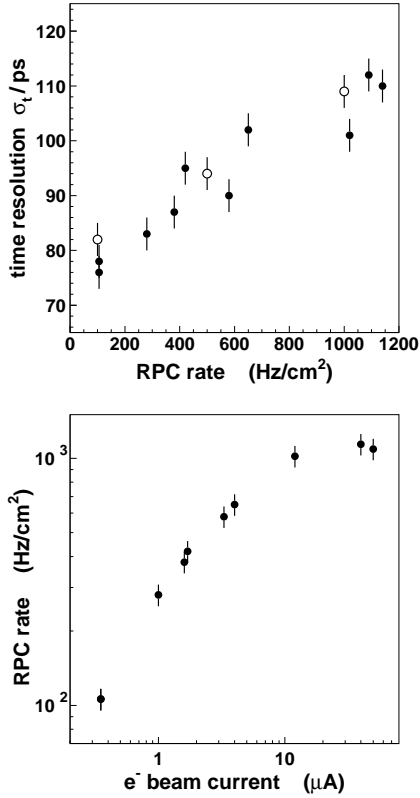
Fig. 3: *Upper panel: The time resolution vs. count rate of the FOPI-MRPC (full symbols) and of one of the IKH-MRPCs (open symbols). The apparent field strength was 110 kV/cm. lower panel: The count rate vs. primary e⁻ beam current of the FOPI-MRPC. A clear saturation effect due to signal degradation as result of the high glass resistivity is visible.*
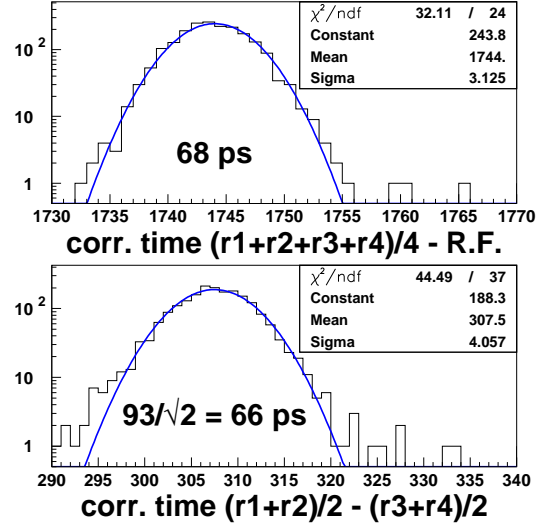
Fig. 4: *Upper panel: The mean timing w.r.t. the accelerator RF of four (time slewing corrected) signals from two strips of two identical IKH-MRPs. For the given resolution a 34 ps contribution of the TDC resolution is quadratically subtracted. Lower panel: The time resolution of the difference between the mean timing of two strips from different MRPCs.*
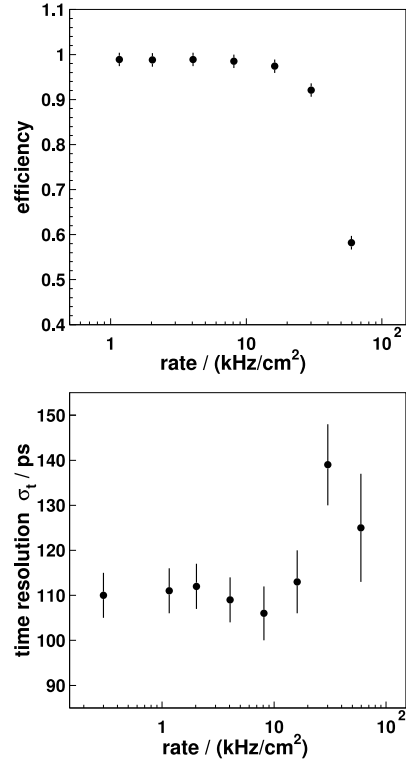
Fig. 5: *Efficiency (upper panel) and time resolution (lower panel) as a function of rate density for the INR-MRPC with low-resistivity silicate glass.*

55

Pneumatic Delivery System for Photoactivation Experiments at the Bremsstrahlung Facility at ELBE

K.D. Schilling, A. Wagner, J. Claussner,[1] M. Sobiella, M. Erhard, E. Grosse,[2] A. Hartmann, A.R. Junghans, M. Langer, C. Nair, A. Saaydi,[3] R. Schwengner, A. Seifert, J. Steiner

The photoactivation method has been introduced at ELBE [1] for the studies of p-process nuclei via (γ,n)-, (γ,p)- and (γ,α)-reactions and for the determination of energy-dependent cross sections needed as input data for nucleosynthesis network calculations.

In order to substantially reduce the limited access time of the procedure described in [2], a pneumatic delivery system has been installed at the bremsstrahlung facility of ELBE [3] allowing spectroscopic investigations of nuclei with very short half-lives.

The new system is based on the pneumatic-tube transport of the samples that are to be investigated from the irradiation position to the measurement site. The diagram displayed in Fig. 1 illustrates this new procedure. The samples are enclosed in cartridges made of polyethylene or aluminum. A stack of up to 10 of such prepared cartridges is stored in station A (cartridge magazine). The cartridges are shot by compressed air through a polyamide (PA) tube to station B into their irradiation position inside the iron casing of the electron beam dump. They are adjusted just behind the vacuum steel vessel containing the graphite electron beam stopper on the axis of the electron beam, thus utilizing the highest bremsstrahlung flux density for the activation of the samples. Immediately after the activation period, the cartridges are transported to the low-level counting setup (station C) directly onto the top of the HPGe detector inside the lead castle that shields efficiently against background radiation. The PA tube lengths between the stations A resp. C (outside the accelerator hall) and station B (inside the accelerator hall) are approximately 30 m. The transport times amount to about 3 - 5 seconds. The samples are precisely positioned on the detector to enable definite efficiency corrections. After each measurement, the cartridges are collected in a radiation shielded container (depot). The pneumatic transport is realized by a compressor and pneumatically controlled by using a diverter and several valves. The whole procedure of activation and measurement is completely automatically controlled for up to 10 cartridges. Moreover, activation and decay measurement can proceed simultaneously.

[1] M. Erhard, A. Wagner et al., IKH Annual Report 2003, FZR-401 (2004) 13

[2] M. Erhard, E. Grosse et al., IKH Annual Report 2004, FZR-423 (2005) 13, 14

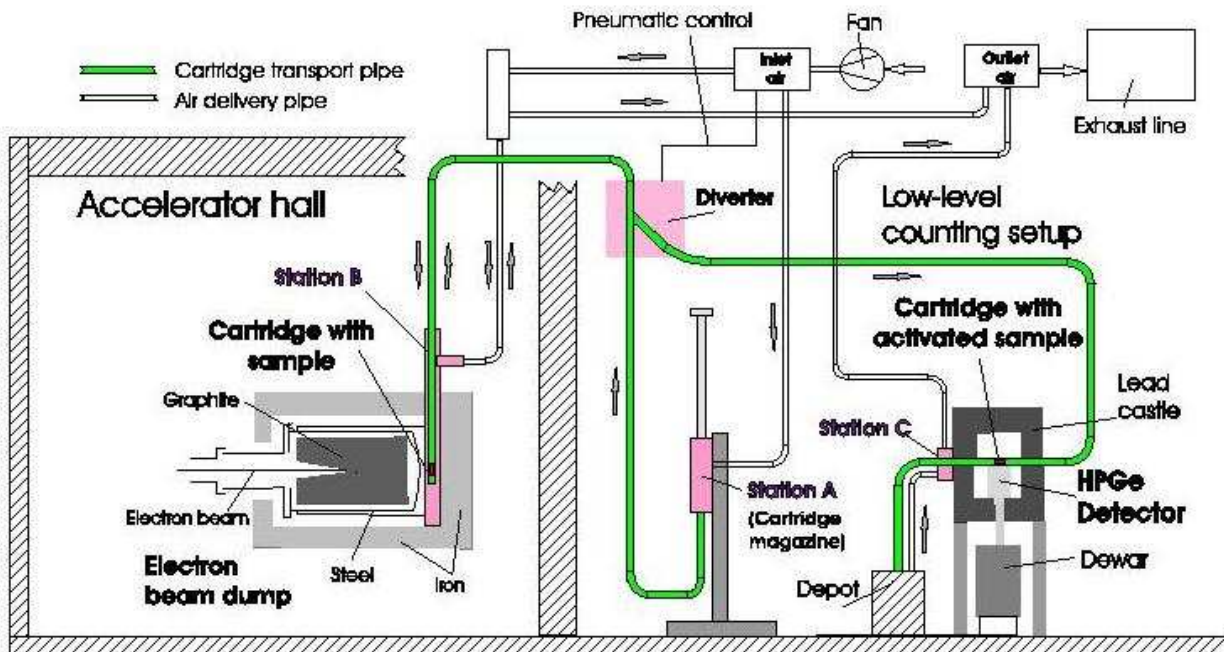[3] K.D. Schilling, M. Döring et al., IKH Annual Report 2004, FZR-423 (2005) 15

Fig. 1: *Diagram of the pneumatic delivery system for photoactivation experiments at the bremsstrahlung facility.*

[1] *FZ Rossendorf, FWF*
[2] *also TU Dresden*
[3] *FH Lausitz, Senftenberg*

The EPOS-Project at ELBE: Status Report 12/2006

G. Brauer[1], R. Krause-Rehberg[2], A. Krille[2], M. Jungmann[2]

A detailed description of the ambitious intentions to realize the EPOS project has already been published [1]. However, this realization is not straightforward and sometimes several options have to be considered and tested before a reasonable solution to a certain problem is found. The present status report intends to review our main activities - with respect to different parts of the whole system - and progress made so far. In order to convey these activities succinctly, a sketch of the EPOS positron production site, beam line, and capital equipment [1] is given in Fig.1. In detail, the following achievements can be reported:

Radiation converter: Physical details regarding the overall design of our converter have already been reported elsewhere [1]. The converter has been manufactured from a stack of 50 pieces of tungsten foil having 0.1 mm thickness, and being separated 0.1 mm from each other (Fig.2). Various housings of this converter are currently being designed and tested in order to guarantee a required cooling water flow of ≥ 13.5 l/min.

Beam dump: The dump, containing a stainless steel tube of four windings to allow the cooling water flow, was cast from high purity aluminium at Bergakademie TU Freiberg. At the face directed towards the electron beam, a stainless steel flange ring has been incorporated by electron beam welding to facilitate future mounting of the target vacuum chamber. An aluminium rack was constructed (Fig.3) to hold the heavy dump ($\sim$250 kg), which is designed at the same time for a precise positioning of the dump with respect to the electron beam axis at its corresponding location in cave 111b at ELBE.

Target vacuum chamber: Construction of a purpose-built target vacuum chamber, based on commercially available parts of radiation resistant aluminium, is underway and has been partly completed.

Vacuum tube into positron laboratory: A serious problem to be solved is how to mount this tube through the concrete channel of 3.2 m length in the basement (Fig.4). This solution requires the construction of a special movable transport system, by which the assembled pieces of the vacuum tubes can be moved step by step into this channel. An additional difficulty arises from the fact that these vacuum tubes have to carry copper wires in order to produce a magnetic guiding field for the positron beam, plus coils made of copper wire to correct for perturbing magnetic fields, like that due to the Earth and various miscellaneous stray fields.
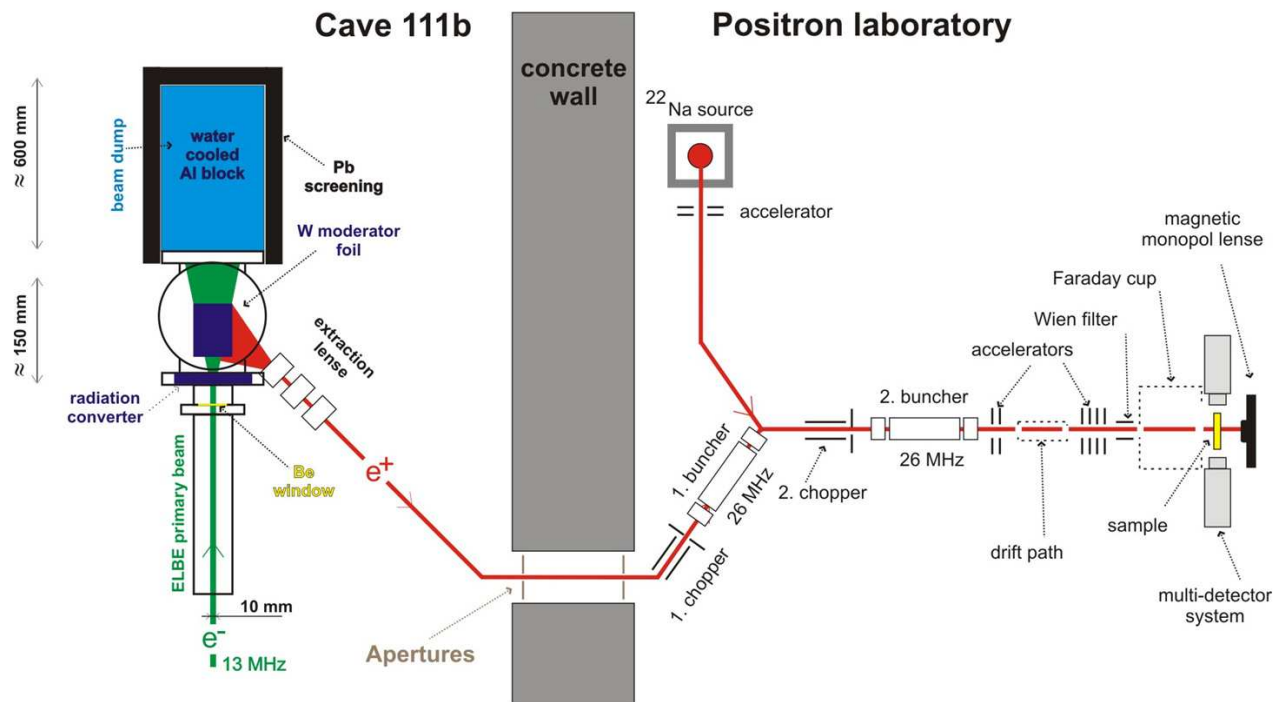
Fig. 1: *Sketch of the EPOS positron production site, positron beam line, and required capital equipment for intended experiments.*

[1] Forschungszentrum Dresden-Rossendorf, Institut für Ionenstrahlphysik und Materialforschung
[2] Martin-Luther-Universität Halle-Wittenberg, Institut für Physik, Friedemann-Bach-Platz 6, 06108 Halle/Saale
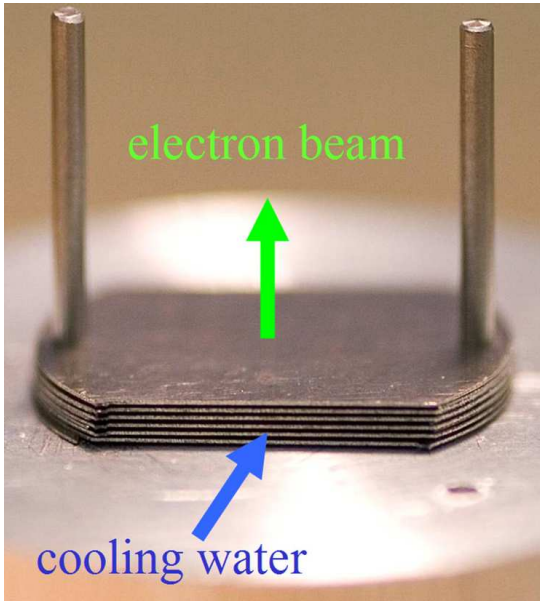
Fig. 2: *Stack of tungsten foils during mounting of the radiation converter. Directions of the intended electron beam path and cooling water flow are indicated for a better imagination.*

Fig. 3: *Aluminium beam dump on its rack (test mounting).*

Chopper/Buncher: The chopper design and its position at the vacuum tube, intended to host and guide the positron beam at its axis, has been simulated (Fig.5). This experimental setup is being built in our mechanical workshop. The electronic components needed to generate pulses required for chopper operation have been designed and are currently being built in our electronic workshop.

Multi-detector system: The energies and the temporal and spatial distributions of the positron annihilation photons carry all the required information about the materials under investigation [2]. Therefore, positron lifetime experiments using commercially available photomultiplier tubes and scintillators, and commercially available energy-sensitive high purity Ge-detectors to measure the Doppler broadening of the annihilation radiation, will be used to set up our measuring system. However, a real challenge of this system is to design and install fully digitized automation and data acquisition systems. This requires the realization of a practical client/server system via corresponding hard- and software, the latter having to be purpose-written.

To date, our efforts have been focused on the realization of positron lifetime measurements, based on a scheme as shown in Fig. 6.

The hardware will consist of a server operating the measurement setup, and four digitizers plus personal computers to collect and evaluate the data. For support, further personal computers may be added to aid the data analysis. In order to achieve a logical separation of functions and higher safety in data handling, virtualisation solutions at the server will be adopted. This will allow independent run-time environments for different tasks of network-security and administration. The software falls into two different parts: (1) server components will be required for the control of adjacencies, automation, and data storage. All these will run as a given entity at the server. (2) A client has to guarantee recording and analysis of measuring signals. In particular, optimally fast analysis of the digitizer output signals has to be performed in order to transfer only the results of this process to the server for further storage.

A prototype of client software has already been written and tested using the output signals of a conventional positron lifetime setup at the Martin-Luther-University Halle-Wittenberg. In Fig. 7, the time resolution curve of such a setup, measured by use of gamma rays from a ^{60}Co source, are presented.
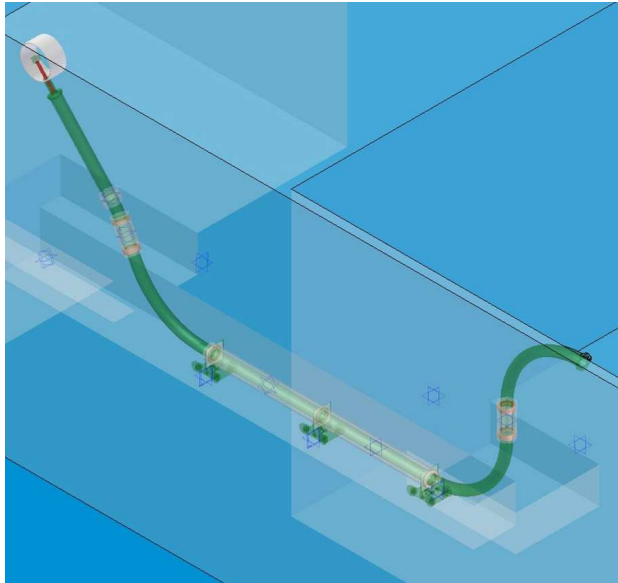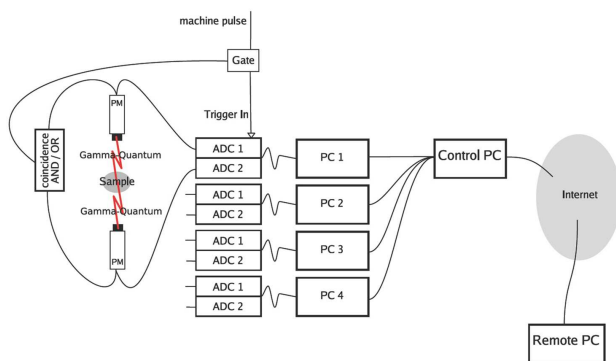
Fig. 4: *Simulation of the vacuum tube construction intended to guide the positron beam into the future positron laboratory.*
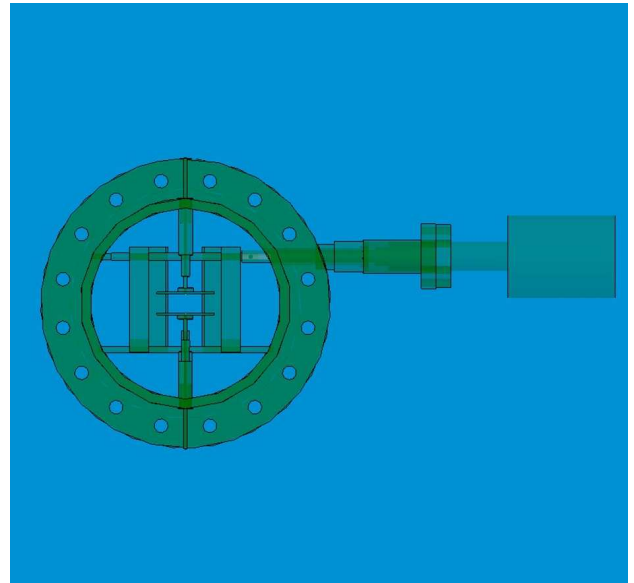
Fig. 5: *Simulation of the chopper design and its position at the vacuum tube intended to guide the positron beam.*

Using analogue electronic components only, a time resolution – as defined by the Full Width at Half Maximum (FWHM) – of ∼200 ps is achieved. It has already been shown that by digital processing of all signals a substantial improvement is possible, as seen from a measured FWHM of ∼167 ps.

[1] R. Krause-Rehberg, S. Sachert, G. Brauer, A. Rogov, K. Noack, Appl. Surf. Sci. 252 (2006) 3106.
[2] R. Krause-Rehberg, H. Leipner, Positrons in Semiconductors – Defect Studies, (Springer, Berlin, 1999).

Fig. 7: *Time resolution spectrum measured using a ^{60}Co source.*

Fig. 6: *Block diagram of the wired multi-detector system for positron lifetime measurements.*

An intense Channeling Radiation Source at ELBE

W. WAGNER, J. PAWELKE M. SOBIELLA, J. STEINER,

A powerful nonconventional X-ray source basing on the production of channeling radiation (CR) in a diamond crystal [1] has been installed at the Radiation source ELBE. The brilliant cw electron beam with an average current of $100\,\mu A$, available in the radiation physics cave, allows to reach photon rates of quasi-monochromatic CR of the order of $10^{11}\,s^{-1}$ per band width of about $10\,\%$. The CR energy can be tuned within an interval from ≈ 10 to ≈ 70 keV by variation of the beam energy.
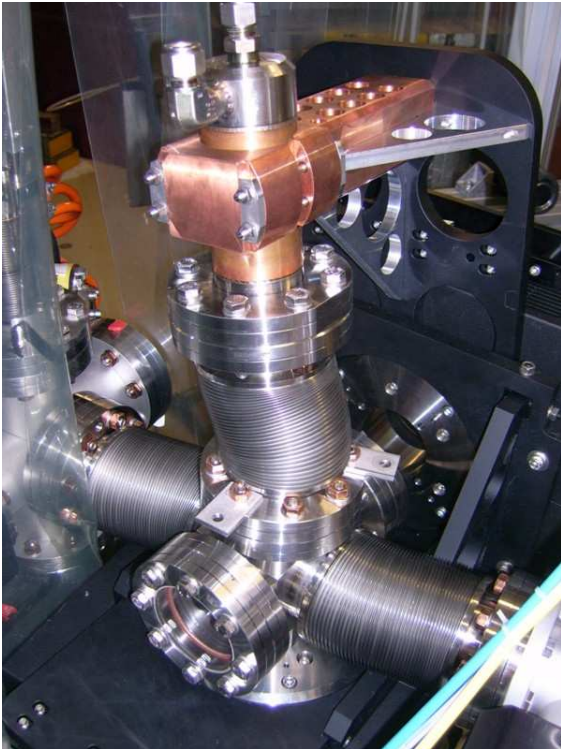

Fig. 1: *Goniometer of the intense CR source at ELBE.*

The core of the X-ray source is a newly constructed remotely controlled goniometer for the target alignment with respect to the beam axis. While the water-cooled target used for radiation production is situated inside the UHV beamline of ELBE, its 3-axes movement is realised by means of external precision motion-systems. Target cooling is necessary for the dissipation of the incidental heat induced by beam energy losses.

The inventive principle of the goniometer bases on the application of three bellows, which are fixed to a small vacuum chamber. The chamber is mounted to a linear stage, which enables its transversal positioning relative to the beam. By means of two rotary stages, a cooling finger extending into the chamber can be rotated around two perpendicular axes, the intersection of which coincides with the beam axis. In this way, an alignment of the crystal is possible in two planes within angular intervals of $\pm 5^{o}$ and with an accuracy

of adjustment of 0.05^{o}. The cooling finger carries two targets, one for the production of bremsstrahlung to be applied for irradiation purposes, and one for the generation of intense CR. A third free position is foreseen for the undisturbed beam setting. The mode of operation of the goniometer is demonstrated in Fig. 1. During commissioning of this new X-ray source, bremsstrahlung as well as quasi-monochromatic planar CR have been produced at average beam currents up to $\approx 70\,\mu A$. The CR has been generated by the 1-0 transition of 14.6 MeV electrons channeled along the (110) plane of a $150\,\mu m$ thick diamond crystal.

Since conventional X-ray spectrometers are unable to operate at the expected extremely high counting rates, a Compton spectrometer has been utilised for the on-line monitoring of the intense CR. A 0.5 mm thick PVC Compton scatterer could be moved into the narrow CR cone outside the beamline behind a thin Be-window. For the registration of the radiation, a Si-pin-diode was placed 1 m away from the scatterer under an angle of 90° with respect to the primary direction of CR inside a 20 cm thick Pb collimator of $\varnothing 3\,mm$. Additional action for shielding of the sensitive detector against the huge amount of background radiation inside the cave has been taken. A measured Compton spectrum of the CR is shown in Fig. 2.
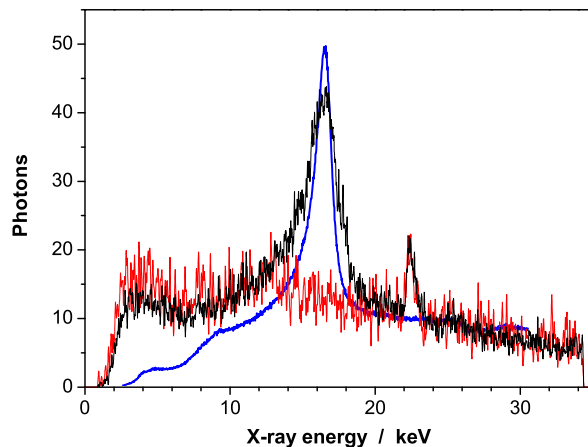
Fig. 1: *Spectra of CR from 14.6 MeV electrons channeled in the (110) plane of diamond. The blue thin-lined spectrum has been registered in forward direction at a beam current of 11 nA and was scaled by a factor of 3×10^{-7}. The thick black-lined Compton spectrum represents the same CR but produced at a beam current of $70\,\mu A$. The corresponding bremsstrahlung background is drawn in red.*

This method enables the checking of the performance of the crystal during CR production at high beam currents.

[1] W. Wagner, B. Azadegan, J. Pawelke, IKH Annual Report 2005, FZR-442 (2006) p. 64

Radiation Background Measurement at the ELBE Channeling X-Ray Beam Line

J. Pawelke[1], B. Naumann[2], W. Wagner[1]

Reliable studies of radiobiological effects on living cells need a maximum irradiation dose rate of about 1 Gy/min and a sufficiently low level of radiation background at the irradiation site. The production of channeling radiation (CR) at ELBE as a source of quasi-monochromatic soft X-rays with the necessary high intensity requires an electron beam of about 100 μA current. Five air-filled ionisation chambers (IC) were placed around the CR beam line (Fig. 1) and the photon background dose rate $\dot{D}_\gamma$ has been measured by two Farmer IC (position I and II), two rigid stem IC (position III and IV) and an LB6701 IC (position V) [1]. In addition, the neutron background dose rate $\dot{D}_n$ was measured with a BF$_3$ counter (2202-D, Alnor, Turku, Finland) at position VI.
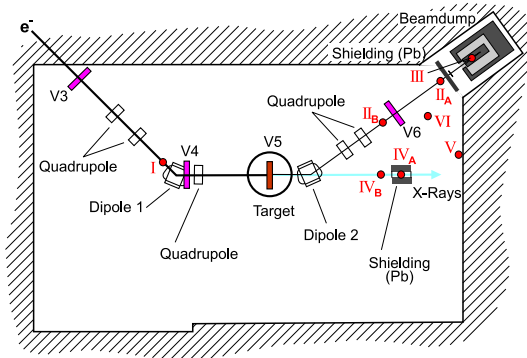

Fig. 1 *Position of the ionisation chambers in the radiation physics cave. The electron beam comes from the accelerator (left) and is stopped in the dump (right).*

After tuning the electron beam of 14.6, 22.5 and 30.0 MeV, respectively, up to 200 μA current, dose rates were measured without any target in the beam (#1). The measurement was repeated after an 18 μm thick Al foil was inserted into the beam at target position V5 in order to study the influence of electron scattering in the target on the beam loss, and corresponding generation of radiation background. The Al foil has been chosen for practical reasons and results in a roughly comparable electron scattering as the thicker

diamond crystals used for CR generation. Upon entering the cave and moving IC II and IV from position A to B the dose rates were measured again (#2) for both cases (with and without target in the beam).

Without passing a target the electron beam can be transported to the dump without loss (see Table 1) which results in a very low level of radiation background at the cell irradiation site (cf. position II$_B$, IV$_A$ and V). In contrast, the electron scattering in the target results in a considerable beam loss and a corresponding overall rise of the radiation background level. However, the commissioning of the second LINAC section at ELBE not only allowed to increase the electron energy up to 35 MeV but also to reduce the radiation background level by more than one order of magnitude at low electron energy (cf. Table 1 with the dose rates reported in [1] for 17.0 MeV). Also, the high photon radiation intensity at the cell irradiation site is mainly caused by bremsstrahlung generated in the target and emitted in forward direction of the electron beam. Only a small bremsstrahlung contribution of about 5 % generated at the beam line reaches the irradiation site (Fig. 2) and the neutron dose contribution is even smaller. Therefore, in a next step the irradiation of cells is prepared.
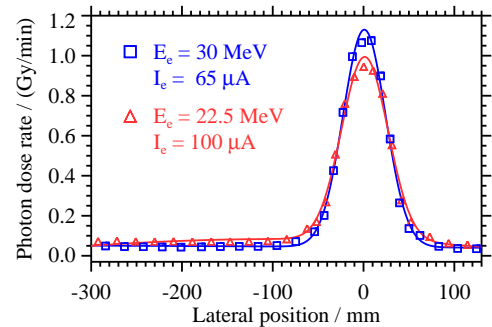
Fig. 2 *Horizontal dose profile measured at position IV$_B$ for the 18 μm thick Al target.*

[1] J. Pawelke, U. Lehnert et al., Radiation Source ELBE Annual Report 2003/04, FZR-428 (2005) 38

Tab. 1 *Comparison of dose rates at different positions measured for an electron beam current of 100 μA.*

E_{e-} /	Target	Photon dose rate $\dot{D}_\gamma$ / (mGy/min)									$\dot{D}_n/$(mSv/h)	
		I		II$_A$	II$_B$	III		IV$_A$	V		VI	
MeV		#1	#2	#1	#2	#1	#2	#1	#1	#2	#1	#2
14.6	no	<0.6	<0.6	990	<0.6	17.1	17.4	<1.3	2.1	2.2	3.2	3.3
	18 μm Al	<0.6	<0.6	11900	630	20.8	24.1	363	32.3	34.3	7.3	7.0
22.5	no	<0.6	2.6	685	<0.6	33.6	33.1	<1.3	0.9	0.9	23.3	21.7
	18 μm Al	<0.6	3.2	8710	2020	42.0	47.5	961	108.4	81.4	63.3	80.0
30.0	no	1.8	6.5	556	<0.6	37.6	37.2	<1.3	0.7	0.7	96.6	104.3
	18 μm Al	2.3	2.8	3382	3281	47.8	63.1	2040	20.5	132.1	200.0	208.1

[1] FZD, Institute of Radiation Physics
[2] FZD, Department of Safety and Radiation Protection

First Experiments on In-Beam PET at Hard Photon Beams

D. Möckel[1], T. Kluge[1], J. Pawelke[1], M. Sommer[2], E. Will[3], W. Enghardt[4]

Since there are good experiences with in-beam PET for quality assurance in carbon ion therapy [1] it is highly desirable to extend this method to other radiation treatment modalities. For example, in-beam PET seems to be feasible for high energy photon irradiation with energies above ~ 20 MeV because of the generation of positron emitters ^{11}C and ^{15}O in tissue by (γ, n) reactions as already shown in simulations [2].

First quantitative results on the activation of phantoms at hard photon beams were obtained by performing off-beam PET experiments. Homogeneous PMMA phantoms were irradiated with high energy photons. After the irradiation the distribution of the generated positron emitters in the phantom was measured using the PET scanner Siemens ECAT EXACT HR+. Furthermore, the depth dose distribution was measured by means of optically stimulated luminescence detectors (BeO).

For the experiments an electron beam at ELBE with a current of $\sim 70\,\mu$A and different energies $E = \{21, 23, 25, 30, 34\}$ MeV was used to generate bremsstrahlung in a $18\,\mu$m thick Al target. The accelerator was operated in the continuous wave mode at a frequency of 13 MHz.

The activity determined by PET was recalculated to the end of the irradiation. Only the annihilation photons of positrons emitted by ^{11}C were detected because of the ~ 30 min time interval between the end of the irradiation and the start of the PET measurement, which corresponds approximately to 15 half-lives of ^{15}O and 1.5 half-lives of ^{11}C.

By dividing this recalculated activity concentration and the measured dose of the BeO detectors the dose related activity concentration was calculated, showing the approximate proportionality between activity and dose outside the dose buildup region. In Fig. 1 one example is shown for an electron energy of 34 MeV.

Increasing the electron energy results in a rising of the generated activity. Energies larger than ~ 23 MeV are required to obtain a sufficient amount of positron emitters.

A remarkable increase of the measured activity is expected if also ^{15}O is detected. Therefore, an in-beam measuring setup at ELBE has been built up combining irradiation and measurement [3]. Higher activity concentrations are determined in comparison to the off-beam PET experiments depending on the oxygen content. Furthermore, a good contrast between materials with various density values and stoichiometry are achieved (cf. Fig. 2).
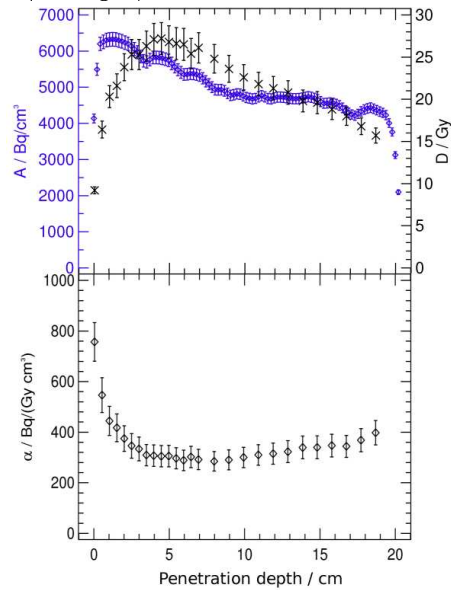
Fig. 1 *Depth dose distribution D and ^{11}C activity concentration A (top) as well as dose related activity concentration α (bottom) in dependence on the penetration depth in a PMMA phantom at the end of the irradiation ($E_{e^-} = 34\,MeV$).*

[1] W. Enghardt, P. Crespo et al., Nucl. Instr. Meth. A 525 (2004) 284
[2] H. Müller and W. Enghardt, Phys. Med. Biol. 51 (2006) 1779
[3] D. Möckel, T. Kluge, J. Pawelke, W. Enghardt, ISP Annual Report 2006, FZD-61
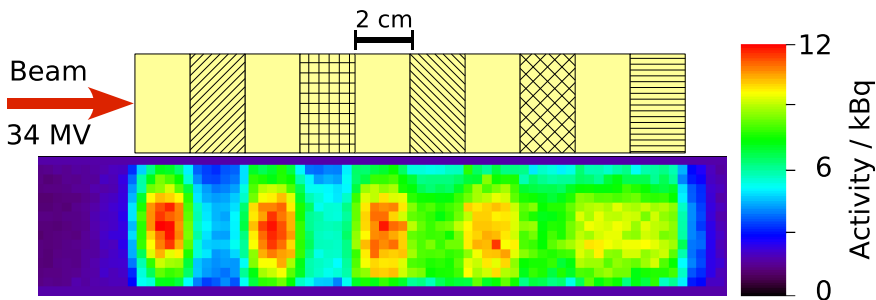
Fig. 2 *Schematical illustration (top) as well as two-dimensional distribution of the generated positron emitters (^{11}C and ^{15}O) in an inhomogeneous phantom for an electron energy of 34 MeV (bottom).*

[1] *FZD, Institute of Radiation Physics*
[2] *TU Dresden, Institute of Nuclear and Particle Physics*
[3] *FZD, Institute of Radiopharmacy*
[4] *TU Dresden, Medical Faculty*

The ELBE Free-Electron Lasers

With the second accelerator stage of ELBE installed at the beginning of year 2005, electron beam energies up to 32 MeV are possible in routine operation making the whole wavelength range of the U27 mid-IR FEl from 4 to 22 μm available. Both in-house as well as external users showed great interest in beamtime at the ELBE FEL which, since February, 2006, is distributed under the framework of FELBE being a member of the IA-SFS of the 6th EU program.

In August, 2006, first lasing of the long-wavelength FEL (U100) was demonstrated. First user experiments could be performed in fall, 2006, already. By now, the whole wavelength range from 20 μm up to 150 μm is routinely available. Lasing has been shown up to 200 μm wavelength.

Major improvements were achieved in the FEL operation. The IR diagnostic station ist now partially remote-controlled supporting short tuning times for the FEL setup. Scanning the FEL wavelength by varying the undulator gap has been automized. A lot of measurements have been done to characterize the IR beam.

There is a broad range of experiments now being performed at ELBE. The main fields of research include the semiconductor physics (ground state vibration population decay, experiments to determine the relaxation times of superlattices or self-assembled quantum dots) and biophysics (IR-induced changes in thin DNA films). Further experiments were performed in environmental and safety research (photothermal beam deflection at actinides), experiments on ellipsometry and nearfield microscopy.

Remote Controlled IR-Diagnostic station for the Rossendorf FELs

W. Seidel, R. Jainsch[1], M. Justus, K.-W. Leege[1], D. Proehl[1], H. Weigelt, D. Wohlfarth

Starting in the summer 2005, FEL beam time has been offered to external users in the frame of the EC funded "Integrating Activity on Synchrotron and Free Electron Laser Science" (FELBE project [1]). It is of great importance for routine user operation at ELBE that, after changing the beam path or after beam interruptions stable operation in all wavelength ranges can be provided within a short time (some minutes). Extensive diagnostics for the optical components of the FEL are very important to achieve fast availability.

We have developed an optical beam diagnostic system (see Fig. 1) to properly characterize and adapt the output of the two FELs (U27 and U100). The present system is compatible with a tuning range from 3 μm to 150 μm, and can be extended beyond 150 μm, if necessary.

The FEL beam from each undulator will be transported separately from the resonator to the diagnostic area through beam pipes using reflective optics. Both lines will be merged on the diagnostic table, which may be purged with dry nitrogen to avoid absorption in air, if necessary. From here both beams follow the same path.

Two flipper mirrors may deflect the beam in a bypass to a plasma switch which reduces the repetition rate from 13 MHz down to 1 kHz (first results see [6]). The switch is based on the principle of photo-induced reflectivity of an optically excited electron-hole plasma [3, 4]. In this way, subsequent FEL micropulses are selected out of the 13 MHz pulse train. An additional focusing mirror ensures the same beam parameters as the direct beam has.

From the main beam, approximately 1-5 percent of the total power is separated by a scraper mirror on a translation stage for wavelength measurement and power monitoring.

The transmitted beam passes an attenuator and can be delivered to 6 optical laboratories. In this attenuator precisely fabricated metal grids diffract a calibrated percentage of power (3, 5, and 3 × 10 dB) out of the beam. The rejected light is absorbed in the walls of the housing. The mode structure and other properties of the transmitted beam including the divergence and the M^2 parameters are fully preserved, the polarisation as well [7]. Finally, a non-collinear background-free autocorrelator system is used to determine the length of the ultrashort FEL pulses. We use a CdTe crystal as SHG medium [2, 5] since it is transparent for a wide wavelength range in the infrared.

The part of the beam deflected by the scraper mirror goes through a synchronized chopper for measurement in CW-mode. Next to this, the outcoupled beam is deflected by a mirror or a diamond beam splitter (350 μm thick, under 45 degrees, deflection 15 %) at a pneumatic translation stage (this part of the diagnostic is described in detail in [8]). The beam transmitted through the diamond beam splitter (85 %) is transported to the spectrometer. The spectrum is measured with a Czerny-Turner type spectrometer which contains a turret with three different gratings to cover the whole wavelength range from 3 μm to about 200 μm. In the near future the monochromator will be equipped with a 48-channel pyroelectric linear array detector. We use the second side-exit slit equipped with a single Hg-Cd-Te or Ge-Ga detector for measurements with higher sensitivity.
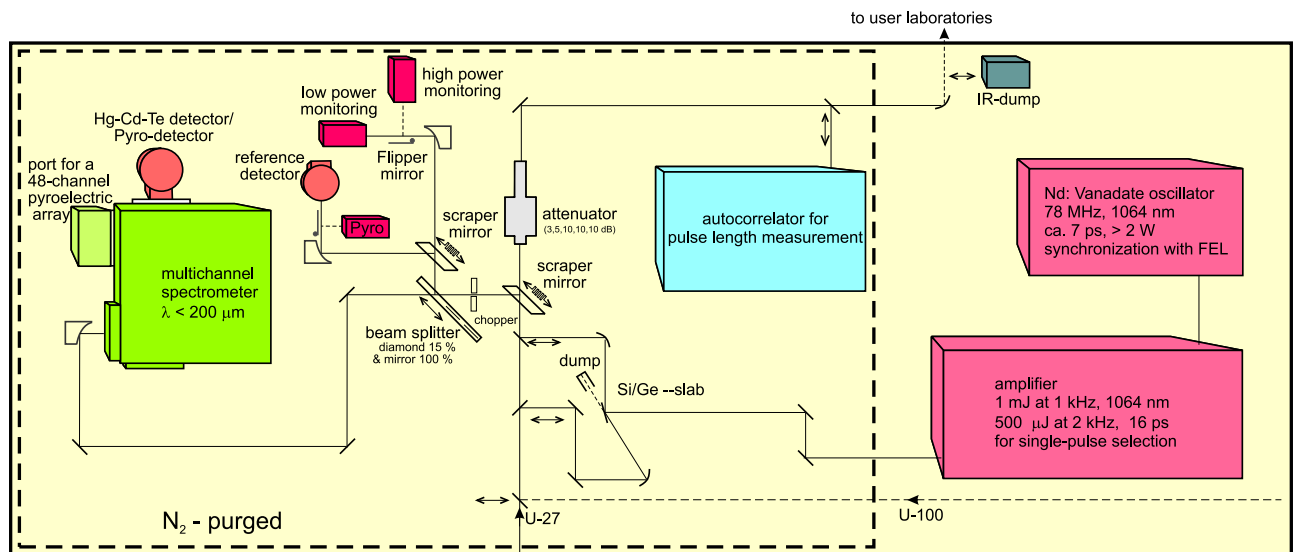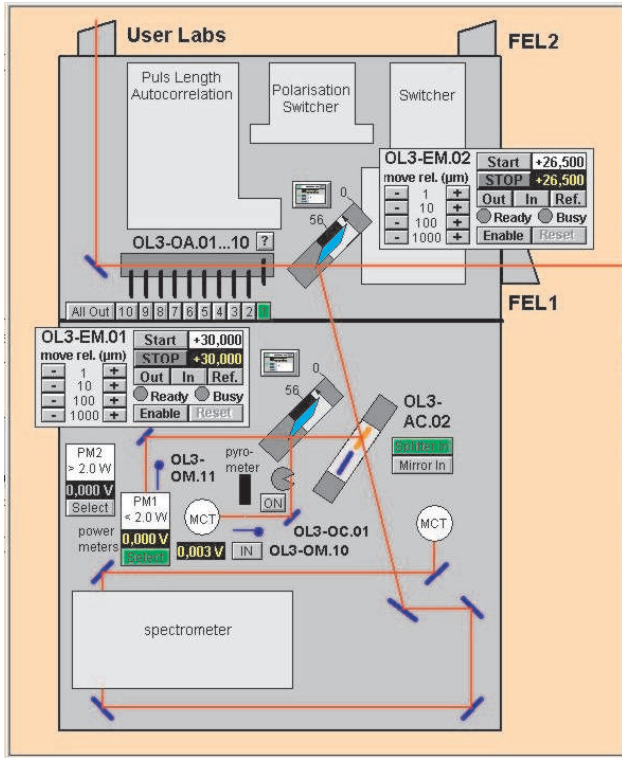

Fig. 1: *Arrangement of the different optical components and devices on the table.*

[1] Department of Research Technology

The part reflected from the pneumatic device is distributed with another scraper mirror and two flipper mirrors to different power meters (<2 W and >2 W) and reference detectors (Hg-Cd-Te and pyro-Detektors) for monitoring the lasing process (see Fig. 2).


Fig. 2: *Interface of the remote controlled part of the IR-diagnostic station. One attenuator, two scraper mirrors on stepper controlled stages, one mirror and one beam splitter on a common pneumatic stage, spectrometer and different power meters are indicated. The red lines show different paths for the radiation when both scraper mirrors are not entirely within the beam.*

The FEL diagnostic instrumentation has been integrated into the existing Programmable Logic Control (PLC) and Human-Machine-Interface (HMI) environment of ELBE (see Fig. 3). It ensures the access both for operators and users of the FEL. The basic technologies are the WinCC server/client system, the SIMATIK PLC system and distributed I/O by Beck-hoff Automation for controlling the pneumatic components (i.e. attenuators), analogue data logging (FEL power, MCT) and other instrumentation. The stepper control drivers for the scraper mirrors are integrated system components, whereby expensive separate controllers could be avoided.

[1] http://www.fzd.de/felbe
[2] J. Xu et al., Opt. Comm. 197 (2001) 379-383
[3] P. Haar, Ph.D. thesis, Stanford University (1996)
[4] E.H. Haselhoff et al., Nucl. Instr. and Meth. A358 (1995) ABS28
[5] W. Seidel and D. Stehr, Pulse length this Report
[6] W. Seidel and S. Winnerl, Switch this Report
[7] F. Keilmann, SPIE Vol. 666 (1986) 213
[8] H. Weigelt, Diplomarbeit, Hochschule Mittweida, 2006
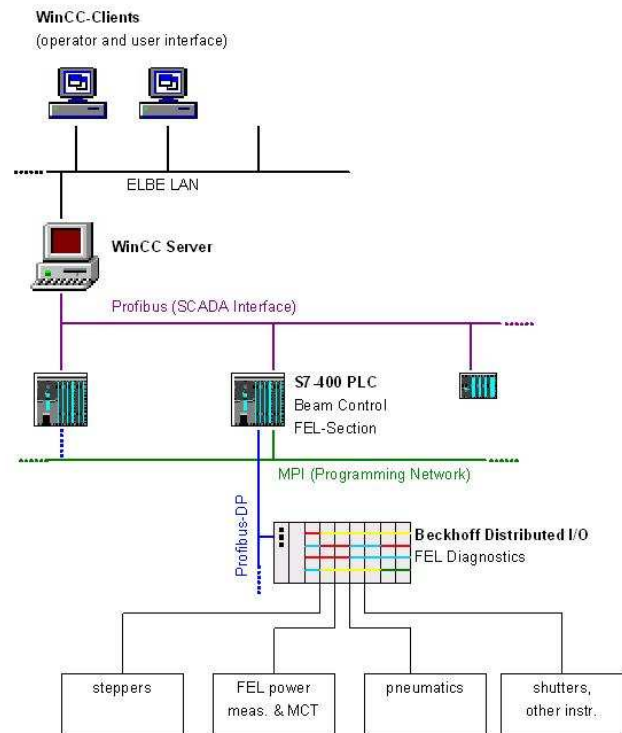
Fig. 3: *The programmable Logic Control (PLC) and Human-Machine-Interface (HMI) environment of ELBE with the integrated FEL diagnostics instrumentation.*

# Laser Gain and Intra-Cavity Losses of the ELBE mid-IR FEL

U. Lehnert, P. Michel, W. Seidel[1], J. Teichert, R. Wünsch[1]

Introduction

The U27 mid-IR FEL of the ELBE radiation source was designed to cover a wavelength range from 3 to 20 μm. The optical resonator is equipped with two spherical mirrors with a free propagating optical mode of fixed Rayleigh length. Therefore, the optical mode size at the mirrors shows a big variation over the whole wavelength range. To achieve a suitable outcoupling different sizes of the outcoupling hole are required. The mirror chamber containing the outcoupling mirror was designed with a mirror wheel which allows to choose between 5 different mirrors. At present outcoupling holes from 1.5 to 4 mm are available. Now, the fraction of outcoupling can be adjusted to ensure the needed laser gain and to optimize the outcoupled laser power.

Gain and Loss Measurements

For measurements of the laser gain and round-trip losses of the optical cavity we switch off the electron beam for a 10 μs period. An MCT detector with a fast readout electronics is used to measure the decay and rise of the optical power (see Fig. 1). The decay can easily be fitted by a single exponential giving the optical losses per round-trip.
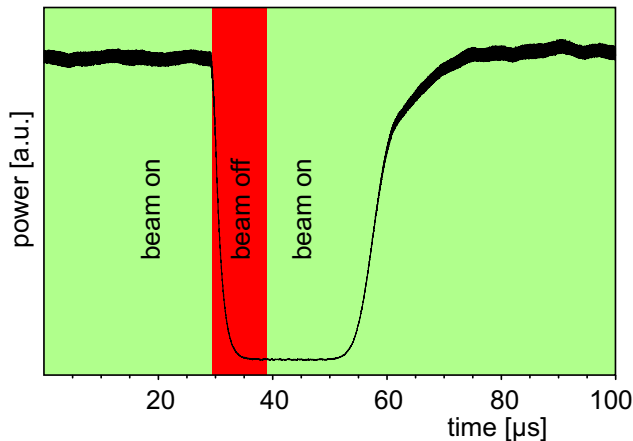

Fig. 1: *Decay and rise of the optical power caused by a 10 μs break of the electron beam.*

Round-Trip Losses

Round-trip losses inside the optical cavity were computed using the GLAD [1] code (see Fig. 2). The computation (totals shown with red triangles) includes the outcoupling of optical power (blue circles) as well as diffraction losses due to the aperture limits of the optical beam path in particular inside the undulator. The amount of outcoupling very well agrees with a simple geometrical model (blue line) except for very short

wavelengths where the optical mode has a tendency to avoid the outcoupling hole. The latter effect was seen experimentally as well. At 5 μm wavelength the measured losses were significanly smaller when using the 3 mm outcoupling hole than with the 1.5 mm or 2 mm holes. In general, the measured round-trip losses show a quite reasonable agreement with the computation.
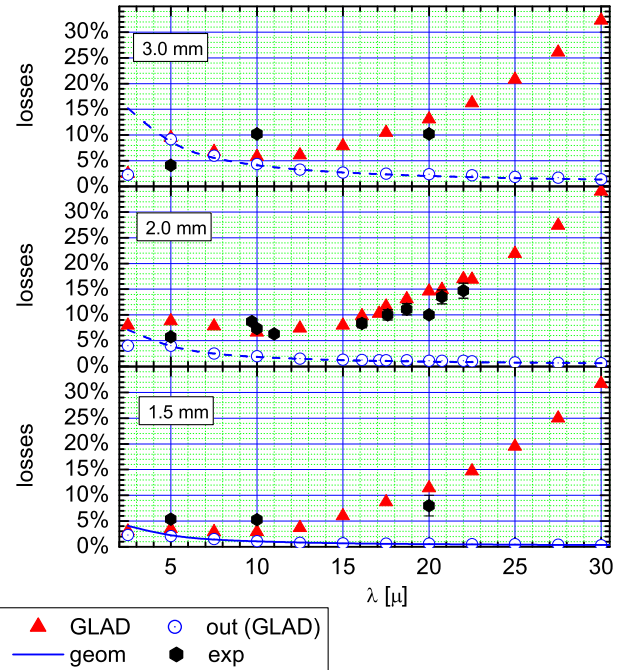

Fig. 2: *Comparison of measured and computed values of the round-trip losses inside the FEL resonator.*

Laser Gain and Power

The rise of the optical power is determined by the net laser gain. However, the rise curves shown in Fig. 1 need a more involved analysis as the gain itself depends on the optical power. We use a simple analytical model (see Fig. 3) to simulate the gain drop at high powers caused by over-bunching and wave-breaking effects. This model very well fits the measured curves of the laser turn-on as shown in Fig. 4. In the example shown we have a 6% small-signal gain over 7% round-trip losses. The laser saturates at 50 MW optical power. At this point the gain has dropped to just match the losses.

---

[1] FZD, Institut für Strahlenphysik
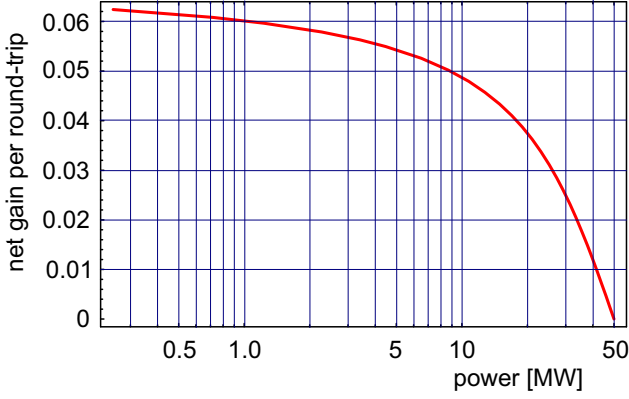
Fig. 3: *Analytical model of the gain drop at high laser powers approaching saturation.*
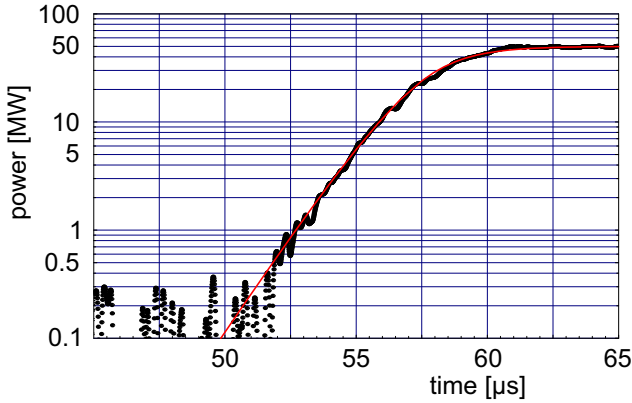
Fig. 4: *The rise of the optical power computed from the model in Fig. 2 very well fits the measured power data.*

The Optimal Outcoupling

The measurements performed at 10 μm wavelength demonstrate that there exists an optimal outcoupling hole for a given cavity and beam setup. The data

shown in Table 1 were measured with a 22 MeV electron beam with 50 pC bunch charge. The round-trip losses roughly correspond to the computed ones considering that the losses at the mirror surfaces are not included in the calculations. Going from 1.5 mm to 2 mm outcoupling hole size one sees the expected rise of the losses (approx. 2%) due to the outcoupling and the increased diffraction losses at the hole. At this power level the gain changes quite rapidly with the power. So the needed 2% higher gain translates only into a small drop of the intra-cavity power. The outcoupled power is increased. But when going further to 3 mm hole size the increased losses yield a much lower saturation power inside the cavity. Despite the higher outcoupling fraction the outcoupled power drops. The measured power levels again roughly confirm the gain model shown in Fig. 3.

[1] GLAD, Applied Optics Research, Woodland, WA 98674, USA.

Table 1: Parameters of the optical resonator of the U27 FEL measured at 10 μm wavelength for different sizes of the outcoupling hole. The intra-cavity power is estimated using the computed fraction of outcoupling. To scale it to the saturation power a pulse length of 2 ps was assumed which was previously measured for a minimum-detuning setting of the optical resonator.

| out-coupling hole size	1.5 mm	2.0 mm	3.0 mm
measured average power	16.8 W	24.8 W	13.9 W
measured round-trip losses	5.25 ± 0.25 %	7.25 ± 0.25 %	10.0 ± 0.6 %
computed round-trip losses	2.9 %	6.6 %	5.8 %
out-coupled fraction	1.1 %	2.0 %	4.4 %
average intra-cavity power	1600 W	1300 W	330 W
intra-cavity saturated power	62 MW	50 MW	13 MW

68

Spectral Width and Duration of the IR-Pulses from FELBE

W. Seidel, D. Stehr[1]

From a user's perspective, the three valuable characteristics of the free electron laser FELBE (among the wavelength range) are its peak power, variable picosecond optical micropulse length, and variable transform limited spectral bandwidth. Precise control of the FEL optical pulse has been essential for many time-resolved measurements performed at FELBE. The optical pulse length can sensitively be tuned by varying the FEL resonator length with respect to the nominal length resulting from the electron bunch repetition rate. At minimum detuning one yields the highest saturated power and the shortest optical pulse length. By detuning the resonator, the spectral width can be decreased simultaneously increasing the pulse length.

To characterize the ultrashort pulses generated by the FEL we built a non-collinear background-free autocorrelator system. We used a CdTe crystal as SHG medium [1], since it is transparent for a wide wavelength range in the infrared. We measured the autocorrelation function at maximum power in the detuning curve at a wavelength of 11.09 μm (see Fig. 1) generated in the FEL-U27 [2].

We deduced a pulse duration of 0.89 ps (FWHM), assuming a Gaussian temporal pulse shape. The measured FWHM of the spectrum is approx. 176 nm (corresponding to a relative spectral width of 1.6 %). The calculated time-bandwidth product is about 0.4 which indicates Fourier-transform limited operation. Long IR pulses with narrow bandwidth can be obtained
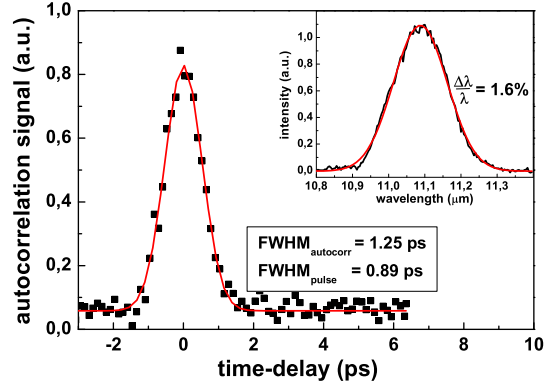
Fig. 1: *Autocorrelation trace and the corresponding FWHM of the wavelength (inset) of 11 μm at maximum of the detuning curve of the FEL-U27.*

from a detuned U27 resonator (pulse duration of 3.4 ps with 0.4 % bandwidth).

First pulse length measurements and corresponding spectra at different detuning points of the FEL-U100 [3] are shown in Fig. 2. Here we deduced the pulse duration by assuming a sech^2 temporal pulse shape, in contrast to a Gaussian pulse shape for the U27.

[1] J. Xu et al., Opt. Comm. 197 (2001) 379-383
[2] W. Seidel, IKH Annual Report 2004, FZR-423(2005)60
[3] Th. Dekorsy et al., IKH Annual Report 2004, FZR-423(2005)65
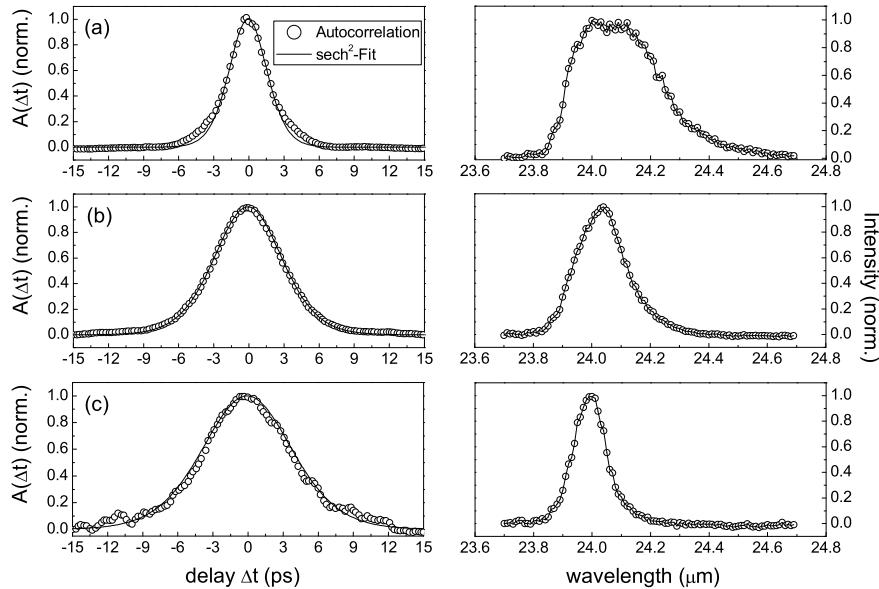
Fig. 2: *Autocorrelation functions (left) and the corresponding spectra (right) for 24 μm radiation at three different detuned resonator lengths of the FEL-U100 (a: ΔL=-2 μm, $FWHM_{pulse}$=2.5 ps; b: ΔL=-14 μm, $FWHM_{pulse}$=4.4 ps; c: ΔL=-24 μm, $FWHM_{pulse}$=5.8 ps).*

---

[1]Institute of Ion Beam Physics and Materials Research

PLC-based Control System for the U100 Optical Cavity

P. Michel

Technical Requirements

A computer based control system was needed for the long wave (20 - 150 $\mu\mu$m) Free Electron Laser U100 [1]. This system would remotely control actuation of the cavity mirrors, the cavity length as well as optical cavity mirror alignment. To optimize the out-coupled infrared laser power, different mirrors with same curvature but different out-coupling hole diameters are required. Therefore the control system also contains a linear mirror drive with three different mirrors (out-coupling holes 2, 4.5 and 7 mm). The required alignment tolerances for the optical cavity, both the high reflector and the out-coupler, pitch and yaw are a few μrad, additionally the mechanics and drive control must be appropriate for this extreme high accuracy. An alignment laser is in-coupled through the out-coupler mirror's hole for this procedure. By using several insertable reference marks and beam position monitors the alignment laser spot can be used to align the optical cavity mirrors before lasing is attempted with the FEL. In order to rapidly change from one machine configuration to another (e.g. FEL wavelength change) at ELBE all important machine data are stored and can be reloaded again if necessary. Therefore the pitch and yaw angles of the mirrors, the transverse out-coupling mirror position and the length of the optical cavity must be available as absolute data with respect to the fixed coordinate system of the FEL. Another important requirement is the stabilization of the optical cavity length. Thermal drift deviations of the optical cavity mirror spacing can be 10 μm per day. Since the laser only works within a cavity length interval of a few μm, this length must be kept constant automatically to ± 1 μm. The measurement of relative longitudinal deviations is done by means of interferometer lasers. The correction of the mirror spacing is realised by a longitudinal motion drive on one of the cavity mirrors. The control loop to stabilize of the cavity length is also a part of the described control system. Fig. 1 shows the elements of the U100 FEL optical cavity.

Main hardware architecture

The control system is based on a programmable logic controller (PLC) OMRON CJ1 with modular input and output units for analog, binary and serial digital signals. The data exchange with the central SIMATIC PLC based ELBE control system has been implemented by using the profibus DP interface. For the autonomous operational controls, all functions can be executed via an OMRON touch terminal NT631 C. Operation of this system via the local terminal is useful during commissioning of the drives. This flexibility in both local and remote control of the optical cavity enables the operator to rapidly respond to unexpected or possibly dangerous situations. Fig. 2 gives an overview of the control components for the optical cavity.
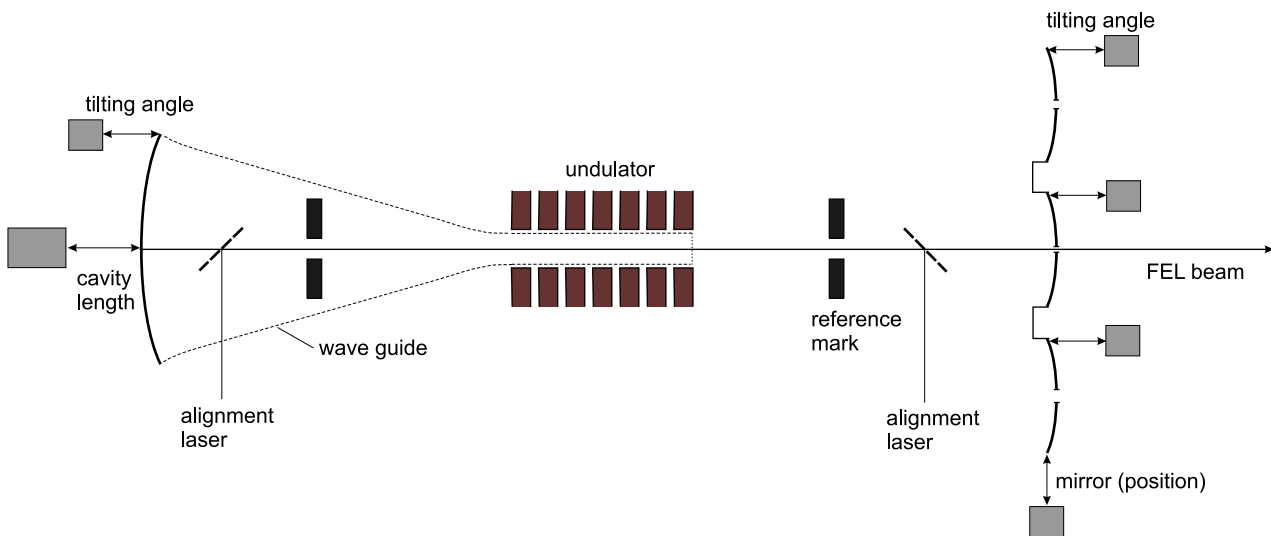

Fig. 1: *Optical cavity of the U100 FEL with actuators for mirror and cavity length motion.*

Mirror position and mirror change in mirror chamber 1 (MC1)

The three mirrors are mounted on a linear translation stage. It is driven by an 800 W step motor with integrated encoder for position detection of the motor axis. The measurement of the mirror position is done by an external linear encoder (glass scale). The motor is autonomously steered and monitored by an Omron motion controller (MCW151) and Omron SHDH-08AE servo drive unit. The connection to the PLC is made by RS422 (115bps). The positioning accuracy corresponds to the smallest division of the encoder and amounts to 0.1 μm. The system works permanently in the closed loop mode so that thermal drift are compensated.

Mirror tilting in mirror chamber 1 (MC1)

Each of the three mirrors in MC1 is equipped with two piezo motors (model 8301-UHV, New Focus) for controlling the mirror pitch and yaw around the X and Y axis. The piezo motors are controlled by an Intelligent Picomotor Control Unit (NEW FOCUS). Execution instructions are transferred via serial protocol from PLC to the control unit. Due to the not reproducible movement of piezo motors the tilting angle of the mirrors must be measured with two external encoders mounted directly to the mirror mechanics. The

encoder signals are read in the PLC counter modules. The PLC software has functions that are implemented for origin search and tilting of pitch and yaw to defined angles.

Mirror tilting and cavity length modification in chamber 2 (MC2)

In Chamber two (MC2), the drive motors are mounted outside of the vacuum system. Thus the installation of DC motors (PI) with integrated position sensors became possible. They are driven directly by intelligent control units (C-848 Multi-Axis DC-Motor Controller, PI). The connection to the PLC is made over a RS232. The positioning accuracy amounts to 0.1 μm. An additional increase of the accuracy is reached by mechanical lever mechanism (lever ratio 30:1). The distance measured between the mirrors of the optical Cavity is accomplished by use of a PC connected to the interferometer laser system (Laser Head HP 5517C and single beam interferometer HP10705A). The computer continuously sends the relative change of the mirror spacing to the Omron PLC over a serial interface. A software routine which is implemented on the PLC, regulates the cavity length drive and thereby holds the mirror spacing stable.
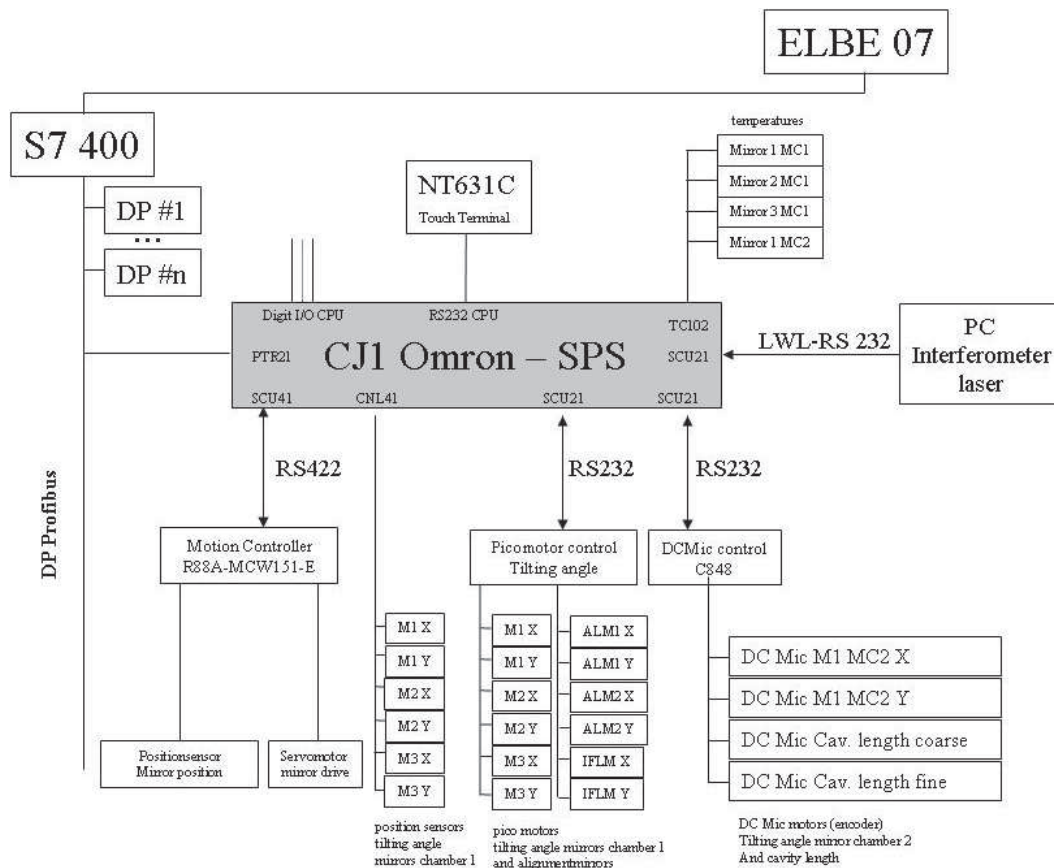
[1] U100 FEL, this report

Fig. 2: *Control system for mirror actuation and cavity length stabilization of the U100 optical cavity.*

Mode Conversion in the Partial Waveguide of FEL2

R. Wünsch, C.A.J. van der Geer [1]

At wavelengths around $150\,\mu$m a freely propagating resonator mode in the long-wavelength FEL2 at the radiation source ELBE is roughly $4\,$cm thick ($4*w_0$). This is in conflict with a reasonably small undulator gap and a sufficiently high magnetic field on the undulator axis. For that reason a waveguide will be installed [1]. It spans from the entrance into the undulator to the downstream resonator mirror and compresses the optical beam vertically. It is $1\,$cm high (inside height) and wide enough to allow a free propagation of the resonator beam in horizontal direction (parallel-plate waveguide). On the upstream side the elements necessary for a correct electron beam formation do not allow to install bulky waveguide plates. Here, the beam propagates freely both horizontally and vertically.

The waveguide allows a minimal undulator gap of $24\,$mm with an undulator parameter $K_{\rm rms} \approx 2.7$. A particular hybrid waveguide mode [2] carries the optical energy practically without loss. Losses arise solely at the waveguide exit where the mode is converted from a waveguide into a freely propagating Gaussian mode and vice versa. The hybrid waveguide $H_{m,n}$ mode shape is Gauss-Hermitian horizontally and sinusoidal vertically. Apart from the principal mode ($m = 0, n = 1$) a number of higher modes with additional maxima may be excited. These modes have a broader field distribution and hence a smaller overlap with the electron beam. Fig. 1 shows that the power density of the principal mode (m = 0) in the center, where the beam overlaps with the electrons, is twice as large as that of an m = 2 mode. Its gain is correspondingly larger.
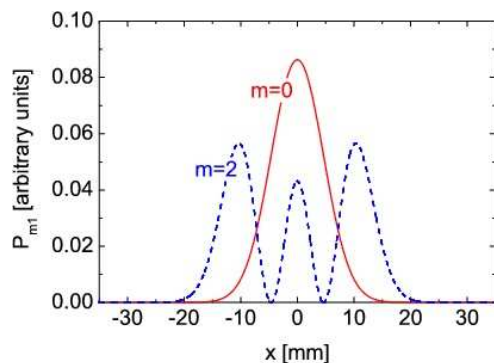
Fig. 1 *Horizontal power distribution of the principal optical mode (m = 0) and the m = 2 mode.*

Modes with more than one field maximum in vertical direction ($n > 1$) propagate with a slightly lower group velocity which reduces the overlap with the electron bunch additionally. At $150\,\mu$m the n = 3 radiation pulse is roughly $2\,$mm behind the n = 1 pulse after one roundtrip. At a resonator length fitted to the n = 1 mode the n = 3 mode does practically not overlap with the short electron bunch and is not amplified. At shorter wavelengths higher vertical modes can be amplified simultaneously with the principal one.

Using a partial waveguide higher order modes can be generated by the conversion of a waveguide mode into a freely propagating one and vice versa. When calculating lasing gain and power [3] and estimating the coupling losses between freely propagating and waveguide modes [4] the assumption was made that solely the principal mode $H_{0,1}$ is present in the waveguide when the appropriate mirror curvature has been selected. We have verified this assumption by means of the software package GPT [5] extended by a code describing the propagation of the optical beam inside and outside the waveguide without the restriction to the principal mode.

	m=0	m=2	m=4	m=6	m=8
no hole	0.982	0.000	0.002	0.002	0.001
d_h=7 mm	0.968	0.010	0.010	0.006	0.006

Table 1: *Coupling matrix of the principal waveguide mode (m = 0) with higher modes calculated for one roundtrip of a $150\,\mu$m beam through the FEL2 resonator.*

Table 1 illustrates the coupling between the various waveguide modes. It verifies that an optical field starting as a principal waveguide mode basically returns as a principal mode after freely propagating through the downstream side of the resonator. Only a few percent of the power (3.6 % without outcoupling and 6.3 % for a 7 mm hole) is converted into higher modes. These values are in nice agreement with the losses calculated by means of the computer code GLAD [6].

Due to the larger absorption and the lower gain of higher oder modes they are less amplified during the lasing process and, after a sufficient number of roundtrips the final profile contains less than 1 % of higher order modes at the outcoupling mirror even at 7 mm hole. Altogether the results confirm the assumptions and restrictions made when calculating the roundtrip losses by means of the optical code GLAD.

[1] Th. Dekorsy et al., IKH Annual Report 2004, FZR-423 (2005) 65
[2] L.R. Elias and J. Gallardo, Appl. Phys. B31 (1983) 229
[3] R. Wünsch, IKH Annual Report 2004, FZR-423 (2005) 67
[4] R. Wünsch, IKH Annual Report 2004, FZR-423 (2005) 66
[5] Pulsar Physics, General Particle Tracer (GPT), http://www.pulsar.nl
[6] E. Grosse et al., Proc. 27th Int. Conf on Free Electron Lasers, Stanford, USA, http://accelconf.web.cern.ch/AccelConf/f05/PAPERS/TUPP031.PDF

[1] *Pulsar Physics, The Netherlands*

72

# The IR Beam Line from the FELs to the High Magnetic Field Laboratory

W. Seidel, A. Winter[1], R. Wünsch, S. Zvyagin[2]

A beam line connecting two free-electron lasers (FEL) in the ELBE building [1] and experimental high magnetic field setup located in the building of the Dresden High Magnetic Field Laboratory (HLD) of the Forschungszentrum Dresden - Rossendorf has been designed. The ELBE FEL can produce short, a few picosecond long pulses with a repetition rate of 13 MHz of radiation in medium- and far-infrared region (between 3 and 200 μm). The repetition rate can be reduced down to 1 kHz. The average radiation power does not exceed a few tens of Watts. The light is linearly polarized. Owing to the large wavelength range we use reflective optics with metal mirrors (gold coated copper or stainless steel) have been chosen. Their reflectivity is larger than 97.5% in the operated wavelength range.

The ELBE-HLD beam line is one of the branches of the general line which delivers the laser light from the IR FELs in the ELBE building to several user laboratories [2]. The beam is guided by pipes which are either evacuated or purged with nitrogen gas. It starts at the outcoupling holes of the resonator mirrors of the U100 and U27 of FEL, respectively. The size of the outcoupling holes can be varied. Hole diameters of 2, 4.5 and 7 mm are available for the U100 FEL, while 1.5, 2, 3 and 4 mm holes can be used at the U27 FEL. The beam line has to be adapted to the different outcoupling holes and to the resulting beam divergence which, in addition, depends strongly on the wavelength of the beam. Positions and focal lengths of used mirrors have been determined to achieve better propagation conditions of the light inside the pipe (including passing through several bottlenecks, e.g. at the window between the preparation room and the magnet lab, waists in the HLD building, etc.). We use the Method of Equivalent Gaussian Beam [3] to calculate the propagation of radiation along the beam line. Beam radii w are calculated according to the Gaussian beam propagation laws.

First, the beams are transported from the outcoupling holes using separate lines to a diagnostic table in the neighboring room (see Fig. 1). The beam profile has a waist on the diagnostic table. Waist size and position are the same for beams coming from two FEL, and independent of the wavelength. On the other hand, the size of the waist depends upon the diameter of the outcoupling hole. The narrow beam size in the vicinity of the waist is used for various beam measurements and modifications. Behind the diagnostic table the beam is distributed between user laboratories using one line. By inserting the plane mirror MH1 into the beam line the beam is becoming bent down to a specific line,

guiding the beam via mirrors MH2 - MH4 into a tunnel (27 m long) on the basement level and connecting the ELBE building with the HLD. Arriving the tunnel, the beam is refocused (MH4), becoming a nearly parallel beam. However, diffraction effects increase the IR-beam size much stronger than that in the range of visible light. Towards the end of the tunnel the beam is too thick for a 10 cm pipe and the pipe diameter has to be increased to 20 cm. The beam size calculated along the beam line is illustrated in Figs. 2 and 3.
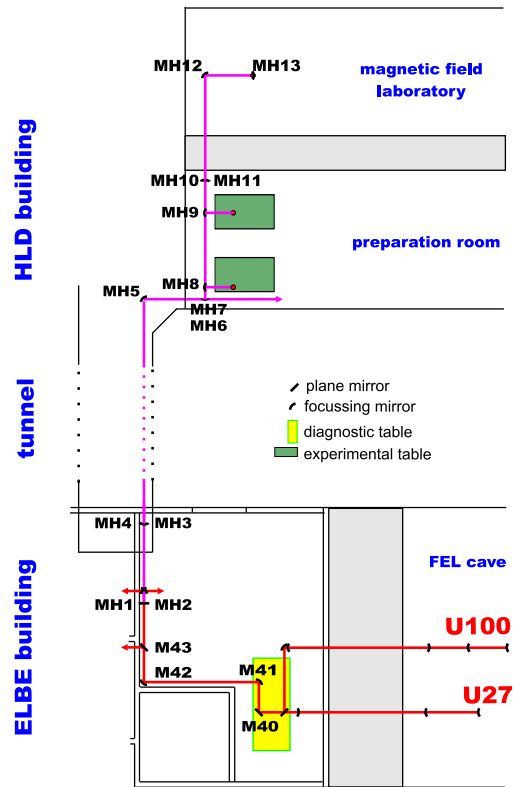
Fig. 1: *Top view of the beam line from the U100 and U27 FEL in the ELBE building to user stations in the HLD building via diagnostic table and tunnel.*

In the HLD building, the beam has to be deflected within shorter distances. The deflecting mirrors can be used to refocus the beam and to keep the necessary pipe diameter at 10 cm. We assume that a diameter of 3*w is sufficient in this branch of the beam line. Behind the mirror MH5 at the end of the tunnel the beam size is rapidly decreased. Mirror MH6 focuses the beam additionally, and deflects it upwards to the experimental preparation room in the ground floor. This mirror can be removed to guide the beam to other laboratories in future. Mirror MH7 brings the beam into horizontal direction 108 cm above floor level. Two removable focusing mirrors (MH8, MH9)

---

[1] Department of Research Technology
[2] Dresden High MagneticField Laboratory (HLD)

can direct the beam to an experimental table, where a beam waist is located approximately 90 cm behind the mirror. Here, the beam is only a few millimeters thick ($2*w$). The beam going straight on enters the magnet laboratory through a safety window. Since the window is 46 cm higher than the beam, the beam is brought to the same level by means of mirrors MH10 and MH11. In the magnet laboratory, a first beam waist is shortly behind the wall. Here, the beam is between 5 and 15 mm thick ($2*w$), depending on wavelength and size of the outcoupling hole. The small beam size allows us to insert a diamond window at this place. After the window, the beam is deflected by the mirrors MH12 and MH13 and focused onto the entrance of a circular waveguide which finally guides the beam into the cryostat of the high-field magnet. Another diamond window is designated 10 cm in front of the entrance into the waveguide at the end of the beam line.

The mirrors are adjusted by means of a He-Ne laser beam introduced into the beam line and aligned with the IR-beam. A first alignment beam starts behind the resonator mirror. It is used in the laboratories of the ELBE building. Towards the end of the tunnel this beam gets rather wide and improper for adjusting the mirrors farer away from the resonator. We therefore introduce another He-Ne laser beam into the beam line between mirrors MH2 and MH3. This beam is aligned with the first one and can be used for adjusting the mirrors in the HLD. Furthermore, the HLD users may use this beam for setting up high-field experiments.

A broad range of high-field experiments using the FEL facility at the Forschungszentrum Dresden - Rossendorf can be performed. It includes Electron Cyclotron Resonance in metals and semiconductors; Electron Paramagnetic, Antiferromagnetic and Ferromagnetic Resonances in varies magnetic dielectrics; investigation of non-linear parametric processes in materials of functional optics and spintronics, pump-probe experiments on quantum wells, high-resolution time-domain spectroscopy of highly-correlated electron systems (including high-T_c materials, heavy-Fermion systems, etc.).

[1] http://www.fzd.de/elbe, 12.01.2007
[2] Th. Dekorsy et al., Proc. Free Electron Laser Conf. 2002, pp. 35,36
[3] H. Kogelnik, Appl. Opt. **4** (1965) 1562-1569
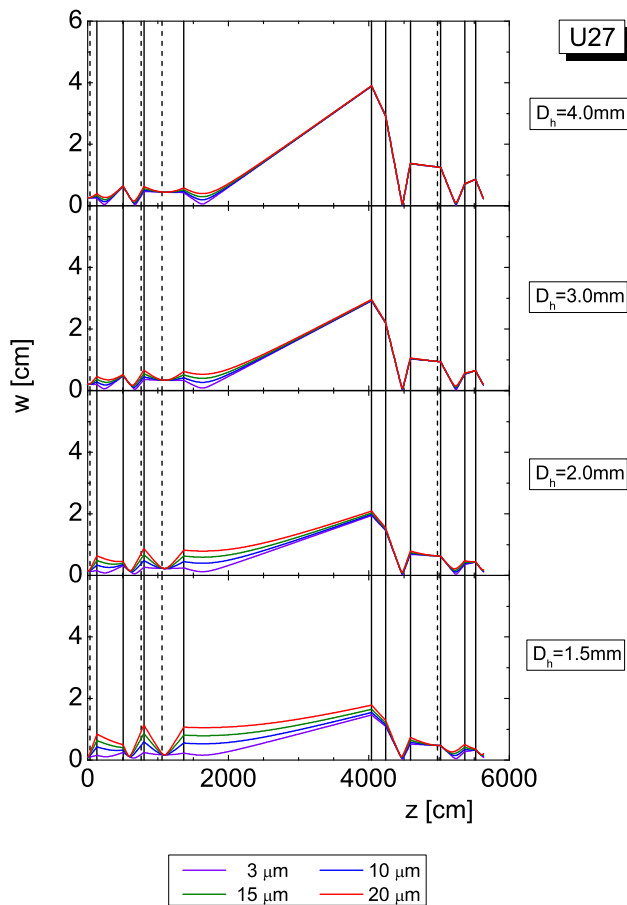
Fig. 2: *Radius w of the U27 FEL beam calculated from the waist on the diagnostic table to the HLD for different hole sizes D_h and wavelengths. The vertical solid and broken lines indicate the positions of focusing and plane mirrors, respectively.*
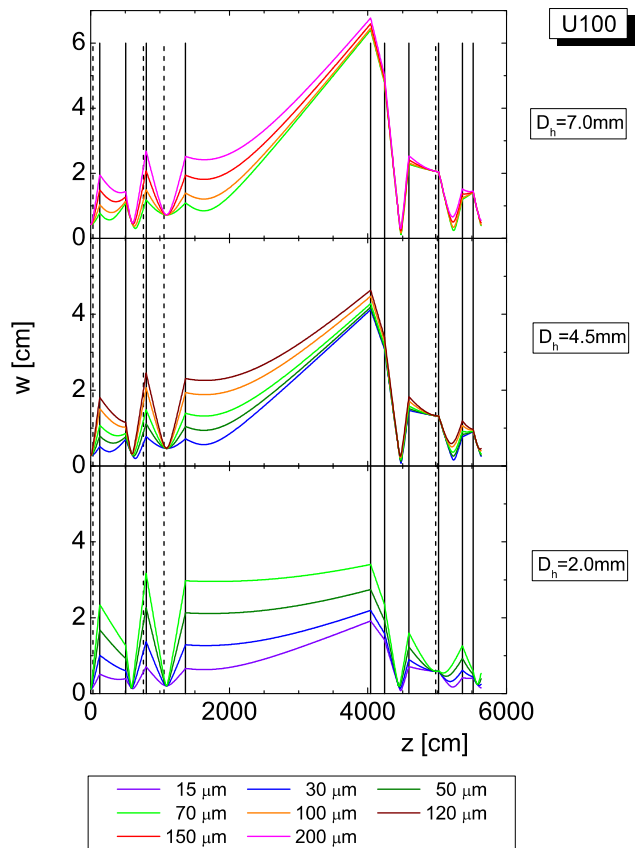
Fig. 3: *The same as in Fig. 2 for the beam from the U100 FEL.*

Extraction of Single FEL Radiation Pulses Using a Laser-Activated Plasma Switch

W. SEIDEL, S. WINNERL[1]

In order to decrease the average radiation power of the Rossendorf free-electron laser FELBE (FELBE project [1]), as required for certain experiments (high pulse energies but moderate or low average power), the FEL repetition rate can be reduced from 13 MHz to 1 kHz. To this end, plasma switching of FEL radiation pulses was demonstrated for cw operation.

The plasma switch is based on the principle of photo-induced reflectivity by an optically excited electron-hole plasma [2, 3]. Germanium serves as semiconductor material for the switch. The semiconductor was illuminated by a Nd:YAG laser amplifier system (1 kHz, λ = 1064 nm, $\tau \sim$ 16 ps, <1 Watt), generating an electron-hole plasma at the front surface of the semiconductor. The generation of a sufficient plasma density leads to a variation of the optical semiconductor properties for the infrared FEL-radiation (strongly focused and under Brewster's angle of 76°). For realizing the pulse selection the frequencies of both laser sources (FEL and Nd:YAG) were synchronised with RF electronics. For the exact timing of both laser pulses, when they hit the semiconductor, they were detected with a photon-drag detector or a fast pyro-electric detector (FEL) and a photo diode (Nd:YAG) and were adjusted on each other with cables, phase-shifter (trombone) and through moving a precision linear stage. Fig. 1 shows the experimental set-up. A gold mirror served as a reference for determining the reflectivity of the Germanium. The selected FEL pulses were detected by a fast MCT detector with a bandwidth of 20 MHz. Fig. 2 shows the switched pulse in two amplitude scales. The signal from the switch laser (photo diode) is shown in red. From the comparison of the black and blue curves we obtained an amount of dark pulses in the switched beam of about 0.5 % due to the angle of beam spread from the focussing. The time-resolved measurement of the reflectivity yields an exponential decay with a time constant of 590 ps. For the highest value of the Nd:YAG laser amplifier peak fluence of 25 mJ/cm^2, a reflectivity of Ge for FEL radiation ($\lambda = 11 \mu m$) of 100 % was achieved (see Fig. 3). We thus succeeded to extract single FEL radiation pulses out of the 13 MHz pulse train, indicating that this plasma switch is most suitable for the Rossendorf FEL. Further examinations will concentrate on achieving similar results for shorter wavelength. To integrate this plasma-switch into the existing diagnostic station we have to build an additional by-pass to the Germanium or Silicon slab which is under Brewster's angle (see [4]). The selected micro pulse will be refocused to the waist parameters outside of the by-pass line and transported to the user stations.

[1] http://www.fzd.de/elbe
[2] P. Haar, Ph.D. thesis, Stanford University (1996)
[3] E.H. Haselhoff et al., Nucl. Instr. and Meth. A358 (1995) ABS28
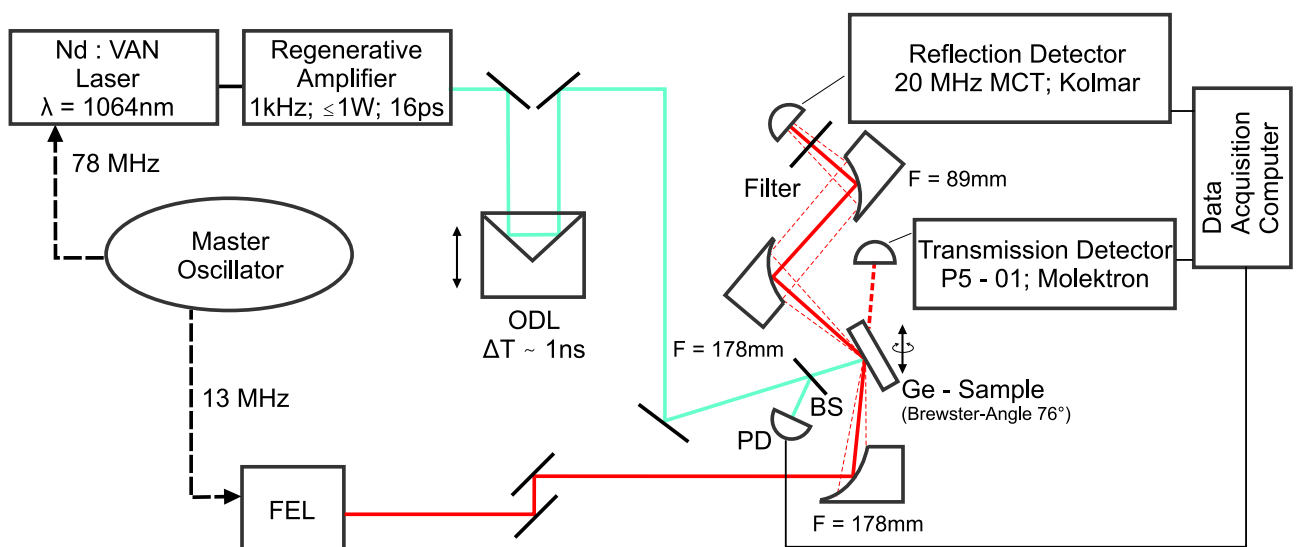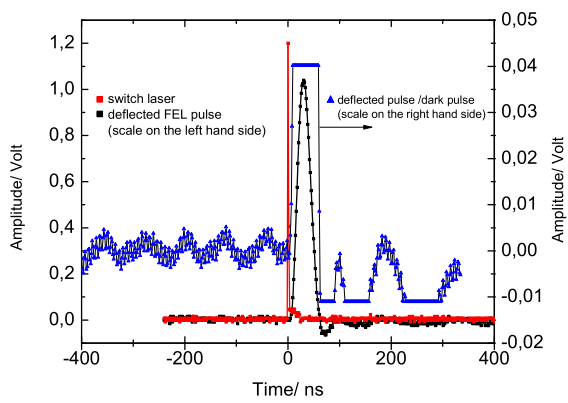[4] W. Seidel et al., Diagnostic this Report

Fig. 1: *Setup for the plasma switch (for details see above)*

[1]Institute of Ion Beam Physics and Materials Research

Fig. 2: *The switched FEL pulse at 11 µm in two different amplitude scales is measured by a fast MCT detector with a bandwidth of 20 MHz. The signal from the switch laser (photo diode) is shown in red. From the comparison of the black and blue curves we obtain an amount of dark pulse in the switched beam of about 0.5%.*
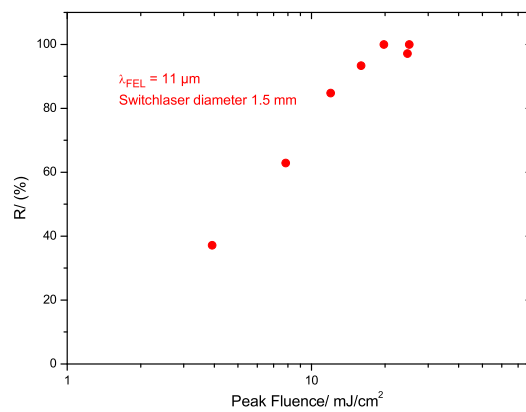
Fig. 3: *Dependence of reflectivity on the pump-laser peak fluence.*

Dynamics of FEL-Light-Induced Changes in thin DNA films Observed by Brewster Angle Microscopy

M. Sczepan, G. Furlinski, D. Wohlfarth, W. Seidel, K. Fahmy

The function of biopolymers is determined by their structural dynamics. Investigation of the structural dynamics is thus important for understanding the processes and superstructures involved in the function of biomolecules. A large number of superstructures is particularly important for DNA function. Our experiments aim at the induction and kinetic analysis of the IR-induced transitions between such states.

In order to observe changes induced in thin DNA films by FEL irradiation, Brewster angle microscopy, which is a proven technique for the evaluation of thin organic films [1] has been employed. If a sample is observed under Brewster angle conditions, small changes in the refractive index of the surface can be detected and thus thin layers on the surface of a substrate or liquid can be made visible. Small changes in the refractive index and thickness of a thin film as a result of structural transitions will induce changes in the reflectivity of the film.

Experiments have been performed using thin layers of DNA (pUC21 plasmid DNA, PlasmidFactory) on ZnSe and CaF_2 substrates. The thickness of the layers has been estimated to be 50-800 nm by interference fringe counting in combination with absorbance measurements. These samples were irradiated with FEL light at different wavelengths. Fast changes of reflectivity - following the temporal structure of the FEL light intensity which are followed by slow relaxation processes (≈ 30 ms) were observed (see Fig. 1). Experiments to determine the influence of the micropulse energy (20-100 nJ), film thickness, macro bunch length (200-1200 μs) and humidity have been performed and revealed a strong influence of these parameters on amplitudes and time constants of the reflectivity variations.

Analysis of the data for films of different thicknesses - especially for films with thicknesses between 50 nm and 150 nm - reveal that changes in the reflectivity on the longer time scale are the result of a decrease in the refractive index of the sample while the fast ($< 30 \mu$s) changes can be attributed to variations (increase followed by decrease) of film thickness due to heating. A model for the heat transport in the sample has been established, allowing the estimation of the temperature reached in the sample as a function of film thickness and pump power. Estimated temperature jumps were found to be in the 50-500 K range with the equilibrium temperature established within less than 50 μs. For high film thicknesses and pump intensities resulting in high film temperatures, a more complex behaviour of the reflectivity was observed. In this case, thickness changes - probably as a result of variations in sample hydration - seem to contribute to the slow changes in reflectivity. The changes in the refractive index of the sample can be the result of structural changes (base pair stacking, strand opening [2]) as well as of variations in the hydration state of the DNA [3].

In summary, we have shown that FEL-pulses can induce rapid DNA melting, allowing to observe base pair separation and annealing with a time resulution not accessible by conventional experiments on DNA-structural transitions.
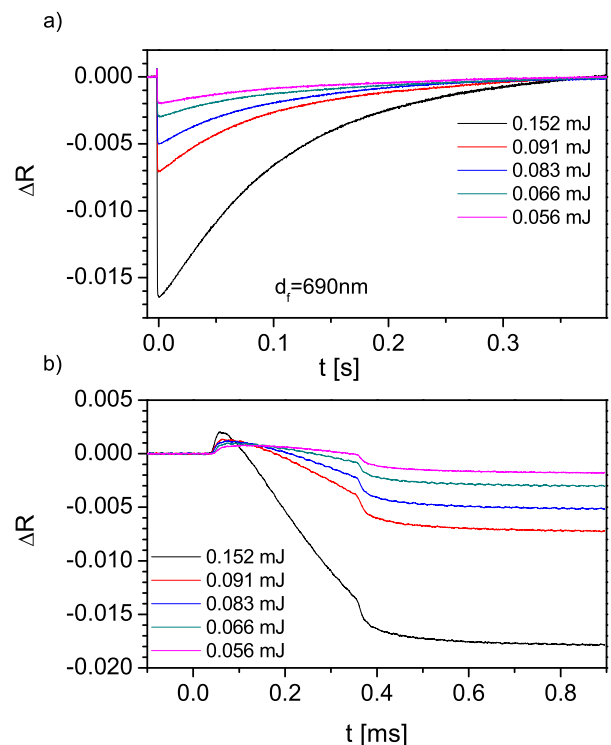
Fig. 1: *Change of reflectivity of a DNA film (thickness 690 nm) during and past FEL irradiation in long (a) and short (b) time scale as a function of light intensity / macro bunch energy.*

[1] S. Hénon, J. Meunier, Rev. Sci. Instr. 62 (1991), 936
[2] S. Elhadj, G. Singh, R. Saraf, Langmuir 20(2004), 5539
[3] S. Weidlich, S.M. Lindsay, A. Rupprecht, Biopolymers 26 (1987), 439

Development of a Superconducting RF photo Gun

The Radiation Source ELBE is a place of research and development for superconducting radiofrequency photo injectors. During the last years very successful results have been obtained and the research topic has attracted high international attention. The highlight was the worldwide first operation of such a superconducting rf photo gun with a half–cell resonator in 2002.

For future SRF linear accelerator projects, FEL light sources or 4th generation synchrotron light sources with energy recovery, the development of high brightness electron injectors is one of the most important challenges. High current electron beams of highest quality must be produced by the source and its emittance preserved in the low energy region. The SRF photo gun is considered as one of the most promising candidates. For the BESSY-FEL in Berlin and the 4GLS at Daresbury such a source is intended to be used. The new SRF photo gun now under development will be a fully utilizable injector for the ELBE accelerator and will produce electron beams of much higher quality (higher bunch charge and lower emittance) than the existing thermionic injector. Due to its great relevance the SRF gun project is encouraged and supported by many national and international accelerator institutes. Especially the European Union supports the SRF gun development within the CARE project (Coordinated Accelerator Research in Europe) and a common national research project with BESSY Berlin, DESY Hamburg and Zeuthen, and the Max-Born-Institut Berlin has launched with financial support of the BMBF.

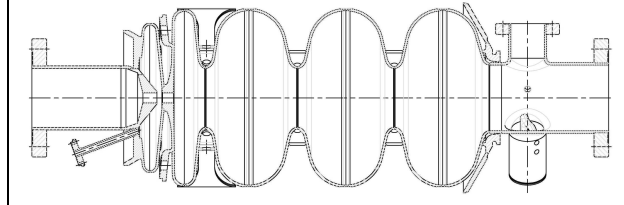# First RF-Measurements of the 3.5-Cell SRF-Photo-Gun Cavity

A. Arnold

Introduction

For future FEL light sources and high energy linear accelerators a high current electron gun with high brilliance is absolutely essential. Thus, an innovative superconducting RF photo injector (SRF gun) is under development at the Forschungszentrum Dresden Rossendorf (ELBE). This gun allows continuous wave operation at an energy of 9.4 MeV and an average current of 1 mA. Simultaneous it generates short pulses and high-brightness electron beams, as known from conventional photo-injectors. The following text deals with the treatment and the first rf measurements of the cavity. Table 1 shows some important RF parameters and a cross-section of the design.

Tab. 1: *RF cavity parameters calculated with MWS normalized to 50 MV/m peak axis field.*

stored energy U	32.5 J
quality factor Q_0	$1 \cdot 10^{10}$
dissipated power P_c	25.8 W
geometry factor G	241.9 Ω
acceleration voltage V_{acc}	9.4 MV
acceleration gradient E_{acc}	18.8 MV/m
shunt impedance $R_a = V_{acc}^2/2P_c$	$1.72 \cdot 10^{12}\Omega$
R_a/Q_0	166.6 Ω
E_{peak}/E_{acc}	2.66
B_{peak}/E_{acc}	6.1 mT/(MV/m)

Cavity warm tuning

In order to get the right field distribution and the accurate frequency at operation inside the cryostat, one has to consider different tuning parameters.

The correct frequency at room temperature mainly depends on cool down shrinking, additional chemical treatment and pre-stressing of both cavity tuners. These tuners permit an axial deformation of $\pm 400\mu$m and $\pm 500\mu$m for the half cell and the three TESLA cells, respectively. The induced frequency shifts have been taken into account. Thus, the estimated tuning frequency follows from Table 2.

A non-negligible detuning of the π-mode field, as shown in Table 3, is caused by pre-stressing of the half cell. This measurement has to be considered when pre-tuning to obtain the right field profile in the cryostat. Based on these target values, the tuning process was realized as presented in [1]. It succeeded in the measured field profile shown in Fig. 1 and met the calculated requirements.

Tab. 2: *Evaluation of the estimated frequency at 300 K.*

operating frequency at 2K	1300.0 MHz
cool down shrinking (measured at ELBE)	- 1.97 MHz
50μm BCP at DESY/ACCEL (simulated)	+ 0.55 MHz
pre-stressing half cell (measured)	+ 0.10 MHz
pre-stressing 3 TESLA cells (measured)	+ 0.22 MHz
required frequency at 300K	1298.9 MHz

Tab. 3: *Field detuning caused by pre-stressing half cell.*

detuning	Gun Cell	TESLA1	TESLA2	End Cell
axis field	-7.3%	-1.8%	+1.4%	+3.1%
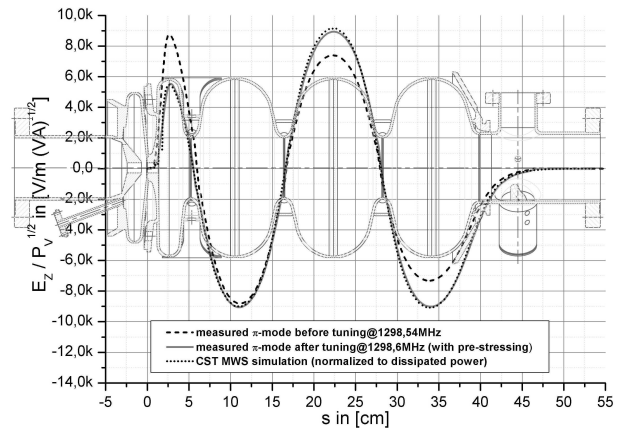
Fig. 1: *Measured vs. simulated π-mode field profiles before and after tuning.*

Ext. Q study main coupler

In order to optimize the RF power transfer from klystron to the electron beam, it is necessary to match the coupling. The applied Rossendorf main coupler is not adjustable, thus the antenna is optimized for a bandwidth of 100 Hz and an external quality factor of:

$$Q_{ext} \sim Q_L = \frac{f_0}{B} = \frac{1.3 \text{ GHz}}{100 \text{ Hz}} = 1.3 \cdot 10^7 \qquad (15)$$

The determination of the suitable distance between antenna tip and axis of rotation is done by an additional probe antenna added at the opposite side of the cavity at room temperature. As shown in equation 2 one has to measure incident and reflected power at the input port, the transmitted power at the main coupler as well as the unloaded quality factor of the cavity.

$$Q_{ext} = \frac{Q_0}{\beta_{ext}} \quad \text{with} \quad \beta_{ext} = \frac{P_t}{P_i - P_r - P_t} \qquad (16)$$

The results presented in Fig. 2, point to the required coupling at a distance of 43.2 mm from axis. An additional calculation, using the results of MWS-simulations with different boundary conditions as shown in [2] gives a similar performance.
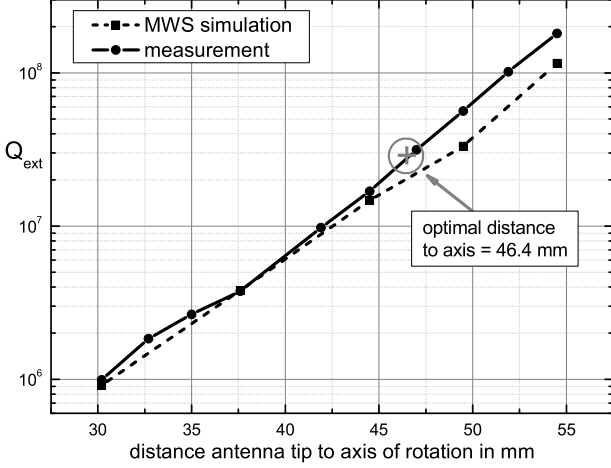
Fig. 2: *External quality factor vs. antenna length.*

Tuning the choke filter

The filter is designed as a coaxial trap filter. We measured the external quality factor versus detuning of the choke cavity by crushing and stretching. For this purpose an antenna probe with the same diameter as the original cathode was used. Thus the power behind the choke filter depending on the dissipated power through the walls can be measured (Fig. 3).
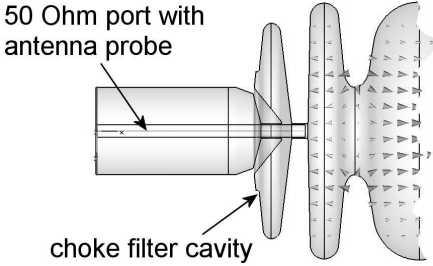
**Fig. 3:** *Assembly to measure π-mode suppression.*
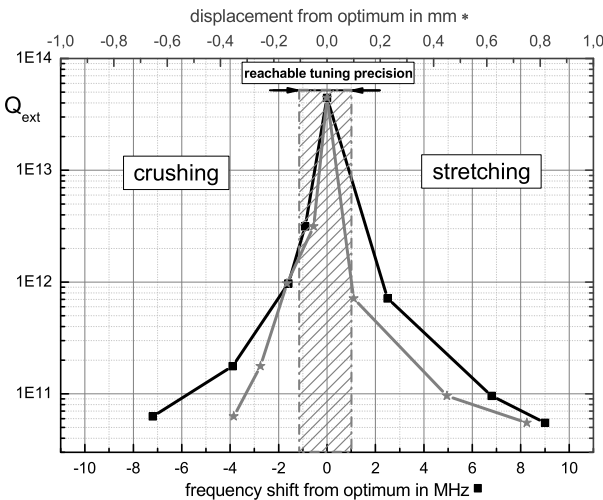
Fig. 4: *External quality factor vs. choke filter detuning measured by frequency shift and deformation.*

As a result one gets a tuning curve shown in Fig. 4. Due to mechanical tolerances during the assembling of

the cryostat, it is hard to improve the accuracy better than ±100 microns. Within this range, the external quality factor is better than $Q_{ext} = 10^{12}$ and the power leakage is less than 1% of the dissipated power.

Tuning the HOM coupler

To estimate the precision achieved by the trap circuit tuning, we measured the external quality factor at the π-mode frequency versus tuning displacement and frequency shift. To prevent crosstalk it is necessary to place the input antenna probe at the opposite side of the HOM couplers. The result is presented in Fig. 5.
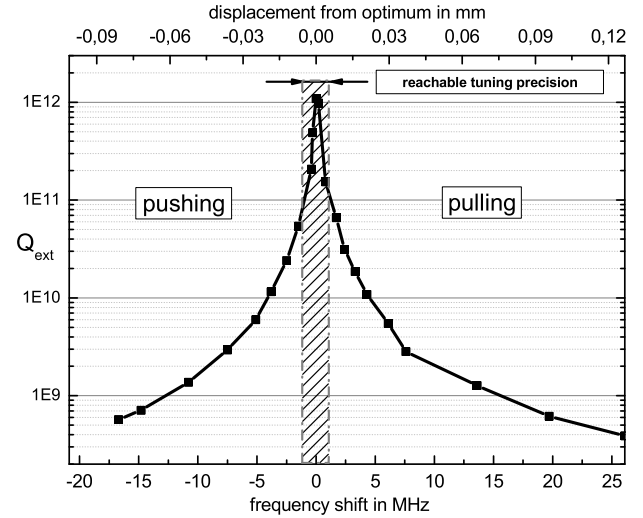
Fig. 5: *External quality factor vs. detuning from best π-mode suppression.*

It is obviously hard to get a better external quality factor than $Q_{ext} = 10^{11}$. In that case less than 10% of the dissipated power is transmitted out of each HOM-coupler.

First vertical cold test

Following the tuning procedures the cavity was prepared at DESY Hamburg by buffered chemical polishing (40μm BCP) and high pressure rinsing (HPR). Afterwards the cavity was tested in a vertical cold test, as described in [3]. During the cool down from 4.4 K to 1.6 K the unloaded quality factor was measured at low RF power (Fig. 6). The illustrated surface resistance follows from Eq. 3 and the numerical calculated geometry factor G.

$$R_S = \frac{G}{Q_0} \quad \text{with} \quad G = 241.9\,\Omega \qquad (17)$$

Based on the BCS-theory the surface resistance can also be calculated analytically. Fitting the measured data points by using Eq. 4 leads to the following material parameters:

$$A_S = 2.42 \cdot 10^{-15}\frac{\Omega\,\text{K}}{\text{Hz}^2};\ \Delta = 1.53\,\text{meV};\ R_{res} = 3.43\,\text{n}\Omega$$

82

$$R_S = A_S \omega^2 \frac{1}{T} e^{\frac{-\Delta}{kT}} + R_{res} \quad \text{for} \quad T < T_C/2 \quad (18)$$
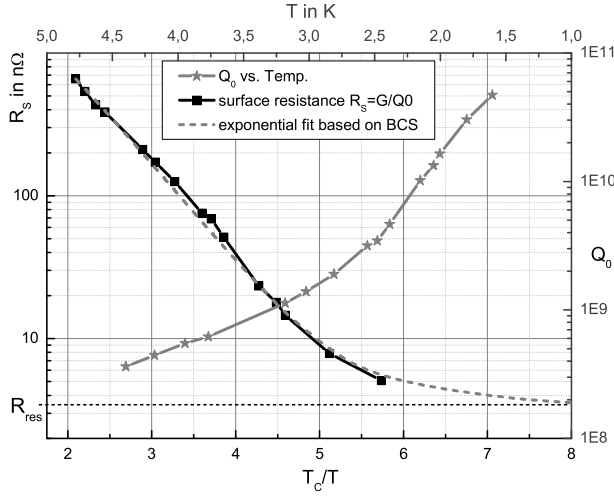
Fig. 6: *Surface resistance and unloaded quality factor versus temperature.*

In view of the measured, unloaded high quality factor of $Q_0(1.8K) = 3 \cdot 10^{10}$ and the calculated low residual resistance of $R_{res} = 3.4n\Omega$ the preparation of the cavity proceeded well. Another matter of substantial interest is the Q vs. E chart. In order to get comparable values, Q_0 is plotted versus peak axis field in the TESLA cells (design value E_{peak}=50 MV/m). Furthermore the radiation caused by field emitters is included into the same chart. As shown in Fig. 7, field emission started early and the quality factor decreases. Further increasing of rf power results in strong field emission and two Q-switches, which are probably caused by thermal breakdown at activated field emitters. After the second Q-switch the field was limited by quench. Especially the behaviour of the Q-switches are most likely due to defects in the bulk niobium or to surface pollution. This might be induced by the hardly cleanable choke filter. Because of the narrow cathode feed through between choke filter and gun cell, direct cleaning of the filter cell wasn't feasible. Furthermore

contaminated water runs out of it into the cavity which leads into polluted surface.
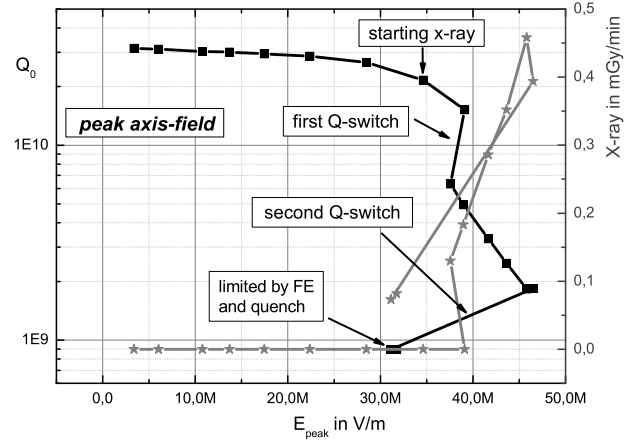
Fig. 7: Q_0 *vs. peak axis field* $E_{peak}(1.8\ K)$.

Conclusion

So far all measurements and tuning procedures yield acceptable results. In the next steps an improved HPR and BCP treatment will be established at ACCEL to achieve the designed peak field. Nevertheless the reached field of E_{peak}=39 MV/m and the high quality factor of Q_0=1.5·10^{10} demonstrates first of all the proper design of the gun cavity.

[1] A. Arnold: "Untersuchungen zur Feldverteilung verschiedener Moden in mehrzelligen Beschleunigerresonatoren", Diplomarbeit, FZD, 2006

[2] P. Balleyguier: "External Q studies for APTT SC-Cavity Couplers", CEA/DPTA, Bruyères-le-Châtel, France.

[3] P. v. Stein, internal report, FZR-227, Forschungszentrum Rossendorf, 1998.

[4] Jens Knobloch: Basic Concepts of Measurements Made on Superconducting RF Cavities, Laboratory of Nuclear Studies, Cornell University, August 1991.

Aufbau eines Feldprofil-Messplatzes mit Tuningvorrichtung für HF-Resonatoren

A. Arnold

Einleitung

Aufgrund fertigungsbedingter Toleranzen des $3\frac{1}{2}$-zelligen Niob Resonator ist die Feldverteilung und die Resonanzfrequenz der beschleunigenden TM_{010}-Mode zu korrigieren. Im Folgenden soll kurz das Mess- und Tuningprinzip sowie dessen praktische Umsetzung dargestellt werden.

Störkörpermessung

Basierend auf der Slater-Formel lässt sich, nach Gl.(1), ein rein elektrisches Feld über die durch einen kleinen bekannten Störkörper verursachte negative Phasenverschiebung quantitativ bestimmen.

$$\frac{|\vec{E_0}|}{\sqrt{\overline{P_v}}} = \sqrt{\frac{-\tan\Delta\varphi \cdot (1 + k_1 + k_2)}{\alpha \cdot \omega_0}} \qquad (19)$$

Die Phasenverschiebung ist proportional zur Feldstärke am Ort des Störkörpers. Damit liefert die durch den Resonator axial bewegte Störung, die Feldverteilung für die vier Grundmoden entlang der Messtrecke. Abb. 1 zeigt den schematischen Messaufbau.
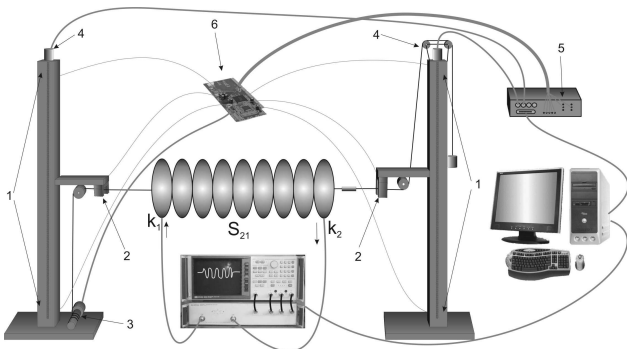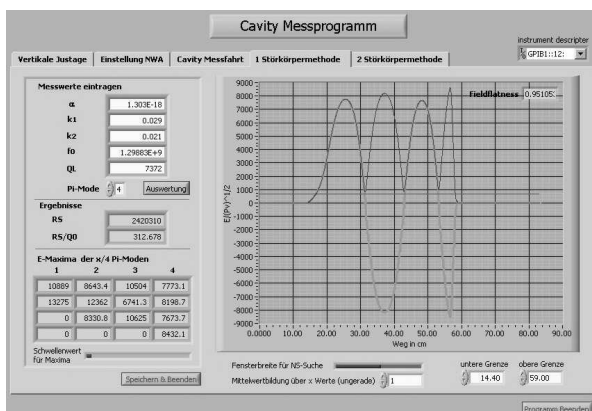

Abb. 1: *Schema des Messaufbaus.*

Abb. 2: *Labview Auswertung für ungetunte π-Mode.*

Die vertikale und horizontale Justage des an einem dünnen Kevlarfaden befestigten Störkörpers erfolgt über Schrittmotoren. Der Transport ist durch einen Gleichstrommotor mit gekoppeltem Inkrementalgeber realisiert. Dieser liefert gleichzeitig über eine parallele Messzeiterfassung den genauen Ortsbezug des Störkörpers im Resonator. Die Phasenverschiebung wird durch den Netzwerkanalysator HP 8753C gemessen. Die gesamte Steuerung und Auswertung erfolgt über Labview und einem PC mit einer Schrittmotorsteuerung (Abb. 2).

Tuning

Eine Aussage über Betrag und Richtung des für jede Zelle erforderlichen Tuningbedarfs liefert ein Tuningalgorithmus aus dem Grundzustand des Resonators (Feldverteilung und Eigenfrequenz aller TM_{010}-Moden vor dem Tunen, vgl. Abb. 3) und der Vorgabe der gewünschten Feldverteilung sowie der Zielfrequenz einer der vier Grundmoden.
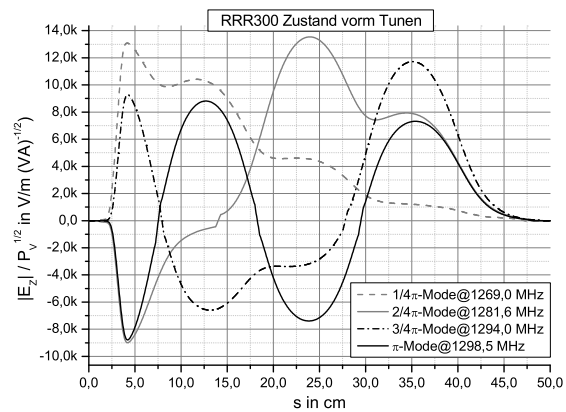

Abb. 3: *Feldverteilung aller 4 Grundmoden vorm Tunen.*

Durch Änderung der axialen Länge lassen sich die Zellen den Vorgaben entsprechend exakt Abstimmen. Um den Resonator nicht zu beschädigen wird eine manuelle Tuningvorrichtung verwendet, die durch speziell geformte Platten die Kraft gleichmäßig über die gesamte Zelleoberfläche verteilt und nur eine axiale Verformung erlaubt (Abb. 4).
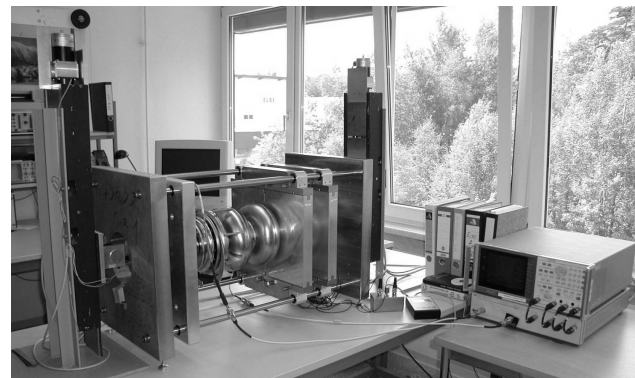

Abb. 4: *Cavity Mess- und Tuningplatz.*

Measurement of the Mechanical Properties of the Tuning System for the Superconducting $3\frac{1}{2}$-Cell Cavity

R. Hempel, A. Arnold, D. Janssen, P. Murcek, J. Stephan, J. Teichert

For the $3\frac{1}{2}$ cell niobium cavity of the new superconducting RF photo electron source a tuning system was developed. The basic design is adopted from the ELBE cryomodule dual spindle-lever tuning system. Due to the different mechanical properties of the half cell and the TESLA cells of the cavitiy, two tuners are used. The two tuners mechanically adjust the $3\frac{1}{2}$-cell superconducting cavity of the SRF gun to the frequency of 1.3 GHz and determine the ratio of the field amplitudes between the half cell and the three TESLA cells of the cavity. For that reason the tuners have to transfer large force within a small range and need high resolution at liquid He temperature.

For operating tests and parameter measurements a test bench for the designed tuning system was built up [1]. This test bench consists of the liquid nitrogen dewar, the leverage of the tuner, a spring packet to simulate the cavity, and the equipment to produce the tuning force, to perform force and length measurements. The photograph in Fig. 1 shows this test bench. The spring packet was variable in order to simulate the half-cell and the three TESLA cells, as well as to measure with preload. For the three TESLA cells a spring constant of 9 kN/mm was taken [2]. The spring constant for the half-cell was assumed to be about three times higher. The preloads were varied between zero and 9 kN. The tuning force was up to 4 kN at the maximum tuning range.

The tuners change the length of the cavity with a resolution less than 3 nm. This corresponds to a resolution of about 1 Hz in the cavity frequency. It consists of a spindle with partly left-hand thread and right-hand thread and two levers. Via the threads and the lever system the rotational motion is transformed into a longitudinal motion performing the length variation. The bearing point of the leverage system has no rotational parts. It consists of two flexible links as it is shown in Fig. 2. The advantage is the lack of any hysteresis due to friction effects and bearing clearance. The third flexible link is connected with a moving bolt which transfers the force to the parts of the He tank joint to the end plates of the half-cell or the TESLA cells.
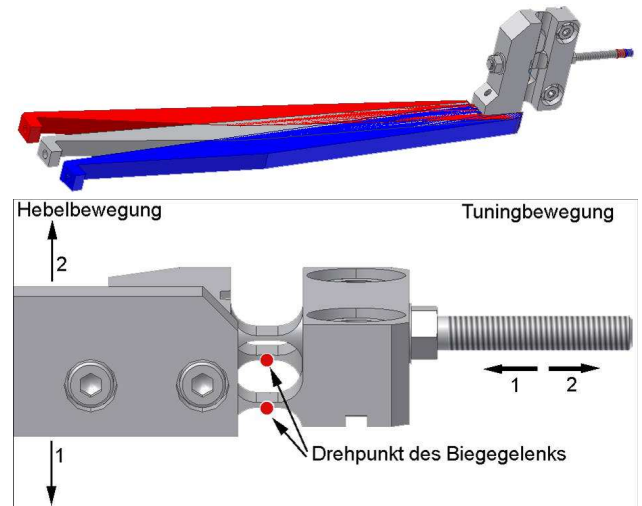

Fig. 2: *Leverage system (above) and flexible link (below) of the SRF gun tuner.*

The measurements confirm that the tuning system accomplishes a sufficiently large tuning range and a tuning resolution of about 1 Hz. The hysteresis measured was caused by the test bench mechanics itself. Fatigue effects were not found. Detailed information can be found in Ref. [1] and [3].

[1] René Hempel, "Messung der mechanischen Eigenschaften eines Tuners für einen supraleitenden HF-Resonator", Diplomarbeit, HTW Dresden, 2005

[2] C. Pagani et al., Proc. of PAC 2005, Knoxville, USA, p. 3456.

[3] J. Teichert et. al., Proc. of FEL 2006, Berlin, Germany, p. 575.

Fig. 1: *Photograph of the Tuner test bench.*
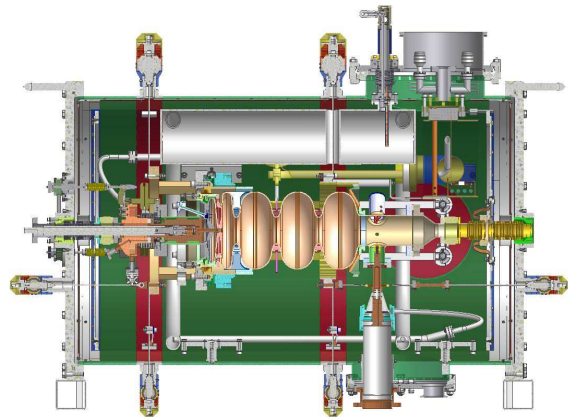
Assembly of the SRF Gun Cryostat

P. Murcek, A. Arnold, H. Büttig, M. Freitag, W.-D. Lehmann, F. Staufenbiel, J. Stephan, J. Teichert

The SRF gun cryostat will contain the $3\frac{1}{2}$-cell niobium cavity which consists of a half-cell with the normal-conducting cathode in it and three acceleration cells with TESLA shape [1]. The cavity will be cooled with liquid He at a temperature of about 1.8 K. The envisaged acceleration gradient of this cavity is 18.8 MV/m which corresponds to a maximum axial peak field of 50 MV/m in the TESLA cells. The geometry constant is 240 Ω and R/Q is 165 Ω. For $Q_0 = 1 \cdot 10^{10}$ and the gradient mentioned above a RF power dissipation of 26 W is expected. The static heat leak will be less than 20 W. The basic design of the SRF gun cryostat was adopted from the ELBE cryomodule [2] which contains two 1.3 GHz TESLA cavities and is developed for CW operation with 10 MeV per cavity.

Fig. 1 shows a sectional drawing of the cryostat. The stainless steel vacuum vessel has a cylindrical shape with 1.3 m length and 0.75 m diameter. The He port and the N_2 port are on top on the right hand side. From the port the He flows through a heater pot and the two-phase supply tube into the chimney of the He tank. For the cooling of the thermal shield, liquid nitrogen is used. The 80 K shield consists of a cylindrical Al sheet welded to two circular tubes filled with N_2. The liquid N_2 tank in the upper part of the module must be refilled after about 5 h from outside. The liquid N_2 is also used for the cooling of the photo cathode stem. The Cs_2Te photo emission layer and the Cu cathode stem are normal conducting. The heat load from the RF field into these parts, estimated to be between 10 and 20 W, burdens the liquid N_2 bath.

The cavity is passively protected against ambient magnetic fields by means of a μ-metal shield, placed between the 80 K shield and the vacuum vessel. Its suppression of the earth magnetic field was measured. In the region where the Nb cavitiy will be placed, the residual magnetic field is below $1\,\mu$T which is the limit during the cool-down [1].

The He tank is made of titanium. Three stainless steel bellows are integrated for the two tuning systems and for the manually tuned choke filter cell. The ten thin titanium spokes support the He tank and allow the adjustment of the cavity position. The 10 kW main power coupler will be the same type like the one in the ELBE accelerator modules.

From outside it is also possible to move the cathode support and cooling system which allows the adjustment of the photo cathode with respect to the cavity. For that reason, three rotation feed-through exist in the backside plate of the vacuum vessel.

Fig. 1: *CAD model cross-sectional view of the SRF gun cryostat.*

In 2005 and 2006 the main components were ordered and fabricated. A photograph of the partly assembled cryostat is presented in Fig. 2. Later in autumn 2006 the cryostat was completely assembled in the workshop. A vacuum check and the cool-down with liquid nitrogen were carried out successfully.
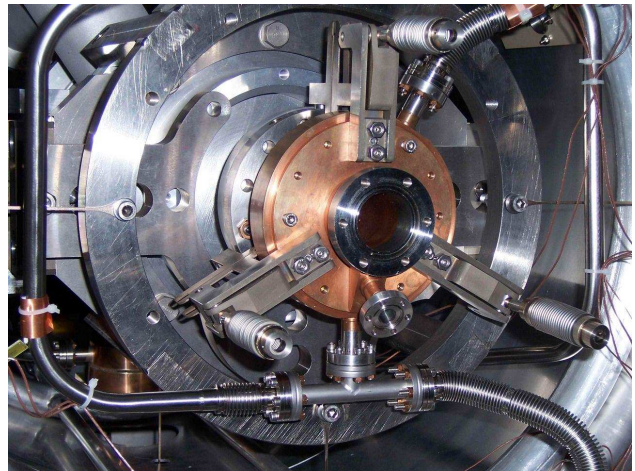
Fig. 2: *Photograph of the cryostat backside with tuning system parts, cathode cooler and flange for photo cathode exchange.*

[1] B. Aune, et al., Phys. Rev. Special Topics, 3(2000) 092001.

[2] J. Teichert, et al., Nucl. Instr. and Meth. A 557 (2006) 239.

[3] J. Teichert et. al., Proc. of FEL 2006, Berlin, Germany, p. 575.

The Preparation of Cs$_2$Te Photocathodes for the SRF Gun

R. Xiang, J. Teichert, F. Staufenbiel, P. Murcek, M. Kersten

In the years 2005 and 2006 a new photocathode laboratory was built in order to provide Cs$_2$Te photocathode with a quantum efficiency (Q.E.) of more than 1 percent for 100 hours working time for the superconducting RF gun project. Because it needs ultra high vacuum, the preparation chamber is installed in a clean room of class 1000. This multi function chamber includes the evaporator unit, cathode heating, DC gap, shutter and mask subsystem, integrating the functions of cathode production, diagnostic and evaluation. Up to now, the vacuum in the preparation chamber has reached 10^{-9} mbar in the cold situation and 10^{-8} mbar in operation.

The Cs$_2$Te photocathode production is performed in two ways: standard method and co-evaporation method. The former is the evaporation of alkaline layer over the tellurium layer on substrate. The later is adopted newly in CERN photoemission laboratory [1] and means to evaporate the two elements simultaneously. Every preparation method needs the same pre- process: the preparation of cathode plug and the source degas and deposition rate calibration, and the post-treatment process.
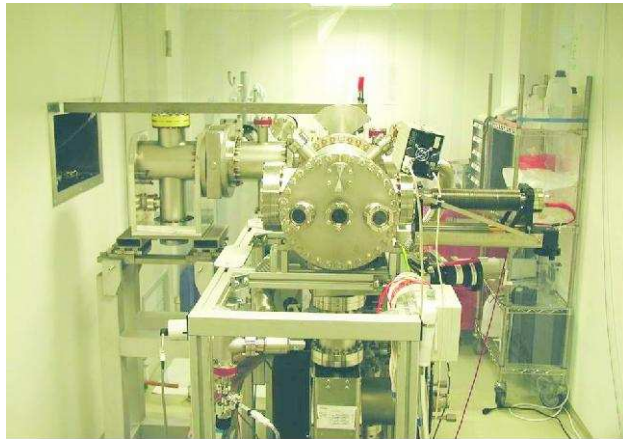

Fig. 1: *Preparation chamber in clean room.*

The surface preparation of the cathode plug prior to the deposition is very important. In our experiment, the cathode plugs are made of molybdenum or copper. Different effects of these two kinds of substrate on the cathode efficiency have not been detected up to now. The process of surface preparation includes polishing, cleaning, degassing and ion beam bombarding. The plugs are manually polished, and the average roughness analyzed by Dektak profiler can reach 17.2 nm. The mechanical polish will be developed soon to ensure the dimensional uniformity of all cathode plugs. After the polishing, ultrasonic cleaning with detergents, pure water and pure alcohol will in turn be used. In the chamber the plug will be degassed in vacuum at about 100°C, but the residual gas contamination will

leave a thin film of 1nm carbon on the surface , and thus in future ion beam bombarding will be performed to clean the substrate surface to atom lever.

Cesium source is commercial dispenser from SAES Getters, and tellurium source is tungsten boat with melted Te. The sources must be degassed in vacuum by loading a small amount of heating power while the cathode surface and the thickness monitors are covered by a shutter. After the chamber vacuum has reached to 10^{-8} mbar, the shutter is removed from the thickness monitor while the cathode surface is still protected. Then the heating power rises to get the proper deposition rates on the thickness/rate monitors. In our case, the tellurium rate is set about 0.1nm/s and the cesium rate is as low as around 0.01nm/s. When the evaporation of the sources keep stable, the cathode surface is exposed in front of the sources, and the deposition on cathode surface starts.
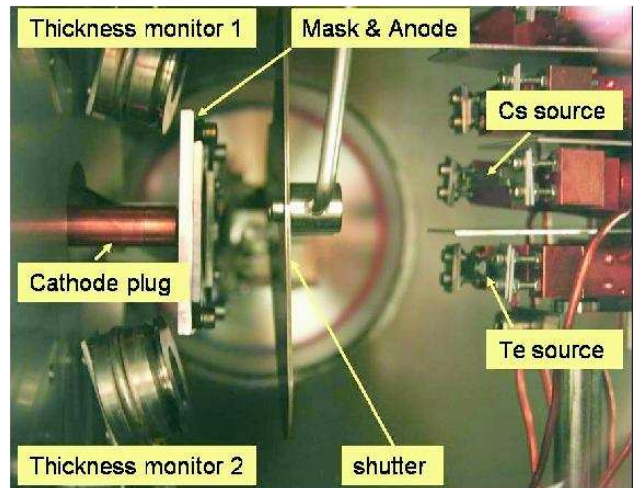

Fig. 2: *Inside view of the preparation chamber.*

For the standard preparation method, the deposition is done in two steps: at first tellurium is deposited on the cathode surface, and then activated with cesium. The temperature of cathode maintains to 120°C during the coating. The thickness/rate monitors calibrate the deposition rates for the cesium and tellurium films. Diagnostic ultra-violet laser illuminates the cathode and the photocurrent is monitored during the deposition. Tellurium film is deposited to about 10 nm, and then cesium is evaporated till the photocurrent curve reaches its maximum and then begins to slide down. This is the most popular method in the photoemission laboratories, and it has been used in our first test. However, sometimes this method will result in inhomogeneous and various stoichoimetric ratios in the photocathode film.
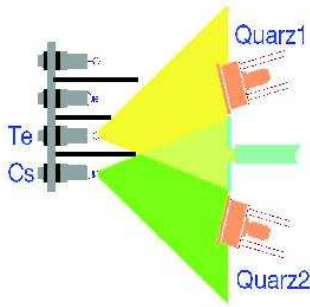
Fig. 3: *Theoretical figure of co-evaporation.*

The co-evaporation method is hopefully a good way to get more proportioned Cs_2Te film than the standard processes if the stoichiometric rate of Cs/Te can be controlled exactly. The Tellurium deposition rate is easy to calibrate, but the open question is how to correctly measure the Cs deposition rate or the Cs film thickness, because Cs is sensitive to contamination gases and it is hard to do measurement with any thickness detector. In our study, an indirect way is developed to calculate the density of Cs atoms in the film and thus the stoichiometric rate of Cs/Te. On the same substrate, at first the whole sample is covered by uniform tellurium film and then only half of the film reacts with cesium while the other half covered by mask. Cesium should be trapped in the Cs-Te bonds so tellurium should be more than enough. Rutherford Back Scattering (RBS) and Proton Induced X-ray Emission (PIXE) are used to measure the density of tellurium atoms in the Te film and the atomic ratio of Cs / Te in the Cs-Te film. These measure methods care about only the number of certain nucleus, but not their chemical status, so they are suitable for the measurement of sensitive Cs element. From these data, the relationship between the atom rate and the thickness/rate monitor displays will be achieved, and this relationship can be repeated for the source group in certain position. After the proper atom rate is reached, try to adjust the heating power of the sources and thus keep the correct displays on the thickness/rate monitors, then the Cs-Te will be formed in right stoichoimetric. Although we have had some experience on this method, it needs more tests to get stable and repetitive result.

After the preparation the cathode will be post-treated. Normally the temperature of the cathode plug will be kept to 120^oC for about half an hour. It is believed that this treatment will let the sensitive photoemission layer solidified, which means dissociative Cesium atoms on the surface will compound with Cs-Te bonds under the surface or react with Oxygen in the surrounding space. Then the distribution of the Q.E. on the cathode surface is supposed to be measured by scanning, and the Q.E. via x-y coordinate will be described to show if the film in the working area is homogeneous. The fine beam travels through the UV window of the vacuum chamber and the mesh onto the cathode surface. The size of the cathode surface is $\Phi8$ mm and the anode-mesh has the period of 0.44 mm. A motorized x-y scanner with angular resolution of 0.7 μrad is performed to steer the beam in two axes. The spot size and position can be detected on the virtual cathode.

In the first quarter of 2007 the photocathodes will be practically used. Until now, we have made some tests but much effort is still needed to improve the vacuum in the preparation chamber and the transport chamber. A website about photocathode in FZD has been developed [2], where the information about the photocathode material and the activity in FZD photocathode laboratory can be found.

[1] http://ucq.home.cern.ch/ucq/Coferences/
     CTF3_col-meet-2003/CTF3_col_meet_Photocat.pdf
[2] http://www.fzd.de/projects/CARE/

The Control Software for the Photocathode Preparation Chamber

J. Teichert, R. Xiang, C. Werner

The photocathode preparation chamber will be controlled automatically outside of the clean room. Figure 1 shows the block diagram of the photocathode preparation control system. A new software "SRF" based on the programming language Visual C++ is developed to perform the preparation control process. In this report the control software will be introduced in two parts: the data acquisition / control and the user interface.

The data transfer is realized by two National Instruments multi function cards PCI-NI6221 and PCI-NI6704, which represent the interface between devices and software. The measuring card PCI-NI6221 receives the analog output from the devices and the control card PCI-NI6704 outputs the analog and digital signal to the devices. In order to protect the cards from high current or voltage interface converters have been used between the devices and the input of the cards.

The user interface includes several modules. We will introduce them separately. The operator can set the voltage for cathode and anode through high voltage controller. At the same time, the photocurrent can be diagnosed from a graphic window with an accuracy of $0.1~\mu A$.

The temperature of the cathode plug is controlled in the range from $20^{o}C$ to $400^{o}C$ by adjusting the power of halogen lamp or setting an expected temperature. The SRF will compare the measured temperature and the expected one and calculate the required power for halogen lamp.

In the evaporator unit control module, user can at first switch on the module and then choose an active source pair. The power loading on the evaporator is controlled with the accuracy of 1 mW. Simultaneously, the current and voltage loaded on the dispenser will be shown to user. Because the resistance of evaporator is very low ($0.06~\Omega$ for Tellurium source and $0.2~\Omega$ for Cesium source), the measurement of resistance is realized by determining the voltage difference at the two ends of evaporator.

The shutter is moved by a step motor, which has four positions: starting point, cover-all, cover cathode only and open-all. The SRF controls the direction and the steps of the step motor through PCI-NI6704 digital ports .

The SRF reads vacuum pressure from the gauge controller, and so the attention will be taken in the whole preparation process on the chamber vacuum. There is a laser switch in SRF and a scan module for the measurement of the Q.E. distribution of the photocathode. An extra scan board is used to steer the x-y scanner. The deposition rate is obtained from the Sycon Thickness Measure (STM) board and shown directly on the monitor.

This control system has been tested in the photocathode laboratory. The detailed information can be found in reference [1].

[1] Werner, Christian, "Entwicklung der Steuer- und Datenerfassungs-software für die Photokathodenpräparation", Diplomarbeit
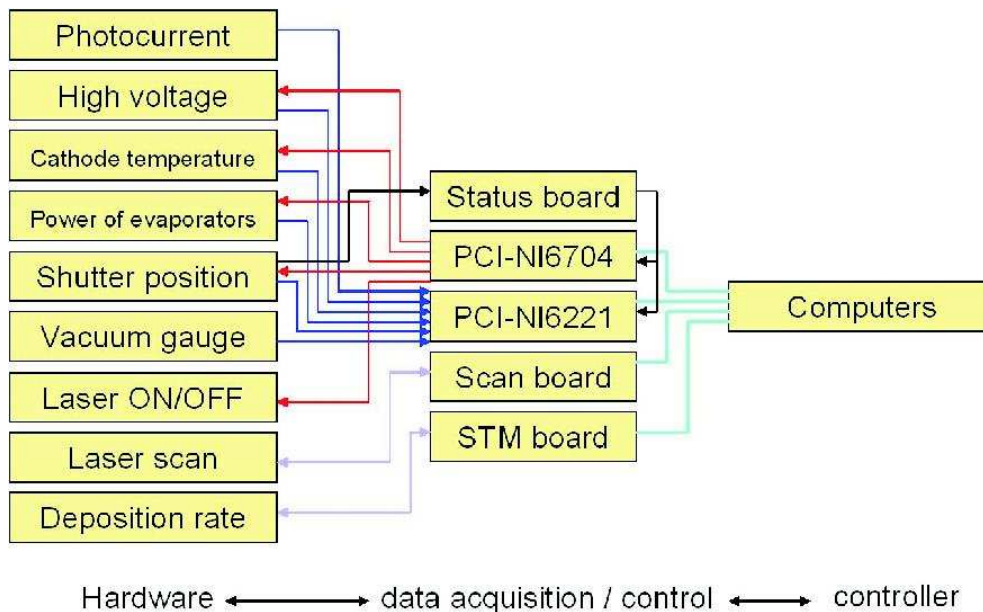
Fig. 1: *The Block diagram of the photocathode preparation control system.*

Test des Photokathoden-Kühlsystems

F. Staufenbiel, D. Janssen, J. Teichert, R. Xiang

In Rossendorf wird eine supraleitende Photoelektronenkanone (SRF-Gun) entwickelt. Die Elektronen werden von einem leistungsstarken UV-Laser aus einer photoelektrischen aktiven Cäsiumtelluridschicht ausgelöst, die auf einer Photokatode aufgedampft ist. Die ausgelösten Elektronen werden danach mittels eines Hohlraumresonators (Cavity) auf ca. 10 MeV beschleunigt. Da die SRF-Gun mit einer normal leitenden Kupferkathode betrieben wird, kann durch die beschleunigende Hochfrequenz ein Wärmeeintrag von geschätzten 10 W und mehr durch die photoelektrische Schicht generiert werden. Der Wärmeeintrag des UV-Lasers beträgt ca. 0.5 W. Durch so eine konzentrierte Wärmequelle kann eventuell die Sprungtemperatur des Hohlraumresonators, welcher auf 1.8 K abgekühlt wird, erreicht werden. Um dieses Szenario präventiv auszuschließen, wird die Kathode über einen massiven Kupferblocks durch ein Reservoir mit flüssigem Stickstoff gekühlt.

In Fig. 1 ist das Kathodenkühlsystem dargestellt. Die Kathode wird durch ein spezielles Bajonett-Verschlusssystem im Kühlkörper positioniert. Die berührenden Flächen sind konisch geformt und zentrieren die Kathode bei gleichzeitiger vergrößerter Kontaktfläche, die einen besseren Wärmeübertrag gewährleistet. Der Anpressdruck wird von einer Feder ausgeübt die eine Kraft von ca. 30 N aufbringt. Beim Test des Systems wird die Temperatur an der Kathodenspitze (Pos. 1), dem Kühlkörper (Pos. 2) und dem Stickstoffreservoir (Pos. 3) gemessen und durch eine Heizpatrone an der Kathodenspitze eine definierte Wärmelast der Kathode zugeführt.

In Fig. 2 sind die gemessenen stationären Temperaturen über der elektrischen Heizleitung aufgetragen. Bei 30 W Heizleistung beträgt die Temperatur an der Kathodenspitze ca. 140 K wobei die Temperatur des Kühlkörpers auf ca. 90 K ansteigt und das Stickstoffreservoir bei fast konstanten 80+K verbleibt. Durch diese Referenzwerte ist es möglich, durch Messung der Temperatur am Kühlkörper, die eingetragene Wärmeleistung während des Betriebs der SRF-Gun zu bestimmen. Somit kann unter anderem ein Wert für die dielektrischen Verluste von Cäsiumtellurid bestimmt werden, welcher nicht in der Literatur vorhanden ist. Ein Wärmeübertrag zum supraleitenden Hohlraumresonator ist nur durch Wärmestrahlung gegeben, da beide Systeme durch einen Vakuumspalt getrennt sind. Bei der gemessenen Temperaturerhöhung beträgt der Wärmeübertrag durch die Wärmestrahlung nach dem Stefan-Boltzmann-Gesetz beträgt nur wenige mW [1]. Somit ist ein Quench-Prozess des Hohlraumresonators, welcher durch die Wärmeverlustleistung der Hochfrequenz in der Photokathode ausgelöst werden könnte, ausgeschlossen.
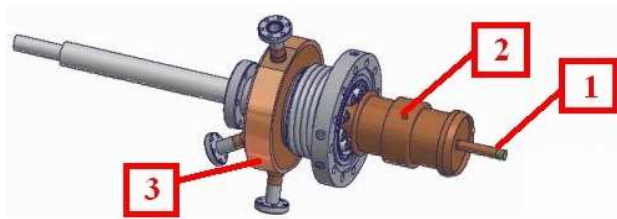
[1] Physica C 441 (2006) 216-219.

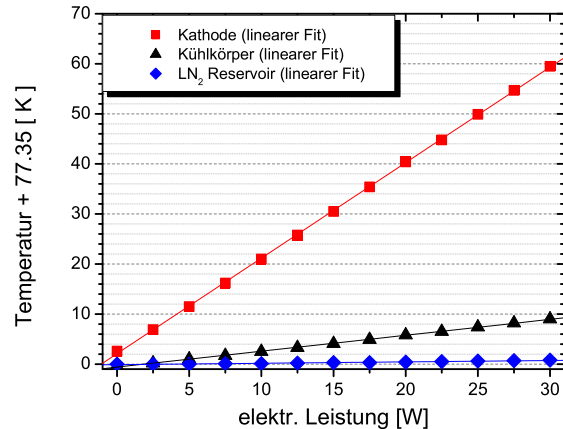**Fig. 1:** *Photokathodenkühlgruppe mit drei ausgewählten Thermoelementpositionen.*

Fig. 2: *stationäre Temperaturwerte an den drei gewählten Thermoelementpositionen bei verschiedenen Heizleistungen.*

Beam Line des SRF-Gun Photolasers

F. Staufenbiel, J. Teichert, H. Tietze

Einleitung

Der SRF-Gun Photolaser erzeugt Pulse im ps-Bereich mit einer Wellenlänge von 262 nm. Die Leistung des Lasers liegt bei etwa 1 W im UV-Bereich. Durch die spezielle Caesiumtellurid-Schicht der Kathode ist die Quantenausbeute für ausgelöste Elektronen ca.1%. Die Laserstrahlung wird mit Hilfe eines Spiegelsystems vom Laserraum in die Beschleunigerhalle geleitet und der Laserfleck mit Teleskopanordnungen auf der Kathode der SRF-Gun abgebildet. Der gesamte Weg der Laserstrahlung beträgt ca.10 m.

Optische Beamline

In Fig. 1 ist die optische Laserbeamline dargestellt. Zunächst wird der Laserstrahl durch eine Schikane unterhalb des Bodenniveaus vom Laserraum in die Beschleunigerhalle geleitet. An Gestellen sind Profile angebracht, auf denen optische Elemente aufgebracht und entlang der optischen Achse verschoben werden können. Die optischen Elemente sind Linsen der Teleskope und ein System aus Blenden und Linsen zur Formung des Laserflecks in transversaler Richtung. Alle Elemente mit einer flexiblen Position z.B. zur Fokussierung etc. müssen auf fernsteuerbaren Lineartischen montiert sein. Ebenfalls ist der vorletzte Umlenkspiegel (3" Durchmesser) in beiden Verkippungsrichtungen fernsteuerbar verstellbar.
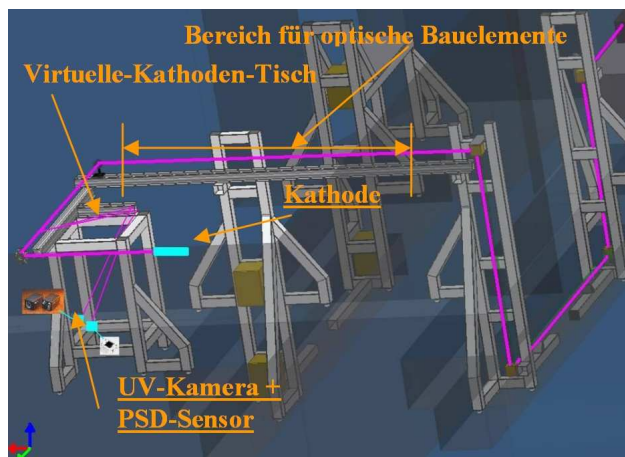

Fig. 1: *Gestelle der Laserbeamline in der Beschleunigerhalle.*

Virtuelle Kathoden

Die virtuellen Kathoden sind zum einen eine CCD Kamera, deren Chip zum Teil im UV-Bereich empfindlich ist, und zum anderen ein ortsempfindlicher Sensor, der die Intensität des Laserflecks und deren Position (Schwerpunkt) in ein elektrisches Signal wandelt (siehe Fig. 2). Der ortsempfindliche Detektor kann örtliche Schwankungen mit einer Frequenz bis 3.5 kHz detektieren. Somit kann der Laserstrahl in seiner Intensität und Lage simultan überwacht und geregelt werden. Die CCD Kamera liefert Informationen über die Intensitätsverteilung und ebenfalls über die Lage des Laserflecks. Für die virtuellen Kathoden wird ein geringer Anteil der Strahlung durch einen Beamsplitter ausgekoppelt. Der nachfolgende zurückgelegte Weg der Strahlung zur Kathode und der zurückgelegte Weg zu den zwei virtuellen Kathoden muss die gleiche Länge aufweisen. Ein Keilplattenpaar mit einem Keil von 2" dient vor dem Beamsplitter als letzte Feinjustierung des Flecks auf den Kathoden. Durch eine unabhängige Drehung der Keilplatten ist eine Parallelverschiebung des Strahls um einige Millimeter möglich. Die Keilplatten werden als bewegliche Elemente motorisiert fernsteuerbar auf Drehtischen betrieben.
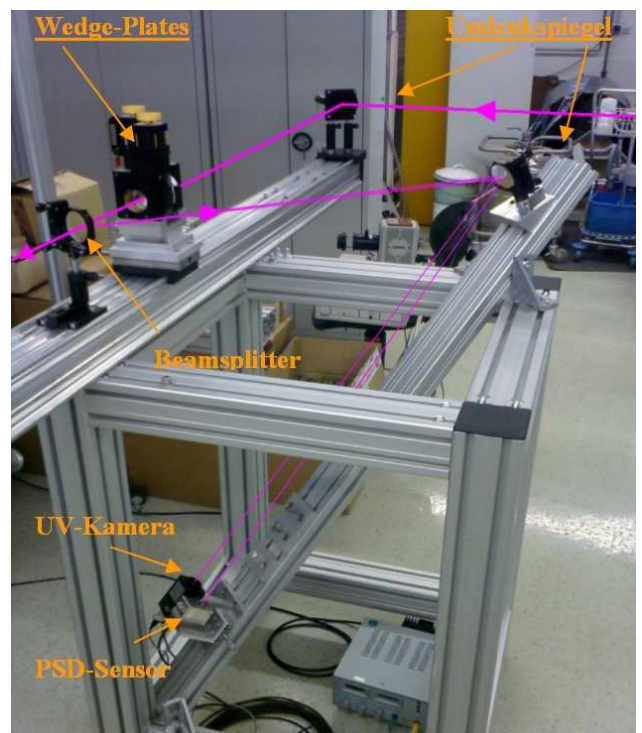

Fig. 2: *Gestell für die Anordnung der virtuellen Kathoden.*

Measurement of the Screening Effect of the μ-Metal Shield for the SRF-Gun

F. Staufenbiel, E. Berger, P. Murcek, J. Teichert

One important aspect for superconducting accelerators is the reduction of the magnetic field flux through the cavity material during cooling down procedure. For the Nb cavity of the SRF-Gun a specially designed μ-metal shield was fabricated and the remained magnetic field inside the μ-metal shield had to be measured. To prevent any effect on the performance of the cavity the remaining magnetic field should be less than about $1\,\mu$T [1]. The magnetic field of the earth amounts approximately $50\,\mu$T.

As shown in Fig. 1 the μ-metal shield lies on a wooden palette. In order to measure the magnetic field inside of the shield in X-Y direction a guide rail was built. With its help it was possible to position the Hall-Probe concentric in the μ-metal shield at reproducible places. The measurements of the Z component could be measured in 3 positions by existing drillings in the μ-metal shield. The probe could be positioned by marks outside the guide rail in equidistant steps of 20 cm.
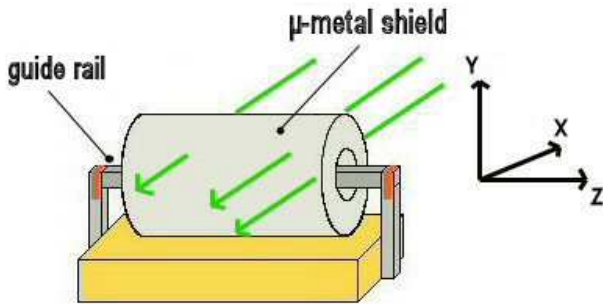
**Fig. 1:** *μ-metal shield with guide rail.*

To determine the magnetic field vector inside the μ-metal shield the components X, Y and Z were measured separately and the amount of the field strength vector was calculated. Analogously, the magnetic field was determined inside the steenless-steel vessel which encloses the μ-metal shield.

The results of the earth magnetic field measurements with and without screening are shown in Fig. 2. The values in X-Y orientation are an average of 3 measurements with a total error of $\pm 0.003\,$G. The unshielded earth magnetic field amounts to approximately $0.5\,$G$= 50\,\mu$T. Inside the μ-metal shield the magnetic field is reduced to approximately

$0{,}007\,$G$=0.7\,\mu$T. The screening of the steel vessel leads to a reduction of the earth magnetic field to approximately $0.4\,$G$=40\,\mu$T. The vessel encloses the μ-metal shield hence the total screening value can be estimated to a magnetic field $<0{,}007\,$G$=0.7\,\mu$T. Furthermore, the measured average of approximately $0{,}002\,$G$=0.2\,\mu$T in X-Y direction shows that the main part of the magnetic field is oriented in Z direction. The μ-metal shield reduces the earth magnetic field total by a factor of about 70. Even in the edge area of the shield a good screening is obtained. The reduction of the magnetic field is relatively constant about the whole length of the μ-metal. With an average value of approximately $0.8\pm 0.5\,\mu$T the requirement to reduce the earth magnetic down to some μT is well done. The position of the superconductive cavity inside the magnetic shield is indicated in Fig. 2. The cavity is by far shorter than the μ-metal shield. Therefore the cavity is not influenced by the less well screened edge areas.
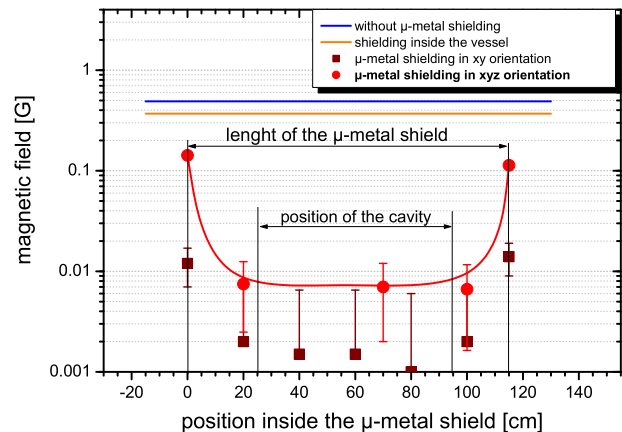
Fig. 2: *Earth magnetic field with and without μ-metal screening.*

Furthermore, a varying screening behaviour of the μ-metal under LN_2 temperature conditions was not observed. The measurement accuracy was $\pm 0.5\,\mu$T. Therefore, a possible shield failing during the cool down procedure is not expected.

[1] B. Aune, et al., Phys. Rev. Special Topics, Vol. 3 (2000) 092001

Correction of the Mirror Charge for a Non-Planar Back Wall of an RF Gun Cavity

D. Janssen, V. Volkov

In the available codes for particle tracking inside an RF gun cavity (ASTRA, PARMELA, GPT) the influence of the conducting cathode plane on the space charge field of the bunch is taken into account by the mirror charge of the bunch behind the cathode plane. If the cathode plane has a curved surface the electric bunch field, obtained in this arrangement, is not perpendicular to the surface. In order to remove this error a FORTRAN code is written, which put additional ring charges behind the cathode plane. The charge values are determined by the condition, that the static bunch field is perpendicular to the cathode surface.

The input parameters of the code are the arrays $\vec{r}_S=$(zs[i],rs[i]), which describe the geometry of the rotational symmetric cathode surface, the arrays $\vec{n}_S=$(dz[i],dr[i]) which are unit vectors tangential to the surface, the external electric field on the surface $\vec{e}_{\text{ext},S}=$(Ez[i],Er[i]), the curvature radius R of the surface at zs[1]=rs[1]=0 and the distance parameter S which is explained below.

In the first step the code calculates the position of the ring charges zc[i], rc[i]. Every charge point is placed perpendicular to the surface and behind a surface point. The distance to the surface is calculated by the average distance between the neighbouring surface points multiplied with the parameter S. For large S values the equation given in Eq.(3) becomes non-linear dependent. For very small S values the electrostatic potential on the surface has an oscillating structure. The optimal value for S is in the order of one.

In the next step the code calculates the charge values. They are determined by the condition, that the sum of the external field and the field of the ring charges is perpendicular to the cathode surface.

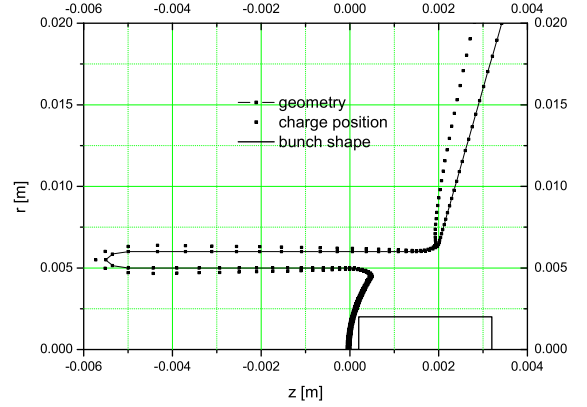$$(\vec{e}_{\text{ch}}(\vec{r}_S) + \vec{e}_{\text{ext},S}) \cdot \vec{n}_S = 0 \qquad (20)$$

The field $\vec{e}_{\text{ch}}$ is proportional to the charge values q and given by

$$\vec{e}_{\text{ch}}(\vec{r}_S) = \sum_k \vec{A}_{\text{S},k} \cdot q_k \qquad (21)$$

Where $\vec{A}$ is a well defined matrix. Eqs. (1), (2) gives a system of linear equations, which determines the charge values.

$$\sum_k \vec{n}_S \cdot \vec{A}_{\text{S},k} \cdot q_k = -\vec{n}_S \cdot \vec{e}_{\text{ext},S} \qquad (22)$$

After solving this equation the code can calculate the field $\vec{e}_{\text{ch}}$ at any point inside the RF gun cavity.

Fig. 1: *Geometry of the cavity back wall with the cathode, position of the ring charges and the bunch shape.*

In order to test the code we calculate the additional field of the ring charges for a special arrangement. The geometry of the cathode and the back wall of the cavity together with the position of the ring charges and the position of the bunch are given in Fig./,1.

For the test calculation a bunch charge of 2 nC has been assumed. The curvature radius R at $z = r = 0$ is 0.02 m. The external field $\vec{e}_{\text{ext},S}$ is created by the mirror charge of the bunch. The values of the additional field created by the ring charges are shown in Fig. 2 and Fig. 3. It is planned to introduce this program into the ASTRA code.
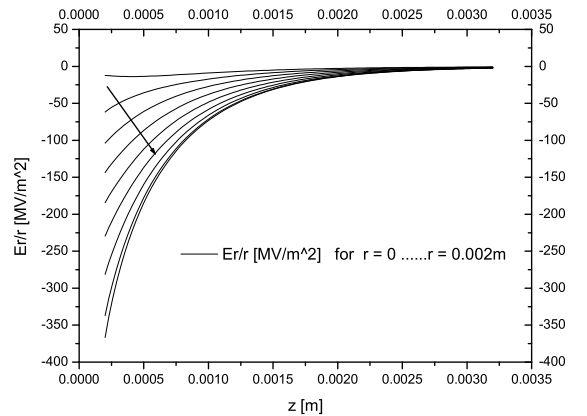
Fig. 2: *Radial electric field of the ring charges at different distances from the axis.*

Simulations for Emittance Compensation of the SRF Gun

F. Staufenbiel, D. Janssen, J. Teichert, R. Xiang

Introduction

For the SRF gun different operation modes are planned. The ELBE mode will be mainly used to drive the infrared FELs at the ELBE accelerator. A small bunch charge of about 77 pC with 13 MHz repetition rate is used to obtain a small transverse respectively longitudinal emittance. In this regime the space charge effects are reduced. Additional calculations for bunch charges of about 40 pC are done in order to achieve very small transverse and longitudinal emittances. In this case the integrated current is halved or the repetition rate must be 26 MHz to achieve the same maximum average current. In all calculations the thermal emittance are included.

The high charge mode will be mainly used to generate neutrons for nuclear reactions analysed by time of flight measurement. Here the repetition rate is determined by the ejectil velocity and limits the pulse frequency to <1 MHz. Therefore, a higher bunch charge is needed to enhance the reaction yield. For all modes, the RF power is restricted to <10 kW by the klystron.
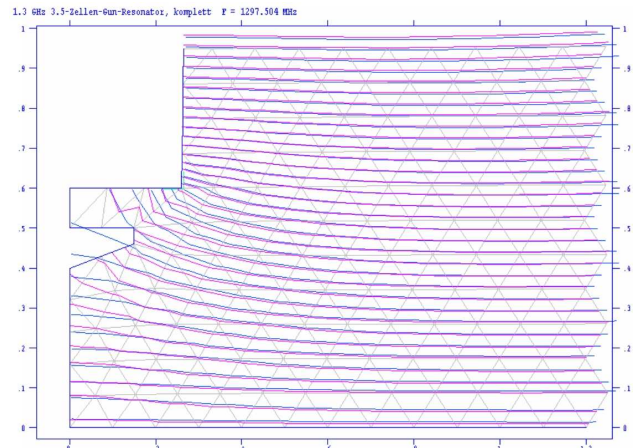
Emittance Compensation

For the SRF Gun three measures are possible to compensate the transverse emittance of the electron beam. Fig.1 shows the well-placed cathode inside the gun half cell. To obtain focusing field lines [1] at the cathode tip the cathode is backtracked by few millimeters. In order to optimize the focusing force with respect to the transverse emittance a visor with a proper shape at the cathode tip is used. Fig.2 shows the small differences of the compared electrical field lines at the tip caused by a cathode visor.
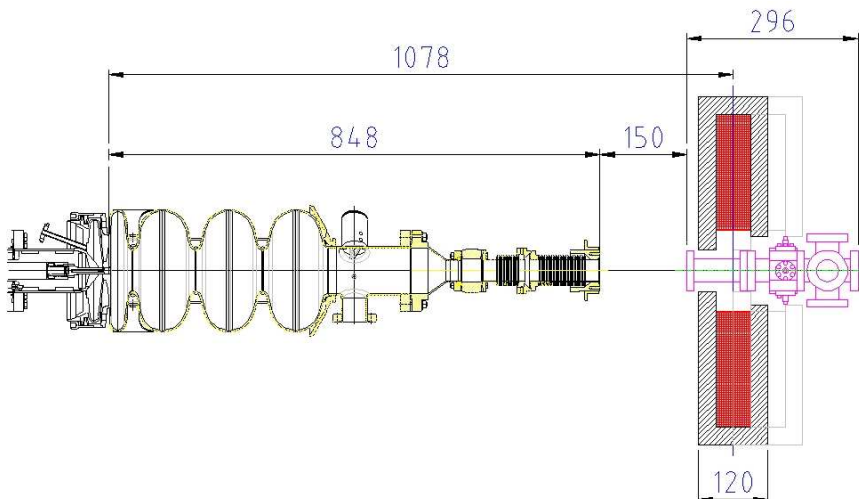
At the exit of the acceleration cavity a solenoid focused the electron beam at 1.08 m distance from the photo cathode shown in Fig.3. After the solenoid the laser port is visible.
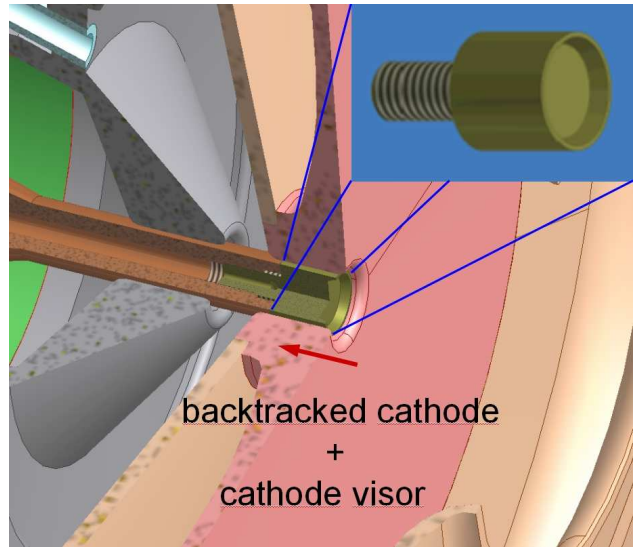
**Fig. 1:** *Backtracked cathode with a cathode visor at the tip.*

Fig. 2: *Compared field lines shows small differences at the cathode tip caused by a cathode visor.*

**Fig. 3:** *Solenoid for beam focusing and emittance compensation.*

Astra simulations

The results of the high charge mode ASTRA simulations [2] with a flat top laser profile and a duration time of about 20 ps are shown in Fig.4. The cathode visor reduces the normalized transverse emittance obviously. The solenoid has a strong effect on the beam diameter and a weak effect on the transverse emittance. The huge peak by the solenoid curve is an effect of the AS-TRA code caused by the solenoid and should not be regarded. The thermal emittance is in all calculations included.
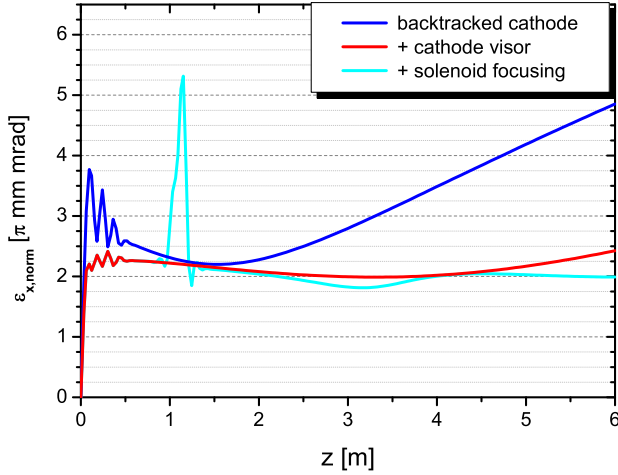
Fig. 4: *ASTRA simulations for different emittance compensation methods at 1 nC bunch charge.*

The results of the ELBE mode ASTRA simulations with a bunch charge of about 77 pC and a Gaussian laser profile and a duration time of about 4 ps (FWHM) are shown in Fig.5. The longitudinal emit-tance via the transverse emittance depends on the starting beam size σ_x. For each beam size a new optimal cathode visor shape is needed. A small transverse emittance causing a large longitudinal emittance and vice versa. Therefore, the balance of the transverse and longitudinal emittance should be conformed to the conceptual formulation. As an example to achieve very small transverse emittances the bunch charge is halved down to 40 pC in order to reduce the dispersive space charge.
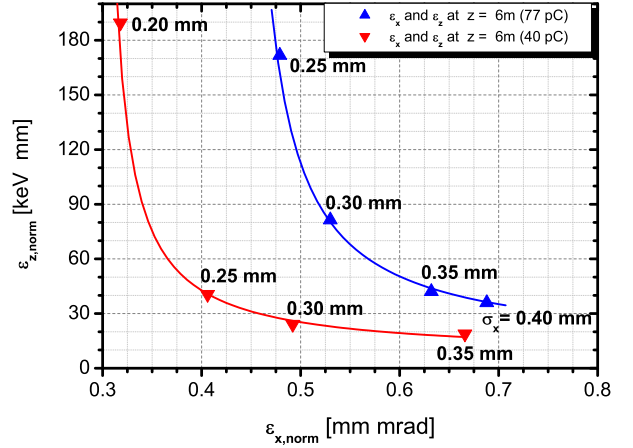
Fig. 5: *ASTRA simulations for 77 pC and 40 pC bunch charge.*

[1] D. Janssen, V. Volkov, Nucl. Instr. and Meth. A452 (2000) 34.

[2] K. Flöttmann, ASTRA, A Space Charge Tracking Algorithm (2007), http://www.desy.de/ mpyflo